UNIVERSIDADE FEDERAL DE MINAS GERAIS
PROGRAMA DE PÓS-GRADUAÇÃO EM SANEAMENTO, MEIO AMBIENTE E RECURSOS HÍDRICOS

EVALUATION OF MEMBRANE SEPARATION PROCESS FOR THE TREATMENT OF GOLD MINING EFFLUENT

Laura Hamdan de Andrade

Belo Horizonte
2016

EVALUATION OF MEMBRANE SEPARATION PROCESS FOR THE TREATMENT OF GOLD MINING EFFLUENT

Laura Hamdan de Andrade

Laura Hamdan de Andrade

EVALUATION OF MEMBRANE SEPARATION PROCESS FOR THE TREATMENT OF GOLD MINING EFFLUENT

Tese apresentada ao Programa de Pós-graduação em Saneamento, Meio Ambiente e Recursos Hídricos da Universidade Federal de Minas Gerais, como requisito parcial à obtenção do título de Doutor em Saneamento, Meio Ambiente e Recursos Hídricos.

Área de concentração: Meio Ambiente

Linha de pesquisa: Caracterização, prevenção e controle da poluição

Orientador: Profa. Dra. Míriam Cristina Santos Amaral

Belo Horizonte
Escola de Engenharia da UFMG
2016

Laura Hamdan de Andrade

EVALUATION OF MEMBRANE SEPARATION PROCESS FOR THE TREATMENT OF GOLD MINING EFFLUENT

Thesis presented to the Post-Graduate Program in Sanitation, Environment and Water Resources of the Federal University of Minas Gerais, as a partial requirement to obtain the title of Doctor in Sanitation, Environment and Water Resources.

Focus area: Environment

Research line: Characterization, prevention and control of pollution

Advisor: Prof. Dra. Miriam Cristina Santos Amaral

Belo Horizonte
School of Engineering, Federal University of Minas Gerais
2016

Página com as assinaturas dos membros da banca examinadora, fornecida pelo Colegiado do Programa

AGRADECIMENTOS

Mais uma etapa chega ao fim... Foram 4 anos de muito aprendizado, desafios e crescimento; e agora é hora de finalizar um capítulo da vida para começar a escrever vários outros.

Agradeço a todos que contribuíram com a realização dessa tese! Primeiramente, à minha orientadora Miriam. Obrigada por ter me apresentado o incrível mundo das membranas, quando eu ainda era aluna de graduação, e por ter contribuído tanto para minha formação. Obrigada por confiar no meu trabalho e por ter me oferecido tantas ótimas oportunidades de crescimento e conhecimento ao longo de todos esses anos de convívio.

Agradeço a todos os bolsistas que participaram do projeto pelo indispensável apoio no laboratório. Gi, Gabi e Luiza Procópio, obrigada por nos ajudarem a obter os primeiros e comemorados dados da nanofiltração. Luiza da Barros, obrigada por seu cuidado e dedicação com o projeto, pela sua grande disponibilidade e vontade de ajudar, e por largar a indústria para vir agregar competência à área acadêmica (rs). Wadson, não tenho nem palavras para te agradecer! Como gosto de dizer, sem o Wadson, eu não teria doutorado. Obrigada por sua alegria contagiante, por seu ombro amigo, pelas brincadeiras infinitas que deixaram todo esse processo mais prazeroso e por sua incalculável boa vontade e disponibilidade para ajudar.

Aos professores da banca, Prof. Cláudio Habert, Prof. Cristiano Piacsek e Profa. Liséte Lange, que gentilmente aceitaram avaliar e contribuir com o melhoramento desse trabalho.

Agradeço imensamente ao Romulo, que faz minha vida mais feliz e completa e me dá força e apoio para superar os desafios. Obrigada pela paciência, compreensão e carinho de sempre.

Ao meu pai Álvaro e meus irmãos, Danilo, Vitor e Gustavo, pelo amor, confiança e apoio. À Zetinha pelos cuidados amorosos, pela preocupação e por tornar os dias mais saborosos. Ao Gibbs, meu tutuquinho, companhia doce em todos os momentos, que me alegra tanto e me faz rir todos os dias.

Agradeço à minha mãe, que não está aqui para comemorar esse momento, mas que com certeza estaria transbordando de orgulho e alegria. Obrigada por ter me ensinado com gestos e exemplos os verdadeiros valores: bondade, humildade e amor.

A todos os colegas e amigos do GEAPS e do DESA, com quem tive a excelente oportunidade de conviver durante todo esse tempo. Em especial, agradeço à Barbrinha por sua verdadeira amizade, infinita ajuda e generosidade. Obrigada por ser um exemplo de gentileza e bondade para todos. Um dia quero ser inteligente e ganhar coxinhas igual a você! À Kerninha, minha amiga para toda a vida, mesmo que esteja em outro hemisfério. Obrigada pelas ótimas conversas, risadas e conselhos e por ser um modelo de competência profissional, retidão e dedicação. À Alice, que tanto nos ensinou com sua luta e superação, por sua grande ajuda, companheirismo e vontade de contribuir de sempre. À Natalie por se dedicar tanto ao crescimento de todo o nosso grupo. À Pri por sua doçura e invejável bom humor. À Bia pela amizade e ótima companhia. À Thaís por toda sua boa vontade e valiosa ajuda. À Olívia pela contribuição com o projeto. A todos outros colegas que fazem parte do GEAPS: André, Carol, Rosi, Eduardo, Marcelo, Mari, Ana, e vários outros, pelo companheirismo. E aos amigos que seguiram outros caminhos, mas que deixaram sua eterna marca no meu coração: Paulets, Danusa, Nath, Marcella, Rê, Fábio, Gabriel, Tainá.

À Flávia, Altair, Naiara, Lucélia e toda equipe da empresa parceira por acreditarem no nosso projeto e nos proporcionarem as condições para que ele pudesse se tornar realidade.

Gostaria de agradecer também a todos que contribuíram para realização das diversas etapas do trabalho: Mirna e Lucilaine (DESA/UFMG), sempre tão atenciosas; Orlando (Engenharia Metalúrgica/UFMG), pela grande contribuição com as análises de ângulo de contato; Profa. Helen e João (COPPE/UFRJ), pela disponibilidade em nos ajudar com o potencial zeta; Alexandre (Engenharia Química/UFMG), pelas análises de absorção atômica; Profa. Luzia e Késsia (Química/CEFET), pela análise de infravermelho; Jéssica, Breno e Renata (Centro de Microscopia da UFMG), e tantos outros...

Finalmente, agradeço à Capes pela bolsa concedida.

E a todos amigos e familiares que participaram de alguma forma da realização dessa tese.

Muito obrigada!!!

RESUMO

Essa tese objetivou realizar uma avaliação sistêmica e detalhada dos processos integrados de ultrafiltração (UF) e nanofiltração (NF) aplicados ao tratamento de efluente de mineração de ouro, o qual é caracterizado por elevadas concentrações de sulfato, cálcio e arsênio e pH ácido. As condições operacionais tipo de processo (osmose inversa ou NF), tipo de membrana, aplicação de pré-tratamento, pH de alimentação, temperatura e grau de recuperação de permeado (GR) foram avaliadas em escala de bancada. As melhores condições encontradas foram: membrana de nanofiltração NF90, com pré-tratamento com UF, ajuste do pH da alimentação para 5,0 e temperatura ambiente. O elevado grau de supersaturação do sulfato de cálcio limitou o GR do primeiro estágio de NF a 40%. O procedimento de limpeza química também foi estudado, e a melhor eficiência de limpeza foi a obtida com recirculação de solução de HCl 0,2% por 90 minutos. Por outro lado, pressão de operação, velocidade de escoamento, adição de anti-incrustante, aplicação de limpeza física e frequência de limpeza química foram avaliados em escala piloto. Observou-se que o aumento da pressão e a aplicação de limpeza física não trouxeram benefícios ao processo, enquanto o aumento da velocidade de escoamento reduziu incrustação e aumentou a eficiência de retenção de solutos. A adição de anti-incrustante também reduziu o decaimento de fluxo de permeado para GR maiores que 40%. A estabilidade da membrana foi avaliada por meio da sua exposição ao efluente e conjuntamente ao efluente e à solução de limpeza. As variações de rejeição e permeabilidade das membranas ao longo do tempo não foram muito expressivas, e as mesmas demonstraram bom desempenho mesmo após 285 dias de exposição. As condições para a precipitação intermediária do concentrado do primeiro estágio da NF foram estudadas. As condições otimizadas para a precipitação de arsênio e cálcio foram, respectivamente, relação molar Fe/As 4,0 e pH 7,0 e relação molar CO_3/Ca 3,5 e pH 11,5. A baixa ocorrência de incrustação irreversível demonstrou ser possível operar com altos GRs no segundo estágio de UF-NF. Apesar de a inclusão de precipitação intermediária e segundo estágio de UF-NF aumentar o custo do tratamento de US$ 1.34/m³ para US$ 6.28/m³, ela permite a geração de 187 m³/h de água de reúso. Dessa forma, esse estudo demonstrou o potencial das tecnologias UF e NF para tratamento dos efluentes de mineração de ouro visando ao reúso de água.

Palavras-chave: Efluente de mineração de ouro; Nanofiltração; Ultrafiltração; Condições operacionais; Vida útil; Precipitação intermediária.

ABSTRACT

This study aimed to carry out a systematic and detailed evaluation of integrated ultrafiltration (UF) and nanofiltration (NF) applied to the treatment of gold mining effluent, which is characterized by high concentrations of sulfate, calcium and arsenic and acid pH. The operating conditions type of process (NF or reverse osmosis), membrane type, application of pre-treatment, feed pH, temperature and permeate recovery rate (RR) were evaluated in bench scale trials. The best conditions found were: NF90 nanofiltration membrane, pre-treatment with UF, feed pH adjustment up to 5.0, and filtration carried out at room temperature. The high supersaturation index of calcium sulfate limited the first-stage NF RR at 40%. The chemical cleaning procedure was also studied and the better cleaning efficiency was found for recirculation of 0.2% HCl solution for 90 minutes. Moreover, operating pressure, cross-flow velocity, antiscalant dosage, application of physical cleaning and chemical cleaning frequency were evaluated on a pilot scale plant. It was observed that the increase in pressure and physical cleaning did not bring benefits to the process, while increasing the cross-flow velocity was able to reduce fouling and increase solute retention efficiency. The addition of antiscalant also reduced the permeate flux decay for RR greater than 40%. The stability of the membrane was evaluated by its exposure to the effluent and to both the effluent and the cleaning solution. The membranes rejection and permeability variations over time were not very significant, and they have demonstrated good performance even after 285 days of exposure. The conditions for intermediate precipitation of the first-stage NF concentrate were studied. The optimized conditions for the precipitation of arsenic and calcium were, respectively, molar ratio Fe/As 4.0 and pH 7.0, and molar ratio CO_3/Ca 3.5 and pH 11.5. It was possible to achieve a 60% RR in the second-stage UF-NF without occurrence of scaling or irreversible fouling, which indicated the possibility of operation at higher RR. Despite the fact that the inclusion of intermediate precipitation and second stage UF-NF increases the cost of the treatment from US$ 1.34 / m³ to US$ 6.28 / m³, it also allows the generation of 187 m³/h of reusable water. Thus, this study demonstrated the high potential of UF and NF technologies for the treatment of gold mining effluents aiming at water reuse.

Key-words: Gold mining wastewater; Nanofiltration; Ultrafiltration; Operating conditions; Membrane lifetime; Intermediate precipitation.

SUMÁRIO

LIST OF FIGURES

LIST OF TABLES

LIST OF ABBREVIATIONS, ACRONYMS AND SYMBOLS

$\Sigma\Delta C$ - Sum of the difference in molar concentrations of concentrate and permeate

a_{im} - Activity of component i on membrane surface

AFM - Atomic force microscopy

ATR-FTIR - Attenuated total reflection Fourier transform infrared

A_w – Pre-exponential factor of Arrhenius equation

C_{ib} – Concentration of the specie i on bulk solution

C_{im} – Concentration of the specie i on membrane/solution interface

C_{ip} – Concentration of the specie i on permeate

C_{pNF} – Concentration in nanofiltration permeate

C_{pUF} – Concentration in ultrafiltration permeate

$C_{raw\ effluent}$ – Concentration in the raw effluent

d_H – Hydraulic diameter

D_i – Diffusion coefficient of component i

EDS - Energy dispersive X-ray spectrometer

E_W - Apparent activation energy for pure water transport through the membrane

FD – Flux decrement

FD_{CP} – Flux decrement due to concentration polarization

$FD_{chem.irrev}$ – Flux decrement due to chemically irreversible fouling

$FD_{chem.rev}$ – Flux decrement due to chemically reversible fouling

FD_{total} – Total flux decrement

h – Half the thickness of the feed spacer

ICP-OES – Inductively coupled plasma optical emission spectrometrometer

$J_{cleaned}$ – Distilled water flux of the cleaned membrane

$J_{effluent}$ – Effluent flux

J_{fouled} – Distilled water flux of the fouled membrane

J_{new} – Distilled water flux of the virgin membrane

J_v – Permeate flux

$K_{cleaned}$ – Distilled water permeability of cleaned membrane

K_{fouled} – Distilled water permeability of fouled membrane

k_i – Mass transfer constant of specie i

K'_{sp} - Solubility product constant based on molar concentration

K_{virgin} – Distilled water permeability of virgin membrane

MF – Microfiltration

NF – Nanofiltration

N_W - Viscosity-corrected water permeability

P_i – Permeability of solute i

Q_{feed} – Feed flow rate

r_1 – Membrane cell input channel radius

r_{lntd} – Average logarithmic radius of the cell

r_p – Membrane pore radius

r_s – Radius of the solute

R – Gas constant

R_{cell} – Radius of stainless steel membrane cell

$R_{chem-rev}$ – Chemically reversible fouling resistance

Re – Reynolds number

R_{firrev} – Irreversible fouling resistance

$R_{fouling}$ – Fouling filtration resistance

R_{frev} – Reversible fouling resistance

$R_{membrane}$ – Membrane filtration resistance

RO – Reverse osmosis

$R_{physic-irrev}$ – Physically irreversible fouling resistance

$R_{physic-rev}$ – Physically reversible fouling resistance

RR – Recovery rate

R_{RMS} – Root-mean-squared roughness

R_{total} – Total filtration resistance

Sc – Schmidt number

SI_m - Supersaturation index over membrane/solution interface

SEM - Scanning electron microscopy

Sh – Sherwood number

SHP – Steric Hindrance Pore

SS – Suspended solids

T – Temperature

u_0 – Feed cross flow velocity

XRD - X-ray diffraction

γ_{im} - Activity coefficient of component i on membrane surface

ΔG – Variation of Gibbs free energy

Δπ – Difference in osmotic pressure of solution at concentrate and permeate streams

σ – Reflection coefficient

υ – Kinematic viscosity

μ – Dynamic viscosity

ρ – Density

1 CHAPTER

INTRODUCTION

1.1 BACKGROUND AND JUSTIFICATION

Brazil has historically occupied a prominent position in the world production of gold. Between 1700 and 1850, Brazil entered its "Gold Cycle" period where the extraction and export of gold and diamond were the main economic activities. During this period, Brazil was the world's largest gold producer, mainly exploring the surface gold ore deposits in the Iron Quadrangle region. Nevertheless, it was only in the 80s that the gold production in Brazil sharply increased from approximately 20 to over 100 tones, because of the beginning of mining in Serra Pelada region and increase in companies' investment (PORTO *et al.*, 2002). Nowadays, the Brazilian gold production has decreased, partly because of the depletion of the natural reserves and partly because of the reduction in gold price; and it reached, in 2013, 79.6 tones (DNPM, 2014).

Gold has an extremely important monetary role as a reserve asset; and a large amount of all the gold produced throughout history is now stored in central banks of several countries. Moreover, the importance of gold is also closely related to jewelry production. Lastly, many other industries, such as electro-electronic, chemical, perfumery, textiles, paper, and plastic, similarly need gold in its processes (NERY and SILVA, 2001). Nevertheless, despite the economic benefits of gold exploration and processing, it can cause various environmental impacts, including the generation of wastewater with high pollution potential.

The idea of unlimited natural resources that could be used unrestrictedly by man is no longer scientifically accepted. Modern society strives to guarantee the preservation of the environment, allowing future generations to enjoy the natural resources needed for survival. As a result, institutions responsible for environmental protection are gaining strength, and expanding its involvement in companies' supervision and pollution control through an increasingly restrictive legislation. In terms of pollution control and rational water usage, in addition to imposing increasingly restrictive wastewater discharge standards, there is a global tendency towards the establishment of taxes for both water intake, and wastewater discharge. The industries situation becomes progressively more critical once the supply of fresh water with appropriate quality to conventional treatments has decreased gradually, which can create serious conflicts over water use.

Although Brazil has a privileged and relatively stable water supply condition, the country has already felt the effects of water shortage because of uneven water distribution and water mismanagement. Since 2012, there has been a gradual reduction in rainfall in some regions of

the country. The availability of water for public supply has been considerably impaired by this climatic change; especially the semiarid region of Brazil, and the Southeast metropolitan areas, which are densely populated and have higher water demand (ANA, 2014). This water shortage may lead to increased water price, or even the restriction of water supply to other users.

Therefore, water reuse has become an environmentally and economically feasible solution for industries. Water reuse can improve the industry's public image, and increase the industry profits because of reduced expenses with water purchase and/or capitation, and decreased dependency on local water sanitation companies. From an environmental perspective, water reuse contributes to a reduction in natural water capitation, and allows the use of this natural resource for nobler purposes, such as public water supply. It also leads to a decrease in wastewater discharge, which reduces the environmental impacts of industrial sectors.

However, advanced treatment technologies with efficient pollutants removal are vital to safely implement wastewater reuse in industrial sectors. While water reuse in industrial, domestic and agricultural applications is a reality in many developed countries (ASANO *et al.*, 2007), in some countries, such as Brazil, it is still difficult to implement. This scenario is mainly caused by lack of knowledge of the advanced processes, lack of investment to adapt the old treatment systems to the new demands, public resistance to new technologies, and dependence on imported products. Therefore, because of these limitations, the use of conventional processes still prevails in Brazil. However, the main conventional wastewater treatment techniques are characterized by high plant footprint, high operational cost, and low removal efficiency per process. Therefore, research projects in advanced processes for wastewater treatment, such as membrane separation one, at the same time increase the knowledge and disseminate these technologies in the country, allowing scientific, technical and technological development. This directly contributes to a more efficient treatment of effluents and an increasingly viable water reuse practice in Brazil.

In the gold mining industries, the effluents are usually treated by neutralization, precipitation and sedimentation processes (LANGSCH *et al.,* 2012). Although this treatment system can produce a treated effluent that complies with the Brazilian legislation for wastewater discharge, it can hardly generate a water with the quality required for reuse (WANG *et al.,* 2007). In this case, the main limitation for water reuse is the high total solids concentration of the treated effluent, since industrial process waters must have low salt concentration to prevent scale and

corrosion problems. As a result, membrane separation processes, especially the ones that can reject dissolved solids, are promising technologies for the treatment of this effluent aiming at generation of reuse water.

According to Habert *et al.* (2006), membrane separation processes are those that use a selective barrier (membrane) which can promote the separation of components of a solution or suspension under a driving force. The membrane separation technologies have significantly developed in recent years, as they have unique characteristics compared to conventional industrial separation processes. Some examples of these unique characteristics include: the absence of phase change for separation (as required for distillation), therefore minimizing energy requirements; they do not require high chemicals addition (as liquid-liquid extraction); allow the processing of thermolabile substances because they can operate at room temperature; have high selectivity; are easily scaled because they have modular design; and do not require extensive labor. Among the membrane separation processes, the importance of nanofiltration and reverse osmosis must be emphasized since these processes are capable of retaining dissolved salts and molecules, and have wide applicability in wastewater treatment and water reuse (ACERO *et al.*, 2010 a; KURT *et al.*, 2012; QI *et al.*, 2011).

Despite the successful cases involving membrane separation processes for the treatment of mining effluents (AL-ZOUBI *et al.*, 2010 a; BUZZI *et al.*, 2011; RICCI *et al.*, 2015; VACLAV and EVA, 2005), further evaluation of the process type, membrane type, best operational conditions and chemical cleaning processes for each specific application is still needed. Besides, studies with synthetic effluents still predominate in literature. These studies do not consider the effect of effluent matrix in process performance and cannot be used for scaling up purposes. Additionally, the evaluation of membrane stability over effluent exposure time is essential for estimating the membrane lifetime, and for discussing the application viability. Furthermore, pilot scale tests are needed to consolidate the bench scale results; however, because of many technical and economic constraints involved in pilot scale tests, few studies with this approach were found in the literature. Lastly, few papers discuss the management of the concentrate produced in membrane separation processes; this concentrate is a residue, and needs to be treated and/or appropriately disposed. In membrane separation processes, concentrate management is especially complex when the initial effluent has high concentration of dissolved solids, since in this case the permeate recovery rate is usually low, and the concentrate flow rate is high.

Therefore, the innovation of this thesis lies in: a) The evaluation of the application of membrane separation processes in the treatment of real gold mining effluents, specially focused on the process valuation through the generation of reuse water, on an understanding of the variables that can influence the membrane retention and fouling, and on the evaluation of the membrane stability after prolonged exposure to mining effluent; b) The study of the continuous operation of an ultrafiltration and nanofiltration pilot scale unit treating gold mining effluent, and the comparison of these results with those obtained in the bench scale unit; c) The proposal and evaluation of an innovative treatment route for mining effluents, which includes the integration of two-stage ultrafiltration-nanofiltration with a two-step intermediate precipitation; the first step aimed at arsenic removal, and the second at calcium removal, in order to treat the nanofiltration concentrate and increase the overall permeate recovery rate in the second nanofiltration stage.

The hypotheses tested in this thesis were: a) that membrane separation processes (particularly ultrafiltration and nanofiltration) are technically and economically advantageous in the treatment of gold mining effluents, and that these processes can produce a treated effluent suitable for industrial reuse; b) that the evaluation of a continuous operation in a pilot scale unit can provide important information that could not be observed in bench scale tests; c) that the innovative treatment route comprised of the two nanofiltration stages and the two-step intermediate precipitation can increase the overall permeate recovery rate and treat the nanofiltration concentrate.

1.2 OBJECIVES

1.2.1 General objective

The aim of this thesis was to evaluate membrane separation processes for the treatment of two gold mining effluents (i.e. the effluent from the sulfuric acid production plant, and water from the calcined dam) and production of reuse water. It focused on the evaluation of the best operational conditions and membrane cleaning procedure, on the study of membrane stability, and on the proposal of a treatment route with two intermediate precipitation steps.

1.2.2 Specific objectives

The specific objectives are:

1. Compare the applicability of nanofiltration versus reverse osmosis for the treatment of two mixed gold mining effluents (effluent from the sulfuric acid production plant and water from the calcined dam) and define the most suitable;

2. Study how the feed pH, process temperature and permeate recovery rate influence the effluent nanofiltration on a bench scale unit;

3. Evaluate the best chemical cleaning agent, the cleaning procedure type (with or without recirculation), and the duration of the chemical cleaning for the nanofiltration membrane;

4. Investigate the chemical and structural stability of the nanofiltration membrane exposed to the mining effluent and to the cleaning solution;

5. Evaluate operating conditions (cross-flow velocity, operating pressure, antiscalant agent usage, and physical and chemical cleaning frequency) in a pilot scale nanofiltration unit and compare bench and pilot scale results;

6. Develop and study a treatment route based on integration of two nanofiltration stages with a two-steps intermediate precipitation (the first step for arsenic removal and the second for calcium removal), as alternative to increase reuse water production and to treat and dispose the concentrate;

7. Conduct an investment estimate of the membrane processes and intermediate chemical precipitation applied to the treatment of gold mining effluents.

1.3 DOCUMENT STRUCTURE

This thesis is divided into seven chapters. Chapter 1 is introductory. It contains the context/justification and the main objectives of work, and publications derived from this thesis.

Chapter 2 is entitled "Operating conditions evaluation of membrane separation processes applied to gold mining effluent". The specific objectives 1 and 2 are contemplated in this Chapter.

The specific objectives 3 and 4 are addressed in Chapter 3. Its title is "Nanofiltration applied in gold mining effluent treatment: evaluation of chemical cleaning and membrane stability".

In Chapter 4, "Comprehensive bench and pilot scale investigation of NF for gold mining effluent treatment: membrane performance and fouling control strategies", addresses the specific objectives 5 and 7.

Chapter 5 is entitled "Treatment of gold mining effluent by a two-stage nanofiltration process: arsenic and calcium intermediate chemical precipitation". It is associated to the specific objectives 6 and 7.

Finally, in Chapter 6, "General conclusions", it may be found the main achievements of the study, and in Chapter 7, the bibliographic references cited in the thesis.

2 CHAPTER

OPERATING CONDITIONS EVALUATION OF MEMBRANE SEPARATION PROCESSES APPLIED TO GOLD MINING EFFLUENT

2.1 INTRODUCTION

Gold mining and ore processing are activities of great economic importance. Gold has been used in many different applications, from raw material for jewelry manufacturing and monetary reserve, to more technological applications such as the production of catalysts and nanoparticles. On the other hand, gold ore exploitation and processing bring forth environmental hazards that may go from natural habitat destruction to highly polluted effluent release that may contaminate the environment (GETANEH and ALEMAYEHU, 2006). Effluents from gold ore processing may carry high concentrations of heavy metals (such as As, Cd, Cr, and Hg), as these elements are often present in minerals disseminated within the gold ore (CHAN and DUDENEY, 2008; LANGSCH *et al.*, 2012). Additionally, when the ore contains sulfide minerals, processing may generate acid effluent (AKCIL and KOLDAS, 2006).

These effluents are usually treated by neutralization, precipitation and sedimentation (AKCIL and KOLDAS, 2006; CORREIA, 2008; LANGSCH *et al.*, 2012), although other technologies such as anaerobic bioreactors (WILDEMAN *et al.*, 2006), sorption (ACHEAMPONG and LENS, 2014; MAGRIOTIS *et al.*, 2014), coagulation and flocculation (ONCEL *et al.*, 2013; YAN *et al.*, 2012), and crystallization (FERNÁNDEZ-TORRES *et al.*, 2012) may also be used. Nevertheless, these methods may be insufficient to adjust effluent properties to meet discharge and/or reuse standards; require high consumption of chemical reagents; and generate large volumes of metal-contaminated sludge (WANG *et al.*, 2007).

Membrane separation processes, specifically nanofiltration (NF) and reverse osmosis (RO), are effective technologies to retain salts and metals from aqueous medium (AL-RASHDI *et al.*, 2013; PAGES *et al.*, 2013) presenting high potential to treat mining effluents for water reuse. NF is an intermediate process between RO and ultrafiltration (UF) that may retain dissolved molecules with molar weight ranging between 200 and 1,000 g/mol and multivalent ions (YU *et al.*, 2010). Many works have shown that NF is an efficient system for secondary or tertiary treatment of effluents intended to supply water for industrial, agricultural and/or indirect reuse as potable water (ACERO *et al.*, 2010 a; ACERO *et al.*, 2010 b; KOYUNCU *et al.*, 2000; SHU *et al.*, 2005). The use of NF has been increasing due to advantages such as reliability, ease of operation, low power consumption and high efficiency (FU and WANG, 2011).

RO systems use membranes that are permeable to water, but substantially impermeable to salts and therefore are suited to separate ions, dissolved metals and organic molecules of low molar

weight (BAKER, 2004). One of the main applications of RO membranes is seawater desalination (FU and WANG, 2011). Moreover, RO membranes have increasingly become popular water recovery technology for industrial effluents (KURT *et al.*, 2012; QI *et al.*, 2011).

Sierra (2013) studied NF process for treating an acid mine drainage from an abandoned mercury mine. NF was able to retain up to 99% of aluminum, iron and arsenic content, and 97% of sulfate content. Other authors (AL-ZOUBI and AL-THYABAT, 2012) tested NF to treat an effluent from a phosphate mine. Retention efficiencies between 61% and 69% for chloride, nearly 100% for sulfate, and 83% for total solids were obtained, ensuring a treated effluent with similar quality to the raw water that fed the system. Chan and Dudney (2008) evaluated wastewater from gold ore bioleaching treated by neutralization, precipitation and sedimentation followed by a post-treatment with RO. It was found that more than 90% of the arsenic that had not been removed by the first treatment was retained by the membrane. Vaclav and Eva (2005) studied a RO pilot plant operation treating three different mine wastewater types, and attained total solid retention efficiencies ranging between 88% and 98%. Another study evaluated NF and RO membrane performance to treat two synthetic acid mine drainage, including one with high and other with low metal content (AL-ZOUBI *et al.*, 2010 a). It was found that NF membrane was more suited for such use as it handled higher permeate flux at lower power consumption, although its rejections were smaller than RO membrane.

Despite the successful cases using different membranes for treating mining plant effluents, membrane fouling limits membrane application in some cases, since it leads to an increase in cost due to increased energy demand, additional labor requirements for maintenance, chemical cleaning costs, and shorter membrane lifetime (SCHÄFER *et al.*, 2005). Accordingly, fouling control is essential for increasing membrane operational lifetime and thus reducing process costs (ARNAL *et al.*, 2011).

Surface fouling matter composition and structure depend on several factors, such as feed composition and membrane surface properties (MADAENI and SAMIEIRAD, 2010). Fouling control strategies include feed pre-treatment, membrane selection, and operation mode (SCHÄFER *et al.*, 2005). Thus, for each specific application, there remains the need for further examination of the most appropriate system (NF or RO) and membrane type selection, pretreatment, and operating conditions such as feed pH, temperature and permeate recovery

rate. Such assessment would be targeted to find ways to decrease membrane fouling formation, increase retention efficiencies, reduce costs and optimize the whole system.

More effective pretreatment can reduce fouling and increase membrane lifetime. Literature suggests that preliminary retention of colloids and fine suspended solids from effluents is required to prevent severe fouling and avoid module damage or system obstruction (MARCUCCI *et al.*, 2003). Membrane separation processes, such as microfiltration (MF) and UF, are often used as pretreatment for NF or RO systems, since these processes are more competitive than conventional pretreatments (such as coagulation, flocculation, sedimentation, or filtration). MF and UF produce high-quality effluent with low fouling potential and do not require sludge treatment; this enables considerable savings in terms of equipment maintenance, repair, and sludge dumping costs (MARCUCCI *et al.*, 2003; VEDAVYASAN, 2000). System productivity is high, since the backwash water from the MF/UF unit can be recycled to the feed tank when no chemicals are added.

There are many mechanisms related to solute rejection through NF membranes, including steric hindrance, the Donnan effect, and dielectric effects (NGUYEN *et al.*, 2009). Thus, factors such as membrane pore size, surface charge, and pore charge directly influence solute retention. Commercial NF membranes are usually hydrophilic and are prone to hydration and ionization in aqueous solution; the conformation and ionization of their polymeric chains will therefore change in different surrounding conditions, especially at different feed pH values and ionic strengths. Due to the nanoscale pore dimensions (~1 nm) and electrically charged materials of the NF membrane, even a minor change in the pore size or charge pattern can have a significant impact on membrane permeability and solute retention (LUO and WAN, 2013). Research has consequently revealed that membrane solute retention efficiency can be highly dependent on feed pH, which in turn can significantly affect the selection of operating conditions for a specific effluent (CAPAR *et al.*, 2006).

Analysis of the effect of feed pH on NF performance is quite complicated since both membrane and solution properties vary significantly with solution pH; these variations are also dependent on membrane material and solute characteristics. Although there has already been extensive study and modeling of NF membrane performance for both single and multi-element solutions of known composition at different feed pH values (CHILDRESS and ELIMELECH, 2000; LUO and WAN, 2013; NGUYEN *et al.*, 2009; TEIXEIRA *et al.*, 2005), its operational

performance when treating complex effluents cannot be easily predicted (KRIEG *et al.*, 2005). Some authors have studied NF of real water or effluent at different feed pH values (CAPAR *et al.*, 2006; QIN *et al.*, 2003; WANG *et al.*, 2007); however, retention mechanisms and membrane fouling were not thoroughly discussed. Understanding the effect of feed pH on NF and then manipulating this can serve to improve wastewater treatment by enhancing the separation performance and reducing fouling.

The effect of feed pH is even more important when NF membranes are used for the treatment of acid mining effluent. Since low pH can cause changes in the membrane's polymeric structure, pH adjustment may be important not only to improve rejection efficiency and permeate flux, but also to increase membrane lifetime. Moreover, pH adjustment is necessary for water reuse or even for effluent discharge into water bodies, and this can be performed before or after treatment or pretreatment.

According to the literature, feed temperature can also influence both permeate flux and solute retention capacity (AMAR *et al.*, 2009; DANG *et al.*, 2014; KAYA *et al.*, 2009; NILSSON *et al.*, 2008). Dang *et al.* (2014) and Amar *et al.* (2009) observed that increasing temperature led to reduced retention of ionic and non-ionic solutes, but the effect on the latter was significantly more marked. These results were attributed to increased pore size, which reduces the effect of steric hindrance responsible for retention of the neutral solute. These observations can also be explained by an increase in solute diffusion and an expansion of membrane matrix at higher temperatures (KAYA *et al.*, 2009).

Industrial processes often include operations associated with combustion, reactions at high temperatures, steam production, distillation, etc.; these produce high-temperature wastewaters streams. When processing gold ores, roasting (during which the ore sulfide is combusted and converted into SO_2/SO_3) is often employed. Due to the high temperatures of the roaster, the temperature of the effluent generated at this stage is above ambient temperature. Thus, it is also necessary to assess the impact of temperature on the NF process, when this is applied to effluent from gold ore processing.

In addition to pH and temperature, other operating parameters have a strong influence on NF process performance. The permeate recovery rate (RR) is the relation between the permeate and the feed volumes or flow rates. It is considered one of the main design parameters of systems with membranes operating under pressure gradient (GREENLEE *et al.*, 2009). While MF and

UF usually operate at 90-96% RR, for NF and RO these values are substantially lower (BI *et al.*, 2014). Since these membranes are much more permeable to water than to solutes, increasing the RR induces an increase in salt concentration near membrane surface, and as well in the concentrate osmotic pressure and in fouling formation. Thus, for a constant operating pressure, increasing the RR on one hand improves system productivity, but on the other, leads to a reduction in permeate flux.

Therefore, the study shown in this Chapter aims to investigate the use of NF and RO for gold mining effluent treatment to obtain water for industrial reuse. Initially, different NF and RO membranes were tested and the one with the greatest application potential was selected. Then, tests were accomplished in order to evaluate the effect of operating conditions (feed pH, temperature and permeate recovery rate) on membrane performance.

2.2 MATERIALS AND METHODS

2.2.1 Effluents from gold mining

Two effluents from a gold mining company in Brazil were studied, i.e., an effluent from a sulfuric acid production plant and the water from the calcined dam. At this company, the gold ore extracted from an underground mine undergoes processing (crushing, gravity separation and flotation), and the concentrate is transferred to a pyrometallurgical processing unit. At this stage, it is subjected to a roasting process by which gases containing sulfur dioxide and calcined solids are produced. At the sulfuric acid production plant, SO_2-rich gas is converted into SO_3, and then it is adsorbed in an acid solution. The effluent from the sulfuric acid production plant was the first one to be analyzed.

The calcined solids undergo a hydrometallurgical process in which the gold is leached with a sodium cyanide solution. The solid residue is separated from the gold-rich extractant solution through a series of thickeners with counter-current flow. Finally, cyanide is oxidized and the sludge residue is placed in a calcined dam. The second effluent was the supernatant water from this dam.

In this study, the effluents were mixed at a 1:1 ratio (corresponding to actual wastewater flow rates generated by the company, which are 140 m^3/h of effluent from the sulfuric acid production plant and 140 m^3/h of water from the calcined dam) before being transferred to the

membrane treatment system. The mixture of effluents is henceforth referred to as "gold mining effluent."

Twelve samples of each effluent were taken over almost two and a half years, between October 2013 and January 2016. The Table 2.1 shows the characterization of effluents and the mixture between them. Analyses were conducted as explained in Section 2.2.5. As can be noted, the effluent from the calcined dam has a basic pH, while the sulfuric acid production plant wastewater has very acid pH and a high concentration of total solids, arsenic, aluminum, iron and zinc. Neither effluent has an elevated concentration of suspended solids and organic matter. On the other hand, the concentrations of sulfate, calcium, and magnesium are high in both effluents and limit the reuse of wastewater.

Table 2.1 – Minimum, maximum, average and standard deviation of the physico-chemical parameters of twelve samples of the effluents studied

Parameters	Effluent from the sulfuric acid production plant				Water from the calcined dam				Gold mining effluent [c]			
	Minimum	Maximum	Average	Standard deviation	Minimum	Maximum	Average	Standard deviation	Minimum	Maximum	Average	Standard deviation
pH	1.20	2.00	1.73	0.23	7.60	9.01	8.22	0.50	1.84	2.54	2.12	0.25
Conductivity (mS/cm)	7.67	17.25	11.21	2.67	2.61	4.04	3.33	0.40	5.49	8.41	6.63	1.05
Color (Hu)	14	185	105	74	13	50	25	17	29	79	58	26
Turbidity (NTU)	28	251	108	79	3	45	14	13	10	133	57	42
Total solids (mg/L)	6034	9506	8383	1053	2118	4076	3136	548	4202	8804	5475	1504
Fixed solids (mg/L)	3492	6781	5100	1106	1435	5718	2920	1325	3164	5653	3942	914
Volatile solids (mg/L)	1481	5536	3284	1223	127	1607	514	554	903	3151	1533	718
Total suspended solids (mg/L)	25	186	83	48	3	44	21	11	15	90	44	23
Fixed suspended solids (mg/L)	17	180	76	49	0	34	14	10	10	89	39	24
Volatile suspended solids (mg/L)	1	18	7	5	2	12	7	3	0	7	4	2
Dissolved organic carbon [a] (mg/L)	2	9	4	2	4	7	6	2	3	8	5	2

Parameters	Effluent from the sulfuric acid production plant				Water from the calcined dam				Gold mining effluent [c]			
	Minimum	Maximum	Average	Standard deviation	Minimum	Maximum	Average	Standard deviation	Minimum	Maximum	Average	Standard deviation
Carbonate [a] (mg/L)	1	1	1	0	80	107	96	11	41	54	48	5
Sulfate (mg/L)	3061	6481	4713	1296	997	1944	1681	299	2091	4126	3135	866
Chlorine (mg/L)	4	254	63	89	4	500	226	161	53	370	162	127
Calcium (mg/L)	273	895	606	292	405	629	519	123	290	507	403	79
Magnesium (mg/L)	193	547	360	145	31	317	132	127	81	420	186	137
Aluminum (mg/L) [b]	-	-	108	-	-	-	0.1	-	-	-	68	-
Cobalt (mg/L) [b]	-	-	1	-	-	-	0.4	-	-	-	1	-
Copper (mg/L) [b]	-	-	13	-	-	-	0.2	-	-	-	8	-
Iron (mg/L) [b]	-	-	100	-	-	-	0.2	-	-	-	34	-
Manganese (mg/L) [b]	-	-	25	-	-	-	< 0.1	-	-	-	22	-
Nickel (mg/L) [b]	-	-	1	-	-	-	0.2	-	-	-	1	-
Potassium (mg/L) [b]	-	-	41	-	-	-	52	-	-	-	44	-
Sodium (mg/L) [b]	-	-	30	-	-	-	168	-	-	-	77	-
Zinc (mg/L) [b]	-	-	79	-	-	-	< 0.1	-	-	-	64	-

Parameters	Effluent from the sulfuric acid production plant				Water from the calcined dam				Gold mining effluent [c]			
	Minimum	Maximum	Average	Standard deviation	Minimum	Maximum	Average	Standard deviation	Minimum	Maximum	Average	Standard deviation
Arsenic $^{5+}$ [a] (mg/L)	92	163	128	50	4	5	4	1	96	96	96	0
Arsenic $^{3+}$ [a] (mg/L)	792	954	873	114	1	3	2	2	378	469	424	64
Total arsenic [a] (mg/L)	885	1117	1001	164	4	9	7	3	474	565	519	64

[a] Only five samples were analyzed by these parameters

[b] Only two samples were analyzed by these parameters

[c] Mixture at a 1:1 ratio of effluent from the sulfuric acid production plant and of the water from the calcined dam

2.2.2 Experimental setup

Figure 2.1 shows a schematic view of the pretreatment UF and NF/RO bench scale setup. The maximum allowed operating pressure of the UF setup was 0.7 bar, with this provided by a diaphragm pump of maximum flow 138 L/h equipped with a speed controller. Pressure was measured using a manometer and was adjusted via a needle-type valve.

With respect to NF/RO setup, the maximum allowed operating pressure was 15 bar, with this provided by a rotary vane pump (Procon) of maximum flow 530 L/h. A needle valve was used to adjust the feed flow rate and trans-membrane pressure. The stainless steel cell had a diameter of 9.8 cm and an effective filtration area of 75 cm². A 28 mil (711 µm) feed spacer was placed over the membrane to promote effluent distribution. Permeate flux was determined by measuring the volume of permeate produced over 60 s for NF and 120 s for RO using a graduated cylinder.

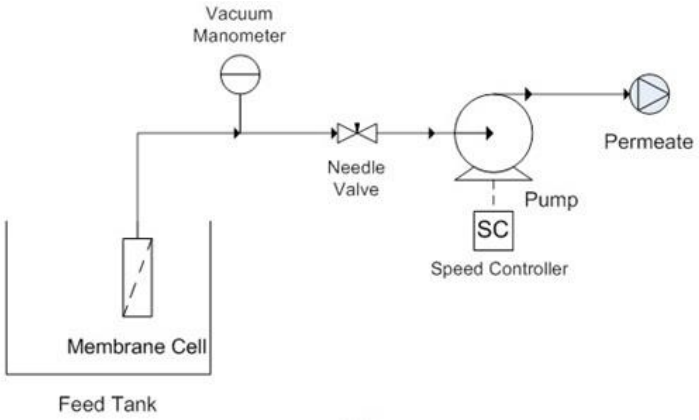

(a)

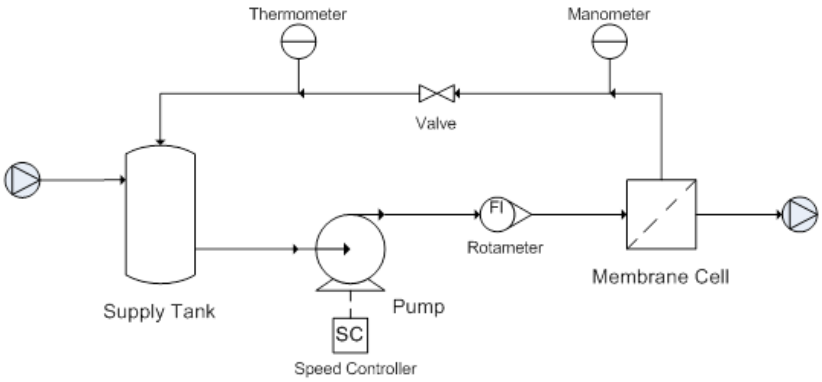

(b)

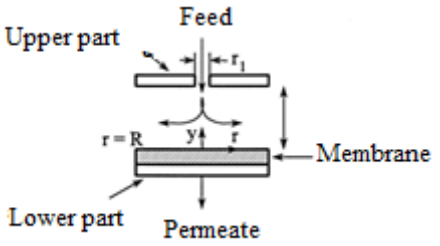

(c)

Figure 2.1 - Schematic illustration of (a) UF and (b) NF/RO units and (c) schematic and photograph of the NF/RO membrane cell

2.2.3 Membranes

Pretreatment was conducted via UF, performed with a commercial submerged membrane module (ZeeWeed by Zenon) with a filtration area of 0.047 m^2, a PVDF-based polymer, and average pore diameter of 0.04 µm.

The performances of five NF/RO membranes were evaluated during the treatment of the effluent from gold mining. RO membranes were TFC-HR and BW30, while NF membranes were MPF34, NF90, and NF270. The characteristics of the membranes studied, as provided by the suppliers, unless otherwise specified, are shown in Table 2.2. The membranes were provided by the suppliers in flat sheets, and were cut to properly fit into the filtration cell.

Table 2.2 - Characteristics of the five tested membranes

Characteristic	TFC-HR	BW30	MPF34	NF90	NF270
Supplier	Koch Membranes	Dow Filmtech	Koch Membranes	Dow Filmtech	Dow Filmtech
Membrane material	Polyamide Composite	Polyamide Composite	Composite	Polyamide Composite	Polypiperazine Composite
NaCl Rejection	99.55% [a]	99.5% [b]	35% [c]	85-95% [b]	n.a.
$MgSO_4$ Rejection	n.a.	n.a.	n.a.	>97% [d]	97% [d]
Molecular weight cutoff (Da)	100 [e]	100 [f]	200 [g]	100 [h]	200-300 [g]
pH range for continuous operation	4 to 11	2 to 11	0 to 14	3 to 10	3 to 10

n.a. Not available

[a] Feed solution containing 2,000 mg/L of NaCl, filtration at 15.5 bar, 25°C, and recovery rate of 15%.

[b] Feed solution containing 2,000 mg/L of NaCl, filtration at 4.8 bar, 25°C, and recovery rate of 15%.

[c] Feed solution containing 50,000 mg/L of NaCl.

[d] Feed solution containing 2,000 mg/L of $MgSO_4$, filtration at 4.8 bar, 25°C, and recovery rate of 15%.

[e] Reference: XU *et al.*, 2005

[f] Reference: GAUTAM and MENKHAUS, 2014

[g] Reference: WANG and TANG, 2011

[h] Reference: ZULAIKHA *et al.*, 2014

2.2.4 Experimental procedure

Experiments were conducted using UF and NF/RO membranes to investigate the effect of type of membrane, pH, temperature and permeate recovery rate on permeate flux, rejection of total solids, conductivity, arsenic, sulfate, chloride, calcium and magnesium, and membrane fouling.

Before each test, UF membrane was cleaned with a 200 ppm NaClO solution in an ultrasound bath for 20 min. The membrane was then flushed with distilled water. All UF experiments were conducted at 0.3 bar.

NF/RO membrane samples were also cleaned by soaking in citric acid solution at pH 2.5 followed by 0.1% NaOH solution in an ultrasound bath for 20 min prior to use. Before each experiment, NF/RO membranes were flushed and compacted with distilled water at 10 bar until the permeate flux stabilized.

While filtrating effluent, the NF/RO setup was operated in semi-continuous mode with concentrate recycling to the feed tank. All NF/RO experiments were conducted at 10 bar and feed flow rate of 144 L/h, which resulted in 1.9 m/s cross-flow velocity and a Reynolds number (Re) of 847. The Re was calculated according to Equation 2.1.

$$Re = \frac{\rho u_0 d_H}{\mu} \qquad \text{Equation 2.1}$$

where ρ is the density (kg/m³) of the effluent, which was assumed to be equal to the water; u_0 is the feed cross flow velocity (m/s); d_H is the hydraulic diameter (m) and μ is the dynamic (N.s/m²) viscosity.

The feed cross flow velocity (u_0) was calculated by Equation 2.2 (MINNIKANTI *et al.*, 1999).

$$u_0 = \frac{Q_{feed}}{4\pi \mathrm{h}\, r_{lntd}} \qquad \text{Equation 2.2}$$

wherein Q_{feed} is the feed flow rate (m³/s); h is the half the thickness of the spacer (m); and r_{lntd} is the average logarithmic radius of the cell, which is calculated by Equation 2.3.

$$r_{lntd} = \frac{R_{cell} - r_1}{\ln\left(\frac{R_{cell}}{r_1}\right)} \qquad \text{Equation 2.3}$$

wherein R is the radius of the stainless steel cell (m); and r_1 is the membrane cell input channel radius (m).

2.2.4.1 UF pretreatment

The benefits of gold mining effluent pretreatment with UF were assessed. For this purpose, 2 L of raw effluent were stored and 3.3 L were ultrafiltered. Nanofiltration of pretreated and raw effluents were carried out for 2 hours using NF90 membrane. NF permeates of pretreated and raw gold mining effluents were analyzed for total solids (Section 2.2.5).

NF permeate flux was measured each 15 minutes. The feed temperature was monitored and permeate flux measures were normalized to 25 ºC. Normalization was accomplished through two correction factors, one related to fluid viscosity and the other to membrane polymeric structure. The fluid viscosity correction factor was defined as the ratio of water viscosity at the temperature of permeation to water viscosity at 25 °C (DRAK *et al.*, 2000). The second correction factor was related to the activation energy for water permeation and was calculated using the Arrhenius equation (KURT *et al.*, 2012) (Equation 2.4).

$$N_w = A_W . \exp\left(-\frac{E_W}{R.T}\right) \qquad \text{Equation 2.4}$$

where N_W is viscosity-corrected water permeability (m³/h.m².Pa), E_W is the apparent activation energy for pure water transport through the membrane (J/mol), A_w is the pre-exponential factor (m³/h.m².Pa), R is a gas constant (J/mol.K), and T is temperature (K). E_W and A_w were calculated by measuring distilled water permeability at 20 ºC, 24 ºC, 28 ºC, 32 ºC, and 36 ºC and fitting the experimental data.

2.2.4.2 Influence of feed pH on UF pretreatment

Process water cannot have acidic pH, as to prevent possible wear and corrosion of equipment and piping. Thus, for reuse of the treated effluent, its pH must be adjusted to approximately 7.0 (ASANO *et al.*, 2007). Such adjustment can be performed before or after the pretreatment and the NF/RO treatment. Therefore, UF was tested at several pH values, namely 2.2 (original effluent pH), 3.5, 4.2, 5.0, 5.5, and 6.0.

A 5.0 M NaOH solution was used for the effluent pH adjustment. After adjustment, 6.6 liters of effluent was ultrafiltered up to a permeate recovery rate of 60%. UF permeate flux were monitored. The conductivity and concentrations of arsenic, sulfate, chloride, calcium and magnesium of raw wastewater and UF permeates were analyzed (Section 2.2.5).

2.2.4.3 Evaluation of several NF and RO membranes performance

NF and RO membranes were investigated regarding their fouling propensity. For this, new membrane water permeability was measured by monitoring the stabilized permeate flux at pressures of 10.0, 7.5, 5.0, and 2.5 bar. Water temperature was also monitored and permeate flux was normalized to 25°C. With the normalized permeability, the intrinsic membrane resistance to filtration ($R_{membrane}$) was calculated according to Equation 2.5:

$$\mathrm{R_{membrane}} = \frac{1}{\mathrm{K_{virgin} \times \mu}} \qquad \text{Equation 2.5}$$

where K_{virgin} is the virgin membrane water permeability at 25°C in m³/s.m².Pa, and μ is the viscosity of permeate (considered to be equal to water viscosity) in N.s/m².

Subsequently, 2 liters of the pretreated effluent were fed into the NF/RO unit. Permeate flux and system temperature were monitored frequently. The total and fouling resistances to filtration (R_{total} and $R_{fouling}$) were calculated by Equation 2.6 and Equation 2.7:

$$\mathrm{R_{total}} = \frac{\mathrm{P - \sigma \Delta \pi}}{\mu \times \mathrm{J_{effluent}}} \qquad \text{Equation 2.6}$$

$$\mathrm{R_{fouling}} = \mathrm{R_{total}} - \mathrm{R_{membrane}} \qquad \text{Equation 2.7}$$

where P is the applied transmembrane pressure (Pa), σ is the reflection coefficient, estimated by the averaged membrane rejection of the major constituents of effluent (MATTARAJ *et al.*, 2008), and Δπ is the difference in osmotic pressure of solution at concentrate and permeate streams. Thus, $P - \sigma\Delta\pi$ is the effective pressure, in Pa. Additionally, $J_{effluent}$ is the permeate flux in m³/s.m².

The difference in osmotic pressure between NF/RO concentrates and permeates obtained with different permeate recovery rates were estimated by the Equation of Van't Hoff, described in Equation 2.8:

$$\Delta\pi = RT\Sigma\Delta\mathrm{C} \qquad \text{Equation 2.8}$$

where R is the universal gas constant (L.Pa/K.mol), T is the permeation temperature (K), and $\Sigma\Delta\mathrm{C}$ is the sum of the difference in molar concentrations of the main dissolved species present in the concentrate and the permeate at a giving recovery (mol/L). For the calculation $\Sigma\Delta\mathrm{C}$, only

concentrations of arsenic, sulfate and chlorine were considered, while for σ estimation, only sulfate was taken into account.

Intrinsic membrane resistance and fouling resistance were calculated for the five studied membranes and compared.

Feed and permeate samples obtained for each test were also analyzed for conductivity, total solids, arsenic, sulfate and chloride (Section 2.2.5). The cyanide concentration was not monitored because it was low (< 0.5 mg/L in the gold mining effluent). Membranes retention efficiencies were calculated and compared. According to fouling propensity and retention efficiency, the best membrane was selected for further trials.

2.2.4.4 Influence of feed pH on NF treatment

The NF90 membrane (the one selected with the highest potential to treat the effluent from gold mining, as will be shown) was tested at pH values of 2.2, 3.5, 4.2, 5.0, 5.5, and 6.0. Tests with pH above 6.0 were not performed because higher pH values did not allowed for better process performance due to high membrane scaling potential.

After pH adjustment with 5.0 N NaOH, the effluent was ultrafiltered and 4 liters the UF permeate was nanofiltrated. During effluent filtration, permeate flux, temperature and accumulated permeate volume were checked every 15 minutes for 4 hours. Permeates for each feed pH value were analyzed for their pH, conductivity, arsenic, sulfate, chloride, calcium and magnesium concentration (Section 2.2.5).

To better understand the membrane behavior at different feed pH values, membrane surface zeta potential was determined using a SurPASS electrokinetic analyzer (Anton Paar GmbH, Graz, Austria). This was calculated from the measured streaming potential using the Fairbrother–Mastin approach (TU *et al.*, 2011), for pH ranges of 2.5–10.0 and for two different background solutions: standard 10 mM KCl solution (electrolyte solution) and a synthetic effluent, with salt concentrations similar to those of the effluent from gold mining (Table 2.3). In the case of the synthetic effluent, only carbonate concentrations differed strongly from those found in real wastewater. Carbonate salts were selected to adjust the concentrations of metallic cations in order to avoid excessive addition of other anions such as sulfate and chloride. However, when the synthetic solution was acidified to pH 1.9, most of the carbonate was expended as a gas. Real effluent was not used, as this could damage the equipment.

Table 2.3 - Characteristics of the real and synthetic effluent used for analysis of membrane surface zeta potential

Parameters	Synthetic effluent
pH	1.80
Sulfate (mg/L)	2,403
Chloride (mg/L)	55
Carbonate (mg/L)	839
Total calcium (mg/L)	559
Total iron (mg/L)	78
Total magnesium (mg/L)	114
Total potassium (mg/L)	61
Total sodium (mg/L)	99

2.2.4.5 Influence of temperature on NF treatment

For NF testing at different temperatures, feed at pH 5.0 (optimal pH, as discussed later) was used. A chiller was used to control effluent temperature at 20 °C, 25 °C, 30 °C, 35 °C, and 40 ± 1 °C. This range of values was selected as real effluent has a temperature close to 40 °C. Pretreated effluent was used to carry out 4-hour nanofiltration tests.

2.2.4.6 NF permeate recovery rate

To establish the optimal permeate recovery rate (RR), 10.0 liters of ultrafiltrated effluent with pH adjusted up to 5.0 were fed into the NF/RO system. The permeation occurred with continuous permeate removal and recycle of the concentrate to the feed tank. Flux was measured for every 100 mL (1% RR) of permeate obtained, while permeate conductivity was analyzed for each 500 mL (5% RR) of permeate. The procedure was performed in duplicate and the results shown are the median from both experiments.

After the filtration, the water flux at 10 bar of the fouled membrane was measured (J_{fouled}). Then, membrane chemical cleaning procedure was performed using two consecutive ultrasound baths for 20 minutes each, first with citric acid solution at pH 2.5 then with NaOH 0.1% solution. Water flux of the cleaned membrane was again measured at a pressure of 10 bar ($J_{cleaned}$). These results, combined with effluent flux measured during the concentration experiment ($J_{effluent}$) and initial water flux through the new membrane (J_{new}) were used to calculate the total flux decrement (FD_{total}) and the portions due to concentration polarization (FD_{CP}), chemically reversible fouling ($FD_{chem.rev}$) and chemically irreversible fouling

($FD_{chem.irrev}$) (Equation 2.9, Equation 2.10, Equation 2.11 and Equation 2.12), by an adaptation of the methodology presented by Capar *et al.* (2006).

$$FD_{total} = \frac{J_{new} - J_{effluent}}{J_{new}} \quad \text{Equation 2.9}$$

$$FD_{CP} = \frac{J_{fouled} - J_{effluent}}{J_{new}} \quad \text{Equation 2.10}$$

$$FD_{chem.rev} = \frac{J_{cleaned} - J_{fouled}}{J_{new}} \quad \text{Equation 2.11}$$

$$FD_{chem.irrev} = \frac{J_{new} - J_{cleaned}}{J_{new}} \quad \text{Equation 2.12}$$

2.2.4.7 Super saturation index calculation

To evaluate salt precipitation on membrane surface which results on scaling, the calcium sulfate supersaturation index on membrane surface (SI_m) was determined for different RR according to Equation 2.13 (HUANG and MA, 2012; SCHÄFER *et al.*, 2005). Calcium sulfate was chosen as representative of salt precipitation as it has low solubility and high concentration on effluent from gold mining (Table 2.1) presenting, therefore, great precipitation potential. It is noteworthy that in aqueous systems the hydrated specie $CaSO_4.2H_2O$ is more likely to be formed, however, the solubilities of the two salts is quite similar and therefore $CaSO_4$ can be taken as scaling model.

$$SI_m = \left(\frac{C_{Ca^{2+}m}\, C_{SO_4{}^{2-}m}}{K'_{sp}}\right)^{0.5} \quad \text{Equation 2.13}$$

where $C_{Ca^{2+}m}$ and $C_{SO4^{2-}m}$ are the molar concentrations of Ca^{2+} and SO_4^{2-} on membrane/solution interface and K'_{sp} is the solubility product constant for calcium sulfate based on molar concentration.

The supersaturation index is important since it can be related to the variation in Gibbs free energy (ΔG) through Equation 2.14. For SI_m>1, the ΔG is less than zero and the precipitation process is thermodynamically spontaneous.

$$\Delta G = -RTln(SI_m) \quad \text{Equation 2.14}$$

Molar concentrations on membrane surface (C_{im}) were determined by Equation 2.15 (SONG *et al.*, 2013).

$$C_{im} = e^{J_v/k_i}\left(C_{ib} - C_{ip}\right) + C_{ip} \qquad \text{Equation 2.15}$$

where C_{im}, C_{ib} and C_{ip} are the concentration of the specie i on membrane/solution interface, bulk solution and permeate, respectively; J_v is the permeate flux; and k_i the mass transfer constant of specie i, determined through Sherwood number (Sh) for a radial cross-flow membrane cell (Equation 2.17 and Equation 2.18) (DE *et al.*, 1995). The permeate (C_{ip}) and feed (C_{if}) concentrations were experimentally determined, whereas the bulk concentration (C_{ib}) were calculated for each permeate recovery rate (RR) according to Equation 2.16.

$$C_{ib} = \frac{C_{if} - RR\, C_{ip}}{1 - RR} \qquad \text{Equation 2.16}$$

$$Sh = \frac{k_i.h}{D_i} = 1.05\left(Re.Sc.\frac{h}{R_{cell}}\right)^{0.38} \qquad \text{Equation 2.17}$$

$$Sc = \frac{\upsilon}{D_i} \qquad \text{Equation 2.18}$$

where Re is the Reynolds number calculated through Equation 2.1; Sc is the Schmidt number; h is the half the thickness of the spacer (m); R_{cell} is the radius of stainless steel cell (m); υ is the kinematic (m²/s) viscosity; and Di is the diffusion coefficient of component i (m²/s) (which was found in Wang *et al.*, (2005)).

K'_{sp} could be then calculated through the solubility product constant based on activities (K_{sp}) as shown in Equation 2.19.

$$K_{sp} = a_{Ca^{2+}m}\, a_{SO_4{}^{2-}m} = K'_{sp}\, \gamma_{Ca^{2+}\mathrm{m}}\, \gamma_{SO_4{}^{2-}\mathrm{m}} \qquad \text{Equation 2.19}$$

where γ_{im} and a_{im} are the activity coefficient and the activity of specie i on membrane surface. In solutions with ionic strength lower than 0.5 M, the activity coefficient can be calculated by Davies equation (SAWYER *et al.*, 2003). Only calcium, magnesium, sulfate, chloride, and hydrogen were considered in calculating the ionic strength of the solution, as they account for approximately 80% of the total ionic strength.

2.2.4.8 Permeate reuse

The final permeate obtained under the best operating conditions (NF/RO membrane, feed pH, temperature and recovery rate) was characterized for its total dissolved solids, conductivity, arsenic, sulfate, chloride, calcium and magnesium concentrations. A sample of process water used by the gold mining company was also collected and analyzed. These results were compared and the industrial reuse possibility was discussed.

2.2.5 Analytical methods

Feed and permeate samples obtained for each test were analyzed for pH (Qualxtron pHmeter QX 1500); conductivity (Hanna conductivity meter HI 9835); arsenic (+5, +3 and total) concentration (DHAR *et al.*, 2004); sulfate, chloride, calcium and magnesium ions (ion chromatograph (IC) Dionex ICS-1000 equipped with AS-22 and ICS 12-A columns) and total solids (APPA, 2005). The initial effluent characterization also included analysis of suspended solids (APPA, 2005); color (spectrophotometer Hach DR 2800); turbidity (Hach turbidimeter 2100AN); the metals aluminum, cobalt, copper, manganese, nickel, potassium, sodium and zinc (inductively coupled plasma optical emission spectrometrometer (ICP-OES) Varian, 720-ES); dissolved organic carbon (TOC analyzer Shimadzu TOC-V CNP); and carbonate. Carbonate concentration was estimated based on dissolved inorganic carbon results from TOC analyzer. The methods from *Standard Methods for the Examination of Water and Wastewater* consulted were 2120 C (Color); 2130 B (Turbidity); 2510 B (Conductivity); 2540 B, D and E (Solids); 3120 B (ICP); 4110 C (IC); and 5310 D (TOC).

In this Chapter, the retention efficiencies of the UF and NF (E_{UF} and E_{NF}) were calculated according to Equation 2.20 and Equation 2.21.

$$E_{UF} = {(C_{raw\ effluent} - C_{pUF})}/{C_{raw\ effluent}}\ x100\% \qquad \text{Equation 2.20}$$

$$E_{NF} = {(C_{pUF} - C_{pNF})}/{C_{pUF}}\ x100\% \qquad \text{Equation 2.21}$$

where $C_{raw\ effluent}$, C_{pUF} and C_{pNF} are the conductivities, ion concentrations or arsenic concentrations in the raw effluent, before pH adjustment, UF permeate and NF permeate, respectively. As shown in Equation 2.20, the E_{UF} includes the removal efficiency of the precipitation caused by the pH adjustment together with the retention of UF itself.

2.3 RESULTS AND DISCUSSION

2.3.1 UF pretreatment

NF permeates fluxes with and without UF pretreatment were monitored for feed pH of 2.2 (original effluent pH) (Figure 2.2). Similar to the results obtained by Debik *et al.* (2010), it was observed that pretreatment reduced the membrane fouling rate. Flux reduction during 2 h of raw effluent nanofiltration was 22%, while over the same period of nanofiltration of UF permeate, reduction was only 7%. Fouling mitigation contributes to increased recovery rate, reduced energy demand, and increased membrane lifetime. Alzahrani *et al.* (2013) reported a case study of an oil refinery in India where UF was used as an RO pretreatment stage in an effluent treatment plant aiming at water reuse. This pretreatment increased membrane lifetime from 1–1.5 years to 4–5 years, in addition to allowing for a permeate recovery rate of 90%.

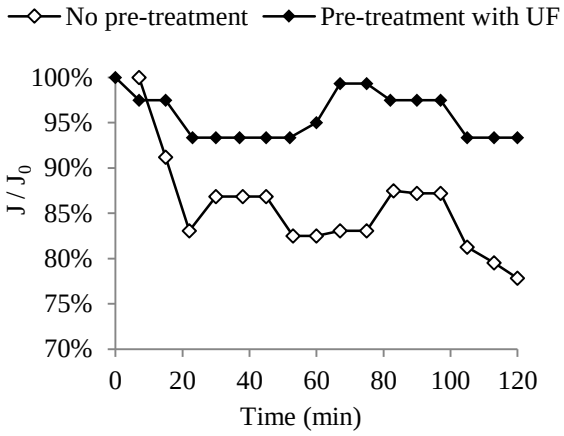

Figure 2.2 - Ratio of permeate flux (J) to initial permeate flux (J_0) as a function of time for effluent from gold mining NF, with and without UF pretreatment

Besides better productivity, UF pretreatment also led to higher rejection of total solids (TS). TS rejection was 96% (NF permeate with TS concentration of 380 mg/L) and 98% (NF permeate with TS concentration of 204 mg/L) for NF of the raw and pretreated effluent, respectively. This means that the amount of TS in the UF-NF system permeate was 46% lower than in the NF system.

2.3.2 Influence of feed pH on UF pretreatment

Table 2.4 shows the ratio of UF permeate flux at the end of the experiment (J_f, at recovery rate of 60%) to initial UF permeate flux (J_0), as well as UF permeate physico-chemical characteristics for each feed pH tested.

Table 2.4 - Ratio of final UF permeate flux to initial flux (J_f/J_0) and physic-chemical characteristics of raw effluent and UF permeates for different pH values

Feed pH	Raw effluent	2.2	3.5	4.2	5.0	5.5	6.0
J_f/J_0 [a]	n.a.	97%	85%	82%	70%	70%	60%
Conductivity (µS/cm)	5,821	4,550	3,330	3,260	3,250	3,310	3,300
Arsenic (mg/L)	275	251	247	230	211	204	203
Sulfate (mg/L)	2911	2785	2783	2931	2832	2871	2891
Chloride (mg/L)	70	52	48	64	50	61	56
Calcium (mg/L)	383	198	193	210	196	207	201
Magnesium (mg/L)	104	71	67	83	69	80	75

n.a. Not applicable

It can be noted that pH increase caused an increase in UF membrane fouling, as evidenced by lower J_f/J_0. This is mainly due to the precipitation of salts and metals at higher pH values, increasing feed concentration of suspended solids, and consequently increasing the concentration polarization phenomenon and the accumulation of solids on the membrane surface and pores (ABDESSEMED and NEZZAL, 2008; GHAFFOUR *et al.*, 2009).

Precipitation caused by pH increase reduces solution conductivity and ion concentration. Arsenic concentrations gradually decreased as pH increased. Since the solubility of arsenic acids is high (USA, 2007), this decrease is closely related to co-precipitation with other metals, such as iron, calcium, and aluminum (JIA *et al.*, 2012). There were no major changes in sulfate and chloride concentrations. Thus, despite causing fouling, increasing the pH after UF contributes to the reduction of permeate salts concentration and the improvement of NF feed quality.

2.3.3 Evaluation of several NF and RO membranes

The membranes used in this study are comprised of a thin selective layer of polyamide. Although the selective layer of all five membranes is formed by the same base polymer, its

complete formation is unknown and are likely to be very different (NGHIEM and HAWKES, 2007). Thus, membrane properties that affect retention capacity and fouling propensity differ from one membrane to another. Although the literature presents several studies evaluating different membranes applied to many industrial effluents (BALANNEC *et al.*, 2005; BELLONA *et al.*, 2012; CHANG *et al.*, 2014; RICHARDS *et al.*, 2010), effluent composition and its specific physico-chemical properties directly influence treatment performance and the results obtained for a given system cannot be simply replicated to another. Thus, membrane evaluation for each given application is required.

The resistance of virgin RO membranes (Table 2.5) is much higher than those of NF membranes, and this is consistent with the dense polymeric structure of the first (TU *et al.*, 2011). That makes permeate flux through RO membranes to be very low, which is, about 7 to 12 times lower than permeate flux through NF membranes. Fouling resistance shows the trend of different membranes to undergo adsorption, pore blocking or solid deposition over membrane surface in contact with the effluent (MATTARAJ *et al.*, 2011). Thus, fouling formation proneness may be related to membrane characteristics such as pore size, hydrophobicity, and surface charge. It can be seen that RO membranes, especially TFC-HR membranes, have prompter interaction with the effluent, and more intense fouling. Conversely, despite the MPF34 membrane have shown one of the lowest fouling formation; NF270 membrane had the highest permeate flux, nearly 60% higher than NF90 and MPF34 membranes.

Table 2.5 - Membranes performance to treat the effluent from gold mining regarding intrinsic membrane resistance, fouling resistance and final permeate flux

Membrane	Intrinsic membrane resistance ($x10^{12}$/m)	Fouling resistance ($x10^{12}$/m)	Fouling in relation to membrane resistance	Final permeate flux (L/h.m²)
TFC-HR	451.4	93.0	21%	7
BW30	470.8	82.5	18%	7
MPF34	60.8	5.4	9%	59
NF90	64.9	10.4	16%	54
NF270	33.0	11.4	34%	89

Table 2.6 shows the results of pollutant retention efficiency obtained for the five membranes tested. Initially, it must be highlighted the high retention efficiencies by both NF and RO

membranes. The high sulfate concentration on the effluent from gold mining is considered the major hindrance to water reuse. Sulfate can precipitate with metal cations causing fouling on equipments and pipes. It can be seen that permeates obtained for all membranes had low sulfate concentration (< 200 mg/L).

Table 2.6 - Results for physico-chemical parameters of the raw effluent and permeates obtained with several membranes and their respective retention efficiencies

Membrane /Sample	Conductivity (µS/cm)	Total solids (mg/L)	Arsenic (mg/L)	Sulfate (mg/L)	Chloride (mg/L)
Raw effluent	5.393	4.342	340	1393	48.7
TFC-HR	244 (95%)	114 (97%)	83 (75%)	8 (99%)	2 (97%)
BW30	555 (90%)	460 (89%)	197 (42%)	55 (96%)	11 (78%)
MPF34	2.715 (50%)	864 (80%)	231 (32%)	182 (87%)	18 (63%)
NF90	314 (94%)	126 (97%)	109 (68%)	23 (98%)	8 (84%)
NF270	1.843 (66%)	710 (84%)	212 (38%)	63 (95%)	24 (51%)

Note: Values in brackets are the retention efficiencies

Among the parameters evaluated, the only one in which the retention was poor was the arsenic. However, it is important to point out that, even though this element may be very hazardous to human health and environment, it has no adverse effect on the industrial process. The main objective of this treatment system is to generate industrial reuse water, which can be used in gold processing for uses that do not involve direct contact with the operators. Therefore, as the treated effluent will not be discharged into water bodies, the discharge standard for arsenic does not need to be met. Moreover, arsenic is not associated with problems of corrosion or fouling and may even act as corrosion inhibitor zero-valent iron (TRISZCZ *et al.*, 2009). Thus, obtaining a final permeate with an arsenic content of 230 mg/L is not critical. The continuous reuse of this effluent would lead to an arsenic buildup in the system, and when steady state was reached the arsenic concentrations of the raw effluent and treated effluent (reuse water) would be 780 and 530 mg/L, respectively (considering the worst retention efficiency of 32%, retention efficiency independent of feed concentrations, and full replacement of process water with the treated effluent with no new water addition).

The reverse osmosis membrane TFC-HR showed the highest pollutant retention efficiency among the tested membranes. According to Fujioka *et al.* (FUJIOKA *et al.,* 2012), the TFC-HR is a low pressure RO membrane typically applied to effluent treatment and reuse processes due to its high efficiency. On the other hand, the second RO membrane studied (BW30) showed lower pollutant retention efficiency. These results are consistent with the findings of Balannec

and coauthors (2005) who evaluated eight different membranes to treat a synthetic dairy effluent.

Among the NF membranes, NF90 showed the best results for the parameters evaluated, and was even comparable to those obtained using the TFC-HR membrane. NF90 and RO membranes have very similar characteristics (KRIEG *et al.*, 2005), including similar molecular weight cutoff (Table 2.2), and therefore NF90 may present high solids retention efficiency, especially for an effluent which the major contaminants are at least bivalent ions (sulfate, calcium, magnesium, etc.), such as the one here studied.

According to Wang and Tang (2011), NF270 membrane has higher water permeability, lower salt retention efficiency, and a surface smoother than NF90 membrane. Additionally, Nghiem and Hawkes (2007) stated that NF270 membrane pores are larger, which may explain its lower performance. MPF34 membrane showed the lowest retention capacity for all the parameters analyzed. By assessing different NF membranes used for sulfate retention in brine, Bargeman *et al.* (2009) also observed lower retention capacity for MPF34 in comparison to NF270. Although the molecular weight cutoff of MPF34 membrane is lower than that of NF270 (Table 2.2), other parameters such as surface charge and hydrophobicity may affect the ions retention capacity in aqueous solution, and may account for the lower retention efficiency observed. Furthermore, the pore size of NF membranes is affected by the ionic strength of the medium (HONG and ELIMELECH, 1997).

The membrane area required for an application is inversely proportional to permeate flux, and the cost of NF or RO systems depends on the membrane area required. Therefore, even though RO systems have shown good pollutant retention efficiency, their use proved to be cost-prohibitive for the application studied. The membrane area required by RO systems in this application is significantly superior, which makes its cost substantially higher. An alternative to avoid the increase in membrane area would be to operate the system at higher pressure. However, to achieve the same permeate flux of NF membranes keeping the same membrane area, the operating pressure of RO ought to be above 70 bar, which is also not feasible due to excessive power consumption. Furthermore, as can be seen in Table 2.6, NF90 retention efficiencies were similar to those of RO membranes, besides allowing for a much higher permeate flux. As a result, NF90 membrane was selected as it showed the highest potentiality for the studied application.

2.3.4 Influence of feed pH on NF fouling

Figure 2.3 shows the ratio of the NF permeate flux to the initial permeate flux (J/J_0) for the NF90 applied at different effluent pHs.

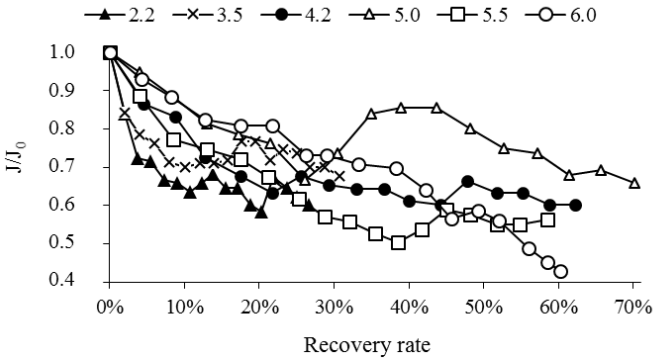

Figure 2.3 - Ratio of effluent permeate flux (J) to initial permeate flux (J_0) as a function of recovery rate and feed pH

NF at original effluent pH (pH 2.2) presented the highest fouling, as can be observed by the lower values of J/J_0 and the lower recovery rate obtained after 4-hour filtration. At pH 2.2, the membrane had a high positive surface charge, leading to higher anion adsorption (especially of sulfate) and causing fouling. Moreover, as anion and cation concentrations were higher at this pH value (UF permeate, Table 2.4), the effects of concentration polarization, fouling and reduction of net driving pressure caused by increment in concentrate osmotic pressure were more expressive.

On the other hand, with the same filtration time, the highest permeate RR (70%) was obtained at pH 5.0. Despite this high RR, which consequently increased concentrate salt concentration, flux decrease was only 34% over 4-hour filtration. Nanofiltration at pH 4.2 also exhibited good performance, with a total permeate flux reduction of 40%.

In addition to causing salt precipitation and changing the feed quality of NF, pH adjustment can also protonate/deprotonate membrane functional groups, change membrane surface charge, and modify its adsorption capacity and the strength attraction/repulsion of cations and anions (CHILDRESS and ELIMELECH, 2000). Thus, to better understand the phenomena involved in nanofiltration, zeta potential was evaluated. Membrane zeta potential was measured using an electrolyte solution (standard 10 mM KCl solution) and synthetic effluent (Table 2.3). Figure

2.4 presents the results obtained. The curve profile is indicative of an amphoteric surface, which, for polyamide membranes, is related to the ionizable functional groups carboxyl and amine (TEIXEIRA *et al.*, 2005).

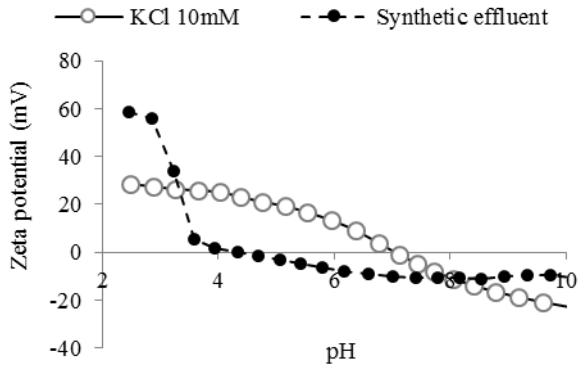

Figure 2.4 - NF90 membrane zeta potential with electrolyte solution and synthetic effluent

As can be noted, the membrane behaved differently when in contact with the two solutions. While exposed to the KCl solution, its isoelectric point was approximately at pH 7.0. This value is higher than others reported in literature (BELLONA and DREWES, 2005; LE GOUELLEC *et al.*, 2007; TU *et al.*, 2011), possibly due to commercial membrane surface heterogeneity or differences in equipment and experimental conditions (background electrolyte solution, pressure, stabilization time, pH change rate, effect of membrane pre-cleaning, etc.). On the other hand, when exposed to synthetic effluent, the isoelectric point was approximately at pH 4.3.

Higher concentrations of cations (25 mM of total cations in synthetic effluent vs. 10 mM in the KCl solution) may cause zeta potential to be higher at low pH values in the case of the synthetic effluent. Cations interact with membrane polymeric material, causing an increase in positive charge at the shear plane region (VAN GESTEL *et al.*, 2002).

At pH values of 8 and above, membrane zeta potential was lower when measured with the electrolyte solution than when measured with synthetic effluent. This can be explained by the lower hydrated radius of the Cl^- ion (anion present in KCl electrolyte solution) compared to the SO_4^{2-} ion (main anion of the synthetic effluent) (MADAENI and KAZEMI, 2008), which allows it to get closer to the membrane surface (CHILDRESS and ELIMELECH, 2000). Moreover, Teixeira *et al.* (2005) noted that the formation of complexes between cations Ca^{2+}

and Mg^{2+} and negatively charged functional groups on membrane surfaces serves to lessen membrane negative charge.

Filtration near the isoelectric point leads to higher permeate flux due to several factors: i) increase in pore size due to conformational changes of the cross-linked membrane polymer structure; ii) increase in process driving force due to reduction of the osmotic pressure at the membrane surface; and iii) decrease of electroviscous effects, thus increasing apparent permeability (CHILDRESS and ELIMELECH, 2000). Both pH 4.2 and 5.0 are close to the membrane isoelectric point (4.3), explaining the higher fluxes. It is possible that small membrane negative surface charge at pH 5.0 served to repel sulfate anions without strongly attracting cations, therefore causing less fouling than at pH 4.2.

Nanofiltration at feed pH > 5.0 led to superior performance than that obtained at lower pH values (pH 2.2 and 3.5); however, permeate fluxes were lower than those obtained with feed pH values near the isoelectric point. Within this range of pH values, the membrane surface was negatively charged. It could thus form complexes with Ca^{2+}, Mg^{2+}, and other cations present in high concentrations in the gold mining effluent, hence leading to flux reduction (CHILDRESS and ELIMELECH, 1996; TEIXEIRA *et al.*, 2005).

To ensure the statistical significance of flux differences as a function of feed pH, the Friedman test for nonparametric paired samples was performed for J/J_0 data using Matlab R2008a software (The MathWorks, USA) at a significance level of 95%. A p value of 2×10^{-6} (<0.05) was obtained, indicating that feed pH affects permeate fluxes. A multiple comparison test was then used to determine which groups of feed pH were significantly different. Results showed that process performance at pH 5.0 differed from that at pH values of 2.2, 4.2, and 5.5 ($p < 0.05$).

2.3.5 Influence of feed pH on NF retention

Table 2.7 shows results for conductivity, sulfate, chloride, arsenic, calcium, and magnesium of NF permeate at different feed pH values, as well as retention efficiencies. Retention efficiencies were calculated based on the NF feed concentrations shown in Table 2.4 (UF permeates at each pH value).

Table 2.7 - NF90 membrane pollutant retention efficiencies for feed with different pH values

pH	Concentration (Retention (%))					
	Conductivity (µS/cm)	Total arsenic (mg/L)	Sulfate (mg/L)	Chloride (mg/L)	Calcium (mg/L)	Magnesium (mg/L)
2.2	382 (92)	116 (55)	18 (99)	10 (81)	22 (89)	2 (97)
3.5	186 (94)	116 (51)	18 (99)	7 (85)	13 (93)	1 (99)
4.2	624 (81)	152 (32)	118 (96)	19 (71)	25 (88)	6 (92)
5.0	274 (92)	126 (39)	38 (99)	9 (81)	6 (97)	2 (97)
5.5	372 (89)	149 (24)	63 (98)	13 (79)	6 (97)	2 (97)
6.0	401 (88)	131 (26)	63 (98)	10 (81)	8 (96)	3 (96)

NF membranes can retain pollutants by steric hindrance and electrostatic repulsion (CHILDRESS and ELIMELECH, 2000; NGUYEN *et al.*, 2009). At isoelectric pH, the membrane surface has a neutral charge. As a result, only the steric hindrance mechanism will prevent solute permeation. This explains the lower retention efficiency of all monitored parameters at feed pH of 4.2.

High sulfate retention efficiencies can be explained by the small ratio between NF90 membrane pore size and the sulfate hydrated radius (Table 2.8), and also by its divalent charge (CURCIO *et al.*, 2010). In contrast, chloride had the lowest retention efficiency due to its smaller hydrated radius and monovalent charge.

Table 2.8 - Hydrated radius of effluent ions

Ions	Cl^-	SO_4^{2-}	Ca^{2+}	Mg^{2+}	H_3AsO_3	$H_2AsO_3^-$	$H_2AsO_4^-$	$HAsO_4^{2-}$
Hydrated radius (nm) [a]	0.12 [b,c]	0.23 [b,c]	0.27 [c]	0.35 [b]	0.24 [c]	0.24 [c]	0.59 [c]	0.78 [c]

[a] Hydrated radius determined according to Stokes equation: $r_s = k.T/(6.\pi.\eta_0.D_i)$, where k is the Boltzmann's constant, T is temperature, η_0 is viscosity, and Di is solute diffusivity

[b] Reference: PAGES *et al.*, 2013

[c] Reference: NGUYEN *et al.*, 2009

Besides steric hindrance related to the size of hydrated radius, charge effects also influence chlorine and sulfate retention. According to Donnan's theory, charged membranes will more strongly repel high-valence co-ions (CURCIO *et al.*, 2010), explaining the lower Cl^- retention efficiency compared to SO_4^{2-} at pH values > 4.2. When the membrane surface is positively charged (i.e., pH < 4.3), two opposite effects may occur. On the one hand, the smaller Cl^- charge

can increase its retention efficiency, since the membrane preferably interacts with and permeates high-valence counter-ions (CURCIO *et al.*, 2010; NGUYEN *et al.*, 2009). On the other hand, retention of co-ions is determined by salt rejection (PEETERS *et al.*, 1999), which means that the high retention of cations requires also high retention of anions to ensure electro neutrality. Because it has higher charge, sulfate acts more efficiently in this balance and there is preferential permeation of chloride (KRIEG *et al.*, 2005). In this study, the electro neutrality effect seems to be stronger than Donnan effect.

Based on study of synthetic effluents, Nguyen *et al.* (2009) proposed that three mechanisms govern arsenic retention by NF membranes: size exclusion, charge exclusion, and ionic preferential permeation. At original feed pH (2.2), As(V) occurs in neutral (H_3AsO_4) and mono-protonated forms ($H_2AsO_4^-$), while As(III) occurs in its neutral form (H_3AsO_3). At this pH value, the NF90 membrane has a highly positive surface charge, which repels cations and attracts anions, especially those with valence of 2 or higher. Thus, if the sole retention mechanism were Donnan's effect, sulfate would permeate preferentially compared to ionic arsenic; this was, however, not the case. Steric hindrance is also unable to explain these results, since the hydrated radius of arsenic compounds is similar or greater than the sulfate hydrated radius. The low arsenic retention observed in this study is thus believed to be caused by the preferential permeation phenomenon. Similar to what was observed with chloride, high retention of metallic cations provided higher sulfate retention in relation to arsenic, guaranteeing effective charge balance on the concentrate.

Moreover, according to Wang *et al.* (2009) the efficiency of arsenic retention by the NF membrane decreases when feed concentrations of arsenic, sulfate, and calcium is high. Furthermore, rejection of As(III) is much lower than of As(V) (<10% vs. 90–100%, according to Xia *et al.* (2007). As effluent contains high concentrations of sulfate, calcium, and arsenic (in both forms), low arsenic retention is also justified.

When pH increased to 4.2, arsenic retention declined. This can be explained by isoelectric point proximity and the consequent decrease in the electrostatic repulsion phenomenon. At pH 5.0, arsenic retention efficiency increased to approximately 40%, with membrane zeta potential at this point of around -3.3 mV. The negative charge increased anion retention capacity, such as that of $H_2AsO_4^-$. Additionally, permeate flux increased at this pH value, leading to dilution of permeate ions and increase, as a whole, of solute retention efficiency.

Conductivity retention efficiency was high (≥87%) under all test conditions except at pH 4.2. After conductivity retention decreased near the isoelectric point, it increased considerably and then tended to decline with pH increase. Within this pH range, membrane zeta potential was progressively negative, and electrostatic attraction and cation permeation progressively increased. As previously discussed, this attraction also increases fouling tendencies at pH values >5.0.

It is clear that the NF retention mechanism is much more complex when treating real effluent, which is comprised of a high number of components, than when applied to single or multi-element solutions. When the NF90 membrane is used to treat gold mining effluent, the retention of high-valence counter-ions to balance retention of co-ions seemed to be an important mechanism.

Based on consideration of permeate flux decay and pollutant retention efficiency, an effluent pH value of 5.0 was selected as most appropriate for the system.

2.3.6 Influence of temperature on NF fouling

Figure 2.5 shows the ratio of NF permeate flux to initial permeate flux (J/J_0) for different feed temperature. One may see that flux decay is bigger for lower temperatures. The effect of increased temperature is increased mass transfer of both water and solutes, with this being according to the Arrhenius relationship (NILSSON *et al.*, 2008). In that way, increased temperature lowered concentration polarization effect on membrane surface, reducing the flux decay and fouling rate.

Operating temperature influences the capacity of the NF membrane to retain sulfate, calcium, magnesium and arsenic (Figure 2.6). The increase in temperature causes thermal expansion of the polymer, leading to changes in pore diameter, thickness, and porosity, consequently reducing solute retention. Dang *et al.* (2014) observed that an increase in feed temperature from 20 °C to 40 °C led to an increase in effective pore radius from 0.39 nm to 0.44 nm.

While retention of neutral solutes is given only by steric hindrance, charged solutes also rely on electrostatic repulsion. Some authors claim that the effect of temperature is more relevant to changes in retention of nonionic solutes (DANG *et al.*, 2014). However, in this work, there was a significant effect of temperature on retention of sulfate ions and especially calcium and

magnesium. This may be related to the vicinity of operating pH (5.0) to the isoelectric point of the membrane (4.3), causing steric hindrance effects to be relevant even to ionic solutes (NILSSON *et al.*, 2008). The greatest influence of temperature on arsenic retention (50% decrease in membrane retention efficiency) was due to the fact that some arsenic is present in the neutral forms H_3AsO_4 and H_3AsO_3.

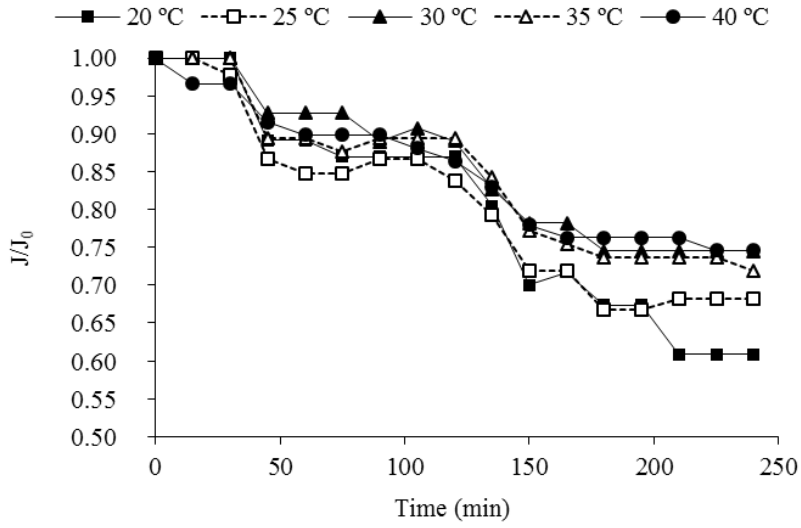

Figure 2.5 - Effect of temperature on J/J_0 for nanofiltration of mining effluent.

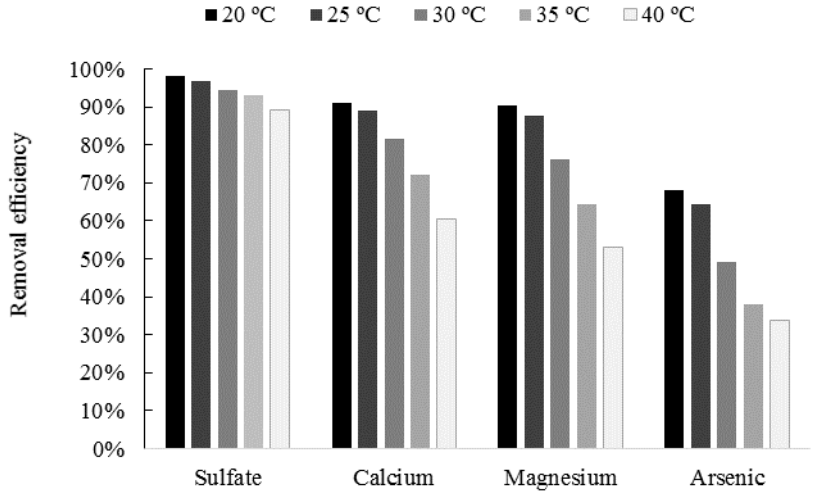

Figure 2.6 - Effect of temperature on efficiency of NF retention of sulfate, calcium, magnesium and arsenic ions

Thus, despite showing less concentration polarization and fouling, nanofiltration at high temperatures caused loss of permeate quality. Near ambient temperatures (20–25 °C) should therefore be used.

2.3.7 NF permeate recovery rate

Increasing the permeate recovery rate (RR) induces an increase in concentrate salt concentration, leading to membrane fouling, as well in concentrate osmotic pressure. Thus, for a constant operating pressure, increasing the RR leads to a reduction in permeate flux. In this study, this decrement occurred in an almost linear shape, that is, $R^2 = 0.947$ linear fit, with a reduction of nearly 0.6 L/h.m² for each 1% increase in the RR (Figure 2.7).

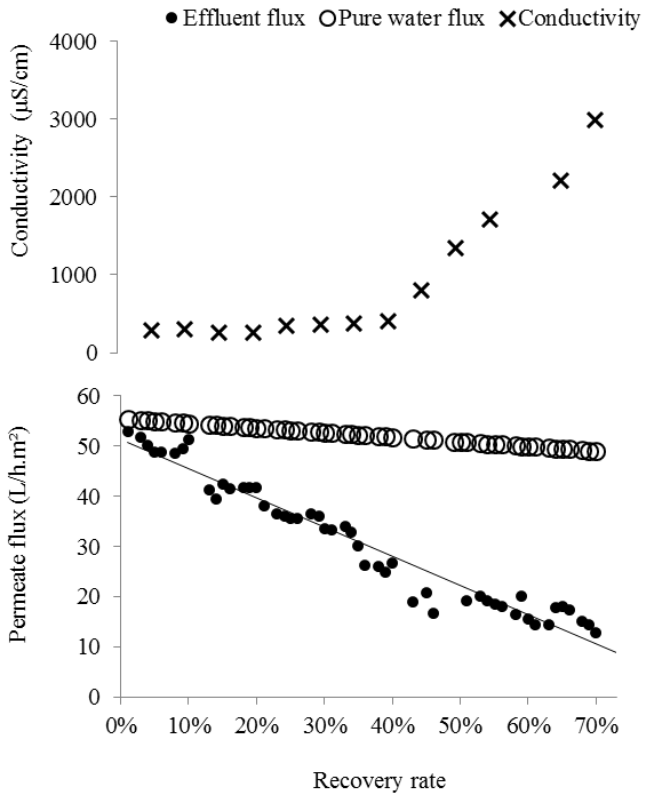

Figure 2.7 – Permeate flux, theoretical pure water flux at instant effective pressure and conductivity as a function of the recovery rate

This decay is partly explained by the reduction in the effective pressure for permeation ($P-\sigma\Delta\pi$). In Figure 2.7, the pure water flux was calculated considering the membrane permeability constant and equal to the one measured at the beginning of the experiment. The pure water flux

reduction is thus only attributed to decrease of effective pressure. However, it can be seen that the effluent flux decay rate is more pronounced, which indicates that fouling is also occurring.

Moreover, it has been noticed that permeate quality remains almost constant up to a RR of 40%. From this point onwards there is a significant increase in permeate conductivity. The permeate conductivity with 5% of RR was 281 µS/cm; this value slowly increased to 398 µS/cm when RR reached 40%. However, for RR above 45%, permeate conductivity reached values higher than 1340 µS/cm. Using a synthetic solution of $MgSO_4$, Bi *et al.* (2014) found that the degree of concentration polarization on NF membranes increased from ~1.00 to 1.45 while RR increased from 20% to 70%, which was found to cause a decrease in its observed retention efficiency (pollutants concentration on permeate in relation to the ones on concentrate solution). However, no significant change was observed in its real efficiency, that is, permeate pollutants concentration compared to concentration on membrane surface. Additionally, the authors stated that concentration polarization degree should be kept below 1.2 in actual applications to be technical and economic feasible. According to Luo and Wang (2013), higher salt concentration also increased bulk viscosity, which decreased solute back-diffusion away from membrane, thus inducing more concentration polarization and passage of solutes to permeate stream.

Table 2.9 presents the percentage of permeate flux decrement during filtration due to concentration polarization, chemically reversible fouling and chemically irreversible fouling. One may notice that when the NF90 membrane is used for filtration of effluent from gold mining with RR of 70%, there will be a 77% decrease in permeate flux in comparison to initial water flux through clean membrane. From these 77%, 30% are due to concentration polarization, 15% to chemically reversible fouling and 32% to chemically irreversible fouling. The high percentage attributed to concentration polarization may be associated with the high RR reached (70%), and it may be controlled in milder operating conditions (lower RR). The percentage of flux decrement due to chemically reversible fouling is related to the formation of loose precipitates over membrane surface, or weak interaction between effluent components and membrane polymeric structure. Finally, chemically irreversible fouling is caused by sticky precipitates that cannot be easily removed by chemical cleanup. Thus, the RR must be kept low in order to: prevent solute supersaturation on the concentrate; reduce the adhesion risk of sticky precipitates that may reduce membrane lifetime; and prevent loose precipitates adhesion which would require more frequent cleaning procedures (NANDA *et al.*, 2010).

Table 2.9 - Percentage of permeate flux decrease during filtration due to concentration polarization and reversible and irreversible fouling formation

Flux decrement	
Concentration polarization	30%
Reversible fouling formation	15%
Irreversible fouling formation	32%
Total	77%

The supersaturation ratio of $CaSO_4$ on membrane surface (SI_m) for different values of RR are presented on Table 2.10. As RR increases, salt concentration on concentrate and concentration polarization process intensify, consequently increasing the SI_m. Its increment was higher when RR rose from 50 to 60% and then from 60 to 70%, when it increased by 18-19%. Moreover, SI_m was higher than 1.0 even at feed solution (RR = 0%). However, although precipitation may be expected when SI_m >1, a significantly higher value of supersaturation ratio must be exceeded to result in scaling, due to kinetics and metastability effects (SCHÄFER *et al.*, 2005). According to Dydo *et al.* (2004), scaling can be prevented if SI_{CaSO_4} < 1.62 to 2.02, which is the case for the studied effluent at RR between ~10 and ~50%. It is noteworthy that the SI calculation was based on the diffusivity coefficient of ions in diluted single-component solutions. As ion mobility in real effluent is smaller, the actual mass transfer coefficient can be lower, and the SI_m, greater than the ones calculated.

Table 2.10 – Supersaturation index of $CaSO_4$ on membrane surface at different RR values

RR	0 %	10%	20%	30%	40%	50%	60%	70%
SI_m	1.32	1.68	1.75	1.84	1.99	2.10	2.49	2.94

A RR of 40% was recommended for this process as operation at higher RR favors the development of both, chemically reversible and irreversible fouling (Table 2.9). Additionally, it was observed that permeate flux decrement was almost constant in relation to RR increase however, a significant reduction in permeate quality was observed at RR greater than 40%. Besides that, values of SI_m show that the risk of scaling from this point onward is high.

It is noteworthy that higher water recovery may be achieved with multiple NF steps, particularly if intermediate precipitation steps are applied. In this approach, a primary NF/RO step recovers water up to a SI_m below the threshold of membrane mineral scaling. Mineral scale precursors

are subsequently removed from the concentrate via precipitation and solid-liquid separation techniques. That lowers the concentrate mineral scaling propensity and thereby enables additional water recovery in a secondary NF/RO step (GABELICH *et al.*, 2011; RAHARDIANTO *et al.*, 2007; RAHARDIANTO *et al.*, 2010). Results regarding intermediate precipitation of gold mining effluent can be found in Chapter 5.

2.3.8 Permeate reuse

To verify permeate applicability for industrial reuse, the physico-chemical properties of the treated effluent obtained with optimal operating conditions (NF90 membrane, at feed pH 5.0, ambient temperature, and RR of 40%) were compared with process water quality used in the gold mining company (Table 2.11). With the exception of arsenic, all parameters showed high retention efficiencies and proved the proposed treatment effectiveness. The permeate met water reuse quality, as its pollutants concentration for all monitored parameters were smaller than those of process water. Arsenic was the sole pollutant to show a higher concentration in the permeate than in process water. However, as already discussed, this metal has no fouling and/or corrosion potential and thus does not qualify as a critical parameter.

Table 2.11 – Quality parameters for the final treated gold mining effluent and cooling water and treatment retention efficiencies

Parameter	Treated effluent	Retention efficiency	Process water
Total dissolved solids (mg/L)	146	97%	1374
Conductivity (μS/cm)	398	91%	710
Chloride (mg/L)	15	89%	20
Sulfate (mg/L)	168	94%	304
Calcium (mg/L)	24	94%	104
Magnesium (mg/L)	6	95%	11
Arsenic (mg/L)	116	58%	<2

2.4 CONCLUSION

In this chapter it may be concluded that:

The use of UF as pretreatment prior to NF increased solid retention efficiency and improved process performance, reducing permeate flux decay. Moreover, increasing effluent pH prior to

UF led to metal precipitation, increasing the concentration of effluent suspended solids. This improved permeate quality, but considerably reduced UF permeate flux.

In an effluent which the major contaminants are at least bivalent ions, such as this effluent from gold mining with high concentration of sulfate, calcium and magnesium, effluent treatment with NF membranes was more effective than with RO membranes, because they allow permeate flux 7 to 12 times higher and compatible retention efficiencies. In this study, NF90 showed the best performance.

With regard to the NF90 membrane, it was noted that there were differences in membrane surface zeta potential with standard KCl solution (electrolyte solution) and synthetic effluent (solution with salt concentration similar to gold mining effluent). This proves that, to understand retention mechanisms and to accurately model membrane processes, analysis of surface charge must be carried out using solutions similar to the solution of interest.

NF retention mechanisms are more complex when treating real effluent,such as the mining effluent studied which includes several components, than when treating mono-or bi-component solutions. We concluded that, when using the NF90 membrane to treat gold mining effluent, the retention of high-valence counter-ions to balance the charge of retained co-ions charge together with steric hindrance were the strongest retention mechanisms.

Feed pH of 5.0 was chosen as ideal for UF and NF treatment of gold mining effluent, since it provides benefits in terms of lower fouling potential and higher pollutant retention efficiency.

The increase in temperature leads to reduction of concentration polarization and fouling due to increased mass transfer of solutes; however, the increase in pore size leads to significant reduction in efficiency of retention of sulfate, calcium, magnesium and arsenic.

Permeate flux decreased linearly as permeate recovery rate increased. Additionally, there was a significant increase in conductivity for RR above 40%. Consequently, RR of 40% was selected as the ideal for this process.

3 CHAPTER

NANOFILTRATION APPLIED IN GOLD MINING EFFLUENT TREATMENT: EVALUATION OF CHEMICAL CLEANING AND MEMBRANE STABILITY

3.1 INTRODUCTION

Nanofiltration (NF) is a separation process that employs membranes with a typical pore size of 1 nm, which corresponds to a molecular weight cutoff (MWCO) of 300–500 Da. NF presents low rejection of monovalent ions, high rejection of divalent ions, and higher flux compared to reverse osmosis (RO) membranes. These properties have allowed NF to be used in many niche applications, especially in the treatment of water and wastewater (MOHAMMAD *et al.*, 2015).

Several authors have studied NF for the treatment of mining effluent and have obtained promising results (AL-ZOUBI *et al.*, 2010 b; AL-ZOUBI and AL-THYABAT, 2012; RICCI *et al.*, 2015; SIERRA *et al.*, 2013). In addition to the cited studies, NF has proved to be a favorable treatment of effluent from the gold mining industry, specifically, from sulfuric acid production plant and calcined dam. As reported in Chapter 2, the NF of the combined streams of these effluents allowed for generation of high quality treated effluent. The permeate met water reuse quality standards, as its concentrations of dissolved solids, sulfate, chlorine, calcium, and magnesium as well as its conductivity were smaller than those of the process water. Despite the excellent performance, membrane fouling management is essential to ensure consistent separation performance with minimal cleaning and membrane replacement.

Fouling has been defined by the International Union of Pure and Applied Chemistry (IUPAC) as "a process resulting in loss of performance of a membrane due to the deposition of suspended or dissolved substances on its external surfaces, at its pore openings or within pores" (MCNAUGHT, 1997). Fouling is a major limitation of NF and is related to operational conditions and to feed stream composition (BEYER *et al.*, 2010). Typically, four categories of potential fouling agents can be found in wastewater: microorganisms, organic compounds, inorganic species, and colloids and particulate matter (MADAENI and SAMIEIRAD, 2010; SOHRABI *et al.*, 2011). Common fouling mechanisms include the following: pore plugging and external pore blocking, resulting from deposition of particles and colloids; precipitation of dissolved materials on membrane pores and surfaces; build-up of a cake/gel-like layer on the upstream face of a membrane; and absorption or adsorption, which is generally the biological mode of fouling (AL-AMOUDI and LOVITT, 2007; GWON *et al.*, 2003; SOHRABI *et al.*, 2011). The main consequences of fouling include flux decline, permeate quality deterioration, and an energy consumption increase. Accordingly, fouling control is essential for increasing membrane operating lifetime and thus reducing process costs (ARNAL *et al.*, 2011).

Feed pre-treatment, membrane selection, module design, operation mode, and membrane cleaning are the main membrane fouling control strategies (SCHÄFER *et al.,* 2005). Membrane cleaning methods are classified into physical, chemical, and physico-chemical. Chemical cleaning is the most common method, especially in NF and RO systems. Chemical cleaning is used to remove fouling by means of specific chemical agents, which typically include acids, bases, chelating agents, and/or surfactants (MO *et al.,* 2010; WEI *et al.,* 2010). The chemical cleaning agent most suitable for a given application depends on several factors, such as feed composition, fouling composition, and membrane surface properties (MADAENI and SAMIEIRAD, 2010). The cleaning agent may act by different mechanisms, which include dissolution of precipitates; morphological changes in fouling layers, e.g., swelling and compaction; change in a foulant's surface chemistry; and chemical reactions such as saponification, chelation, and hydrolysis, among others (MADAENI and SAMIEIRAD, 2010).

The optimal selection of the cleaning agent depends mainly on the membrane material and type of foulant. The ideal cleaning agent should remove the deposited material without damaging the membrane, but often prolonged exposure can result in morphological, structural, and superficial changes, reducing the ability of the membrane to reject solutes. These changes include variations in hydrophobicity, surface charge, and pore size (AHMED, 2013; AL-AMOUDI *et al.,* 2007; BEYER *et al.,* 2010; SOHRABI *et al.,* 2011); ridding the pores of the material that were left from the membrane preparation process (MADAENI and MANSOURPANAH, 2004); surface modifications observed via scanning electron microscopy (SOHRABI *et al.,* 2011); adsorption of cleaning agents within the membrane surface; or degradation of the active layer polymer (AHMED, 2013).

The lifetime of a membrane module is related to the characteristics of the effluent, fouling rate, operating conditions, and hydraulic cleaning cycle (GWON *et al.,* 2003). During the lifetime of NF membranes, a gradual degradation does occur. In some cases, perceptible losses of salt rejection by the membrane can occur due to factors such as surface defects, damage from abrasion, and chemical attacks usually caused by products used in chemical cleaning processes (DA SILVA *et al.,* 2012).

In this context, the objectives of this Chapter were (1) to determine the optimal conditions of chemical cleaning of an NF membrane (NF90) employed in the treatment of gold mining

effluent, and (2) to investigate the effects of continuous exposure to mining effluent and a cleaning agent on NF membrane properties.

Initial cleaning tests were carried out with different chemical agents, and after selection of the most efficient agent, the optimal cleaning procedure, with or without recirculation, and time were determined. Next, membrane characteristics were evaluated for effects from continuous exposure to effluent and to the selected cleaning agent. To perform the evaluation, a set of NF90 membranes was immersed in the effluent and another set immersed in the effluent and periodically subjected to the cleaning process. The exposure period was 285 days and the cleaning processes were conducted monthly. The effects of exposure to the effluent and cleaning agent on the performance of NF90 with regard to rejection of glucose and magnesium sulfate as well as the hydraulic permeability were assessed. In addition, changes in hydrophobicity, effective pore radius, and chemical and morphological characteristics were also evaluated.

3.2 MATERIALS AND METHODS

3.2.1 Effluents from gold mining and description of the effluent treatment process

Two effluents from a gold mining, i.e., the effluent from the sulfuric acid production plant and the water from the calcined dam, were mixed at a 1:1 ratio and, in this study, this mixture is referred to as “effluent from gold mining”. Further information on the mining production process, the collection points of the effluent and their characterization can be found in Chapter 2 (Section 2.2.1).

As discussed in Chapter 2, the treatment process proposed for the effluent consisted of a pH adjustment to 5.0 with a NaOH solution, ultrafiltration, and nanofiltration (Figure 3.1). Ultrafiltration (UF) was performed with ZeeWeed membrane and NF, with NF90. The bench-scale experimental setup description can be found in Chapter 2 (Section 2.2.2).

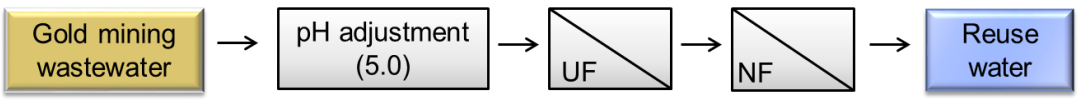

Figure 3.1 – Scheme of the treatment system proposed for gold mining effluent

3.2.2 Fouling evaluation

3.2.2.1 Experimental procedure

To investigate NF fouling, a virgin membrane was cleaned by soaking in citric acid solution at pH 2.5 followed by 0.1% NaOH solution in an ultrasound bath for 20 min prior to use. After that, the membrane was flushed with distilled water. It was then inserted into the NF cell and compacted with distilled water at 10 bar. After flux stabilization, water permeability was measured by monitoring the stabilized water permeate flux at pressures of 10.0, 7.5, 5.0, and 2.5 bar. Water temperature was also monitored and permeate flux was normalized to 25°C by means of a correction factor calculated as water viscosity at the temperature of permeation divided by water viscosity at 25°C (DRAK *et al.*, 2000). The variation of temperature during nanofiltration was significantly lower than that of tests shown in Chapter 2 and therefore the temperature flux correction given by Equation 2.4 was not used here.

Next, distilled water was substituted by 10.0 L of pre-treated effluent (after pH adjustment and ultrafiltration, as detailed in Chapter 2, Section 2.2.4). Effluent NF was performed for 2,200 minutes, with a constant operating pressure of 10 bar and a feed flow rate of 144 L/h, which resulted in 1.9 m/s cross-flow velocity and a Reynolds number of 847 (for details about calculation, please see in Section 2.2.4 the Equation 2.1, Equation 2.2 and Equation 2.3). The system was operated with a continuous removal of permeate and recycling of concentrate back to the feed tank. At the end of the experiment, the final permeate recovery rate (RR) was 72%. The permeate flux and feed temperature were monitored and permeate flux was normalized to 25°C.

Feed and NF permeate samples were collected each 10 % RR and analyzed according to the parameters of conductivity (Hanna conductivity meter HI 9835) and ions of sulfate, chloride, calcium, and magnesium (ion chromatograph Dionex ICS-1000 equipped with AS-22 and ICS 12-A columns). The entire procedure was performed in duplicate and the flux and physico-chemical parameter results presented correspond to the averages from both experiments.

To evaluate salt precipitation on membrane surfaces, which results in scaling, the calcium sulfate supersaturation index on the membrane surface (SI_m) was determined for different RRs. Detailed procedure for calculation is presented at Chapter 2, Section 2.2.4.7. Calcium sulfate was chosen as representative of salt precipitation as it has a low solubility and a high

concentration in effluent from gold mining (Table 2.1) presenting, therefore, a greater precipitation potential.

Following the nanofiltration procedure, two fragments of fouled membranes were obtained. The first fragment was subjected to physical cleaning using distilled water recirculation, at 144 L/h and 0 bar for 30 minutes. After physical cleaning, the water permeability was measured. This result was used to calculate the resistance to filtration (Section 3.2.2.2).

The second membrane fragment was removed from the system. The precipitate formed on the membrane surface was gently removed with a spatula and analyzed by X-ray diffraction (XRD). Samples of virgin and fouled membranes were also analyzed in a scanning electron microscope (SEM) coupled with an energy dispersive X-ray spectrometer (EDS) (Section 3.2.5).

3.2.2.2 Resistances in series calculations

Resistances were calculated using the resistance in series concept. Total resistance (R_{total}) comprises three components (Equation 3.1): intrinsic membrane resistance ($R_{membrane}$); reversible fouling resistance (R_{frev}), which comprised the concentration polarization resistance and the resistance from fouling removable by physical cleaning; and irreversible fouling resistance (R_{firrev}), which cannot be removed by physical cleaning (LI *et al.*, 2015).

$$R_{total} = R_{membrane} + R_{frev} + R_{firrev} \qquad \text{Equation 3.1}$$

Using the virgin membrane water permeability, the intrinsic membrane resistance to filtration ($R_{membrane}$) was calculated according to Equation 3.2:

$$\mathrm{R_{membrane}} = \frac{1}{\mathrm{K_{virgin} \times \mu}} \qquad \text{Equation 3.2}$$

where K_{virgin} is the water permeability at 25°C in m³/s.m².Pa, and μ is the viscosity of permeate in N.s/m².

Equation 3.3 was used to calculate the total resistance:

$$\mathrm{R_{total}} = \frac{\mathrm{P - \sigma\Delta\pi}}{\mathrm{\mu \times J_{effluent}}} \qquad \text{Equation 3.3}$$

where *P* is the applied transmembrane pressure (Pa), σ is the reflection coefficient estimated by the averaged membrane rejection of the major constituents of effluent (MATTARAJ *et al.*, 2008), and $\Delta\pi$ is the difference in osmotic pressure of the solution at the concentrate and permeate streams (Pa). In addition, $J_{effluent}$ is the permeate flux in $m^3/s.m^2$ obtained at the end of the fouling experiment (after 2,200 minutes of filtration).

The difference in osmotic pressure between NF concentrates and permeates obtained with different permeate recovery rates were estimated by the Van't Hoff equation, as described in Equation 3.4:

$$\Delta\pi = RT\Sigma\Delta C \qquad \text{Equation 3.4}$$

where *R* is the universal gas constant (L.Pa/K.mol), *T* is the permeation temperature (K), and $\Sigma\Delta C$ is the sum of the difference in molar concentrations of sulfate, chorine, calcium and magnesium in the concentrate and the permeate (mol/L).

The resistance of the irreversible fouling can be calculated by the water permeability after the physical cleaning process (K_{irrev}) (Equation 3.5).

$$R_{firrev} = \frac{1}{K_{irrev} \times \mu} - R_{membrane} \qquad \text{Equation 3.5}$$

The reversible fouling resistance can be thus calculated by Equation 3.6.

$$R_{frev} = R_{total} - R_{membrane} - R_{firrev} \qquad \text{Equation 3.6}$$

3.2.3 Evaluation of NF membrane cleaning

Cleaning tests were performed with different chemical agents and, after selection of the most appropriate, tests with different soak and recirculation times were carried out. Prior to each cleaning test, a new fraction of NF was separated and subjected to ultrasonication with a citric acid solution at pH 2.5 followed by ultrasonication with a 0.1% NaOH solution, for 20 minutes each. The cleaning test consisted of six steps: (1) compaction of the new membrane at 10 bar with distilled water; (2) measurement of distilled water permeability (K_{virgin}); (3) performance of NF fouling procedure with effluent; (4) measurement of fouled membrane distilled water

permeability (K_{fouled}); (5) accomplishment of the cleaning procedure; and (6) measurement of the cleaned membrane distilled water permeability ($K_{cleaned}$).

In all cases, the measurement of membrane permeability was conducted by monitoring the stabilized permeate flux at pressures of 10.0, 7.5, 5.0, and 2.5 bar. Water temperature was also monitored and permeate flux was normalized to 25°C.

The fouling procedure consisted of feeding 3 L of pre-treated effluent into the NF unit, and performing NF at a constant pressure of 10 bar and a feed flow rate of 144 L/h for 4 hours. Concentrate was recycled to the feed tank and permeate was continuously withdrawn, reaching a final permeate recovery rate between 40-45%.

For tests with different cleaning solutions, the cleaning procedure consisted of recirculating the solution in the NF unit for 90 minutes with a flow rate of 144 L/h and a pressure of 1.5 bar. Different cleaning solutions were tested, specifically: 0.2% hydrochloric acid, 2.0% citric acid, 0.5% phosphoric acid, 0.2% nitric acid, 0.1% sulfuric acid, 0.4% sodium hydroxide, 0.03% dodecylbenzene sodium sulfate (DDBS), and 1.0% sodium ethylenediamine tetraacetic acid (EDTA) (similar to the solutions suggested by the supplier of the membranes (DOWFILMTEC™ a)). A blank test was also conducted using only water.

After that, the cleaning mode (cleaning solution soaking or recirculation) and time were assessed for the best chemical cleaning agent. The procedure consisted of adding the cleaning solution in the NF unit, leaving it in static contact with the fouled membrane for different soak times (0, 15, 30, 45 or 60 minutes), then starting the pump and recirculating the solution with a flow rate of 144 L/h and a pressure of 1.5 bar for 15 up to 120 minutes.

The cleaning efficiency in each test was calculated using Equation 3.7:

$$Cleaning\ efficency\ (\%) = \frac{K_{cleaned} - K_{fouled}}{K_{virgin} - K_{fouled}} \qquad \text{Equation 3.7}$$

3.2.4 Assessment of membrane stability to the effluent and the cleaning solution

3.2.4.1 NF membrane immersion procedure

The effects of continuous exposure to effluent and chemical cleaning solutions on the characteristics of the NF membrane were evaluated by immersing four pristine membrane fragments in NF effluent concentrate (obtained for a permeate recovery rate of 40%, as established in Chapter 2, Section 2.3.7) for a period of 285 days. At four-week intervals, fragments were removed from the solution and rinsed with distilled water. Two of these fragments were immersed in a cleaning solution of 1.0% HCl overnight for 16 hours, and the other two remained immersed in distilled water. The concentration of the cleaning solution and the cleaning time were higher than the ones used in Section 3.2.3 so that the effect of the acid on the membrane could be more readily observed. Subsequently, filtration tests (Section 3.2.4.2) were carried out on two of the fragments, one that was subjected to contact with the effluent and cleaning solution ($NF_{eff+clean}$) and one that was exposed only to effluent (NF_{eff}). For the other two fragments, a fraction was removed for analysis of the morphological and chemical characteristics, as described in Section 3.2.5. After collecting a membrane fragment and proceeding with filtration tests, the immersion solutions were replaced and the fragments were re-immersed. This procedure was repeated until the 285-day period was complete. At the end of the exposure period, tests were also conducted to estimate the effective pore radius of the membrane (Section 3.2.4.3).

3.2.4.2 Filtration tests

The following tests were performed on the fragments of NF exposed to the effluent (NF_{eff}) and NF exposed to the effluent and the chemical 1.0% HCl cleaning solution ($NF_{eff+clean}$) prior to the immersion procedure, and were repeated every four weeks of the exposure period: (1) hydraulic permeability determination; (2) evaluation of magnesium sulfate rejection; and (3) evaluation of glucose rejection.

The hydraulic permeability of the membranes was determined by measuring the stabilized permeate flow rate at a pressure of 10.0 bar using distilled water as feed. Results were normalized to 25ºC.

Magnesium sulfate retention tests were performed using a 2,000 ppm solution as the feed. Two L of solution were fed into the NF unit and nanofiltrated at a pressure of 5 bar and temperature close to 25 °C, until a permeate recovery rate of 15% was achieved (DOWFILMTEC™ b). Feed and permeate were collected and analyzed for conductivity. A calibration curve was constructed and the magnesium sulfate retention efficiency was calculated.

Glucose retention tests were performed using a 500 ppm solution as the feed. Two L of solution were fed into the NF unit and nanofiltrated at a pressure of 10 bar and a temperature close to 25 °C, until a permeate recovery rate of 10% was achieved (GONZÁLEZ *et al.*, 2006). Feed and permeate carbohydrates were analyzed (DUBOIS *et al.*, 1956) and the observed retention efficiencies were calculated.

3.2.4.3 Estimation of the effective pore radius of the NF membrane

In order to assess whether exposure of the membranes resulted in an increase in their effective pores, methanol rejections were also determined as a function of permeate flux for pressures of 4-12 bar for virgin membrane and membranes after 285 days of exposure (NF_{eff} and $NF_{eff+clean}$). Retention tests were performed using a methanol solution of 2,000 ppm. The rejection data were interpreted in terms of real rejection as shown in Equation 3.8.

$$R_{ri} = 1 - \frac{C_{pi}}{C_{mi}} \qquad \text{Equation 3.8}$$

Here R_{ri}, C_{pi} and C_{mi} are the real rejection and concentration of solute i at the permeate and membrane surface (mol/L), respectively.

The concentration of solute i at the membrane surface can be determined by Equation 2.15 (Chapter 2, Section 2.2.4.7). Results of methanol rejections as a function of pressure were analyzed using the Spiegler-Kedem and Steric Hindrance Pore (SHP) models (WANG *et al.*, 1995). The Spiegler-Kedem model equation is given by Equation 3.9 (SCHAEP *et al.*, 1998).

$$R_{ri} = \frac{\sigma(1-F)}{1-\sigma F} \;\; where\; F = \exp\left(-\frac{1-\sigma}{P_i}J\right) \qquad \text{Equation 3.9}$$

where J is the permeate flux, P_i is the permeability of solute i, and σ is the reflection coefficient.

As shown in Equation 3.9, the rejection of a given solute increases as the permeate flux increases, reaching a limit that corresponds to the reflection coefficient. Because the contribution of the diffusive flux of the solute can be neglected if the permeate flux becomes infinite, the reflection coefficient is a characteristic of the convective transport of the solute. A reflection coefficient equals to 1 indicates that the convective transport of the solute is completely prevented or that no convective transport occurs. The last scenario, in which there is no convective transport, represents the ideal case of reverse osmosis membranes in which no pores are available for convective flux. A reflection coefficient smaller than 1 is obtained if the solute is sufficiently small to allow penetration into the pores of the membrane (SCHAEP *et al.*, 1998).

For neutral solutes where the convective flux is not influenced by electrostatic effects, separation occurs according to the size exclusion mechanism. Thus, only the ratio of the radius of the solute (r_s) to the pore radius (r_p) of the membrane determines the reflection coefficient, as indicted in Equation 3.10, which is deduced from the SHP model (SCHAEP *et al.*, 1998):

$$\sigma = 1 - \left(1 + \frac{16r_s^2}{(9r_p^2)}\right)\left(1 - \frac{r_s}{r_p}\right)^2\left[2 - \left(1 - \frac{r_s}{r_p}\right)^2\right] \qquad \text{Equation 3.10}$$

As can be seen from Equation 3.10, the SHP model can be used to estimate the pore radius for a given membrane. For this purpose, the reflection coefficient of a given solute must first be determined by Equation 3.9 and then the pore radius can be calculated using Equation 3.10.

Thus, in this study, the σ and P values were determined from the nonlinear fit of Equation 3.9 to the real rejection data as a function of the permeate flux. Once the σ and P_i parameters were determined, the pore radius (r_p) was determined using Equation 3.10. The solute radius (r_s) was considered equal to the Stokes radius, which corresponds to 0.135 nm for methanol (BELLONA *et al.*, 2010).

3.2.5 Evaluation of morphological and chemical characteristics of membranes and foulants

3.2.5.1 Scanning electron microscopy (SEM)

After the fouling and stability to effluent and cleaning solution tests, membrane surface morphology was analyzed using a FEI Quanta 200 scanning electron microscope (SEM) with

an additional energy dispersive X-ray spectrometer (EDS) analysis. Prior to analysis, membrane samples were air-dried and coated with carbon layer by a sputter coating machine (Leica EM SCD 500 with a pressure of 10^{-2}-10^{-3} mbar and a 2.5 A current).

3.2.5.2 Atomic force microscopy (AFM)

The membrane samples exposed to effluent and chemical cleaning agents were also analyzed by atomic force microscopy (AFM) to observe additional changes in the surface morphology. Tapping mode AFM was performed with an Asylum MFP-3D-SA/AFM microscope (Asylum Research) over an area of 5 × 5 μm². A silicon probe (AC240TS-R3, Olympus) was used. At least three different areas of each membrane were visualized and the mean value of the root-mean-squared roughness (R_{RMS}) was determined using the AFM software.

3.2.5.3 Contact angle measurements

In order to verify changes in the membrane hydrophobicity when exposed to effluent and chemical cleaning agents, contact angle measurements were performed. Water contact angles were determined using a DIGIDROP-DI goniometer (GBX Instruments) equipped with a CCD camera and an automated liquid dispenser, using the standard sessile drop method. Six μL of deionized water droplets were placed at the membrane surface at room temperature and the contact angle was measured. Five droplets were applied to each membrane to establish average and standard deviation.

3.2.5.4 Attenuated total reflection Fourier transform infrared (ATR-FTIR)

In order to evaluate changes in the membrane surface composition, attenuated total reflection Fourier transform infrared (ATR-FTIR) spectroscopy analysis was performed on membrane samples that had been subjected to stability tests. ATR-FTIR experiments were carried out using a Shimadzu FTIR IR Prestige-21 instrument equipped with an attenuated total reflectance (ATR) accessory. The spectrum was obtained in the range of 400–4000 cm^{-1} at a 4 cm^{-1} resolution.

3.2.5.5 X-ray diffraction (XRD)

The precipitate formed on the membrane surface during fouling test was analyzed by XRD. A Philips diffractometer (Panalytical) with an X'Pert-APD system, PW 3710/31 controller, PW 1830/40 generator, and PW 3020/00 goniometer was used. The radiation was emitted from a copper tube (Z = 29) with a mean wavelength K_α of 1.54184Å and $\lambda_\alpha 1$ of 1.54056Å.

3.3 RESULTS AND DISCUSSION

3.3.1 Fouling evaluation

Figure 3.2 illustrates the permeate flux over initial flux (J/J_0) as a function of operation time for the NF of the gold mining effluent. It is evident that the flux decays strongly (~80%) until approximately 770 minutes of NF, followed by a tendency toward stabilization. This flux reduction is justified by the increase in the filtration's resistance due to concentration polarization and fouling (OCHANDO-PULIDO *et al.*, 2014), which is associated with inorganic matter deposition on the surface of the membrane. The high rejection by the membrane of ions present in the effluent cause an expressive increase in the concentration during filtration time (Table 3.1), which intensifies flux decay. The effluent is saturated with calcium sulfate, with a supersaturation index on membrane surface (SI_m) variable ranging from 1.32 to 2.94, for a permeate recovery rate between 0 and 70%, respectively, allowing the salt to precipitate. An X-ray diffraction from the precipitate found over membrane surface indicated the presence of bassanite (hydrated calcium sulfate $CaSO_4.0.5H_2O$) as the only crystalline phase (Figure 3.3).

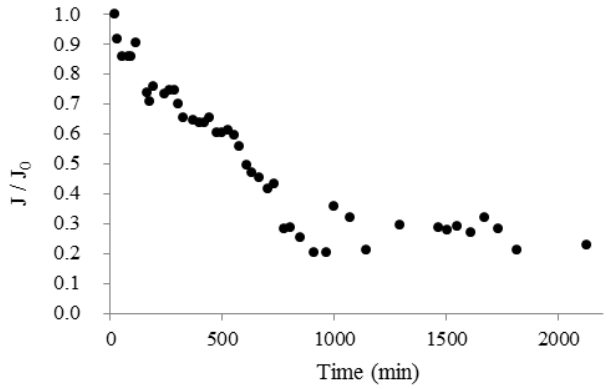

Figure 3.2 – Permeate flux over initial flux (J/J_0) to gold mining effluent nanofiltration

Table 3.1 – Characterization of gold mining effluent and NF permeate

Parameter	Raw effluent	NF permeate at 40% recovery rate	Retention efficiency
Conductivity (µS/cm)	4,550	398	91%
Sulfate (mg/L)	2,620	168	94%
Chloride (mg/L)	196	15	92%
Calcium (mg/L)	673	24	96%
Magnesium (mg/L)	148	6	96%

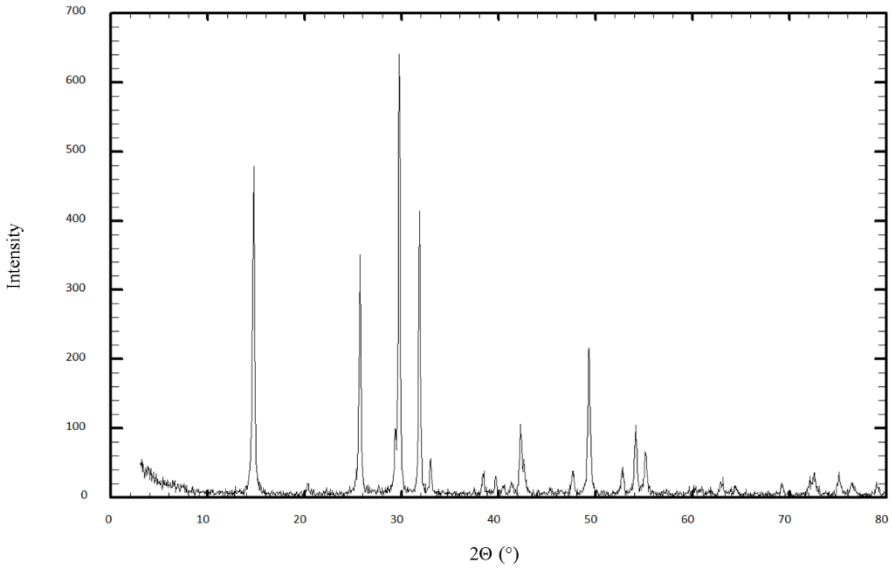

Figure 3.3 – X- ray diffractogram from the precipitate formed over the membrane during the fouling test

Through SEM micrographs of the fouled surface in association with EDS analysis (Figure 3.4), it was observed that, besides crystallized calcium sulfate, the fouling composition included magnesium, sodium, zinc, copper, aluminum, iron, arsenic, and silica precipitated on amorphous structures or adsorbed on the membrane's surface.

The membrane, reversible fouling (physically removed by cleaning with water recirculation), and irreversible fouling (not removed by physical cleaning) resistances were calculated at the end of the fouling test (Table 3.2). It was observed that the highest resistance to NF was due to the membrane itself, which is a typical result of using NF membranes (ANDRADE *et al.*, 2014; MUKHERJEE *et al.*, 2016). Part of the fouling resistance can be removed by physical methods, and thus can be controlled by adjusting the feed flow conditions. However, a significant portion of the fouling is considered irreversible (35%), thus requiring chemical cleaning. The results show the importance of optimizing the chemical cleaning process to ensure the maintenance of membrane permeability and the sustainability of the process.

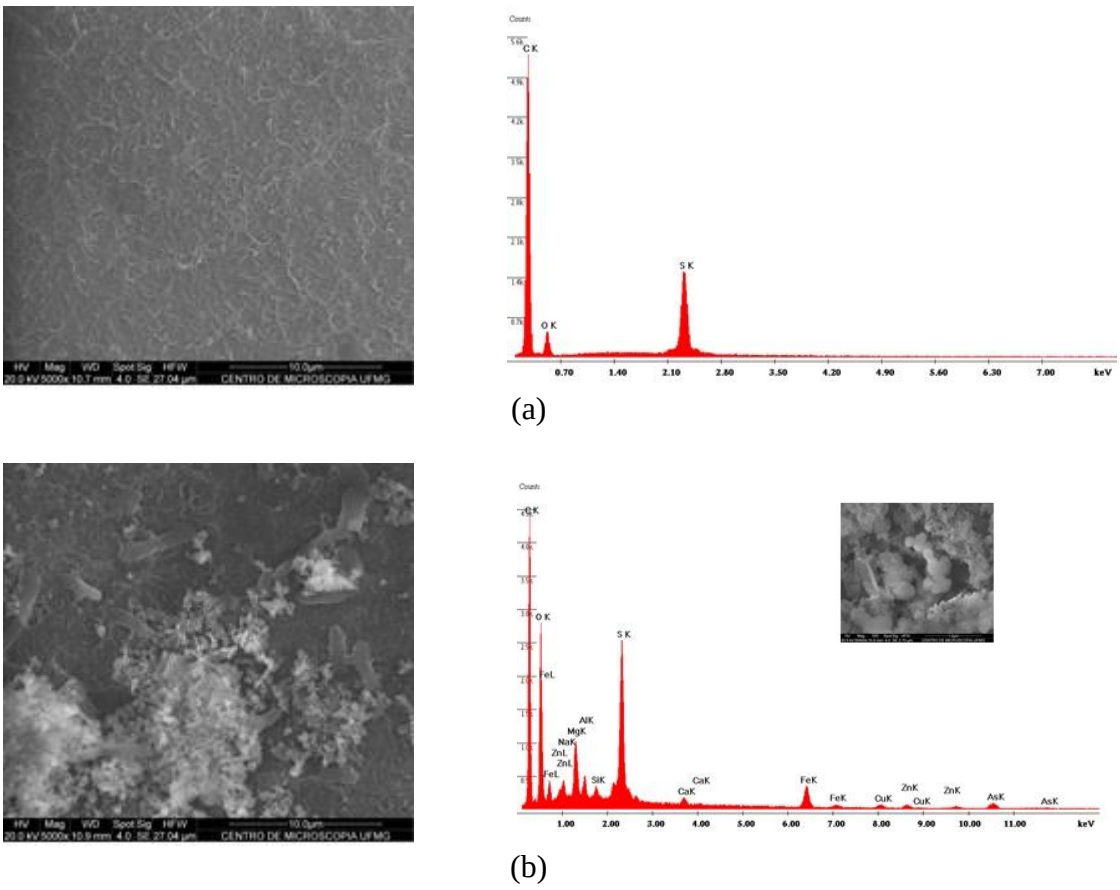

Figure 3.4 – SEM micrographs and EDS spectrum from (a) the virgin membrane and (b) after 2,200 minutes of filtration

Table 3.2 – Resistance of gold mining effluent nanofiltration

Sample	Resistance Value ($m^{-1} \times 10^{-13}$)	Percentage
Membrane	5.85	39%
Reversible fouling	3.99	26%
Irreversible fouling	5.28	35%
Total	15.1	100%

3.3.2 Cleaning membrane evaluation

In order to remove fouling and restore membrane permeability to allow for an increase in the membrane module's lifetime and the process sustainability, several chemical substances were evaluated as cleaning agents (Figure 3.5). The purpose of a cleaning agent is to reduce the foulant-foulant and foulant-membrane interaction in such a way that the fouling layer can be removed from the membrane's surface through mass transfer (WEI *et al.*, 2010). Acid and

chelating agents reduce the inorganic foulant- membrane interaction, while bases act mainly on the organic deposits and amino acids, by hydrolysis and solubilization (MADAENI and SAMIEIRAD, 2010; MO *et al.*, 2010; WEI *et al.*, 2010), and on silica (GWON *et al.*, 2003).

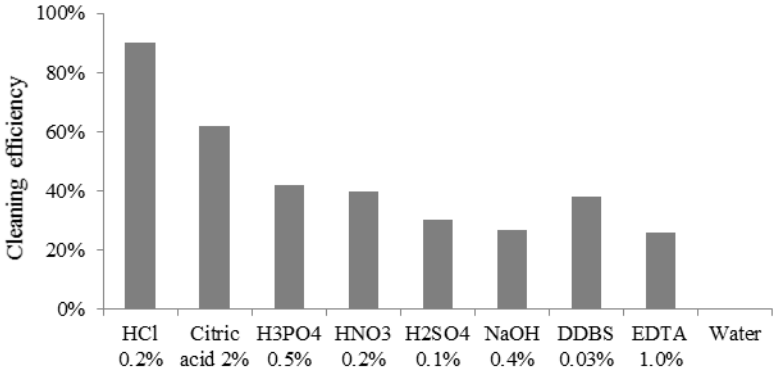

Figure 3.5 – Cleaning efficiency of several chemical agents

Due to the low organic compound concentration found in the effluent (Table 2.1), the NF membrane fouling was caused mainly by inorganic species, as observed in Figure 3.3 and Figure 3.4. Thus, the NaOH solution presented the lowest cleaning efficiency among all chemical agents evaluated.

EDTA is a strong metal-chelating agent. It can react with calcium ions in sulfate and carbonate precipitates to form soluble complexes. It can also react through ligand-exchange with calcium ions in organic matter-calcium complexes (WEI *et al.*, 2010). However, in this study, EDTA did not demonstrate a good efficiency. Al-Amoudi *et al.* (2007) also observed that permeability was not totally restored after cleaning by a mixed cleaning agent that contained EDTA.

Among the acids, the worst performance was observed for sulfuric acid (H_2SO_4), which can be associated with the tendency of formation of sulfate salt precipitate when the solution comes in contact with the calcium presented on membrane surfaces. Phosphoric acid can also provide insoluble calcium phosphate formation (AL-AMOUDI and LOVITT, 2007). Nitric acid did not present satisfactory results, which is consistent with previous results in other studies (MADAENI and SAMIEIRAD, 2010). Despite some suggestions that it is the most efficient cleaning agent (WEI *et al.*, 2010), citric acid had a less relevant effect in this study.

The best cleaning agent was hydrochloric acid. The advantage of HCl over other acids such as HNO_3 and H_2SO_4 is that HCl has no oxidation ability for degradation of organic matter. This degradation may cause formation of secondary fouling. Moreover, the obtained salt from the HCl agent is more soluble compared to the salts from other acids (MADAENI and SAMIEIRAD, 2010). Therefore, HCl was selected as the most suitable chemical for NF membrane cleaning procedures.

The Figure 3.6 shows the cleaning efficiencies obtained with 0.2% HCl solution over different cleaning times. The total cleaning time includes the soak time (ranging from 0 up to 60 minutes) plus the recirculation time.

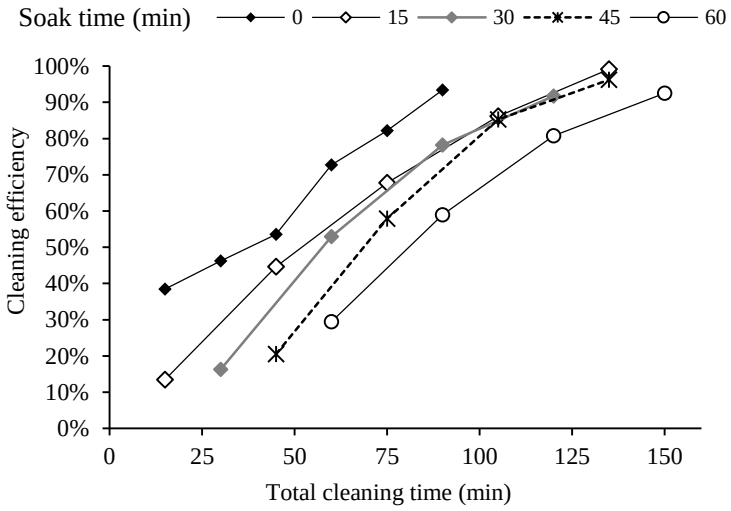

Figure 3.6 – Cleaning efficiencies obtained with 0.2% HCl solution over different cleaning times. The total cleaning time includes soak and recirculation times.

According to Wei *et al.* (2010) during cleaning process, the cleaning agent contacts membrane surface foulants via mass transfer. The agent reacts with the foulants, especially those closest to membrane surface, yielding loosened fouling layer. Then, these reaction products are removed from membrane surface via mass transfer. As hydrodynamic conditions interfere directly in the mass transfer coefficients, cleaning without fluid movement (soak) is not very effective. Thus, it can be seen that the longer the soak time, the greater the total cleaning time necessary to achieve cleaning efficiency > 90%. The condition that required the lower total time to remove fouling was the one with only recirculation cleaning (soak time = 0 min), in which it was possible to obtain 94% efficiency after 90 minutes.

3.3.3 Evaluation of membrane stability to the effluent and the cleaning solution

Figure 3.7 shows the variation in water permeability of membranes exposed to the effluent (NF_{eff}) and to the effluent and the cleaning solution ($NF_{eff+clean}$) as a function of time. The bars represent the positive and negative values of standard deviation. These standard deviations were calculated according to the formula for determining the combined standard uncertainty (Equation 3.11).

$$u_c\,(y) = \sqrt{\sum_{i=1}^{N}\left(\frac{\partial f}{\partial x_i}\right)^2 \times u^2(x_i)} \qquad \text{Equation 3.11}$$

where $u_c(y)$ is the combined standard deviation of the variable y, *f* is the function y=f(x_1, x_2, ..., x_N), and $u^2(x_i)$ is the uncertainty related to the parameter x_i. The water permeability (L_p) can be calculated using Equation 3.12.

$$Lp = \frac{V}{t} \times \frac{1}{\pi \times D^2/_4} \times \frac{1}{P} \times \frac{\mu_{(T)}}{\mu_{(25^oC)}} \qquad \text{Equation 3.12}$$

where *V* is the volume of permeate (L) collected in a given time; *t* is the sampling time (h); *D* is the diameter of the filtration cell (m); *P* is the pressure (bar); and $\mu_{(T)}$ is the permeate viscosity at temperature T. The permeate viscosity was assumed to be equal to water viscosity and thus was calculated at a given temperature T (K) by Equation 3.13.

$$\mu_{(T)} = 2.414 \times 10^{-5} \times 10^{(247.8/T-140)} \qquad \text{Equation 3.13}$$

The combined uncertainty of L_p can thus be calculated by Equation 3.14:

$$u_c(Lp) = Lp \times \sqrt{\frac{u^2(V)}{V^2} + \frac{u^2(t)}{t^2} + \frac{4u^2(D)}{D^2} + \frac{u^2(P)}{P^2} + \frac{u^2(T)(247.8^2)}{(T-140)^4}} \qquad \text{Equation 3.14}$$

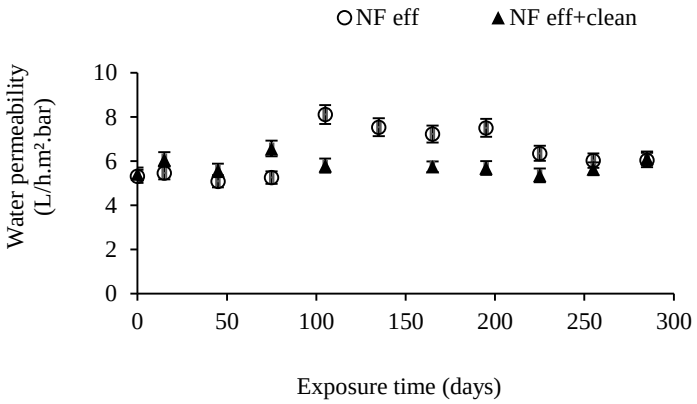

Figure 3.7 – Water permeability variation as a function of time of exposure to the membrane in contact with effluent (NF_{eff}) and in contact with effluent and cleaning solution ($NF_{eff+clean}$)

Retention of magnesium sulfate (ionic solute) and glucose (neutral solute) over the period were also monitored (Figure 3.8). In order to evaluate the changes observed in the permeability and the magnesium sulfate and glucose retentions, contact angle (Table 3.3), SEM (Figure 3.9), and AFM (Figure 3.10) with root mean square (RMS) roughness calculations (Table 3.4) were carried out.

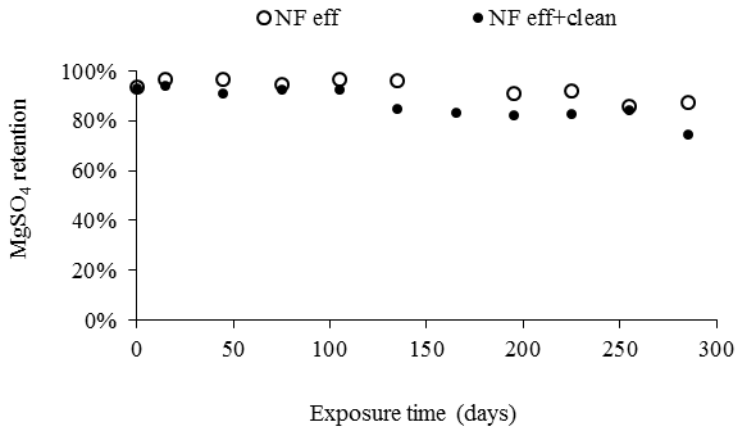

(a)

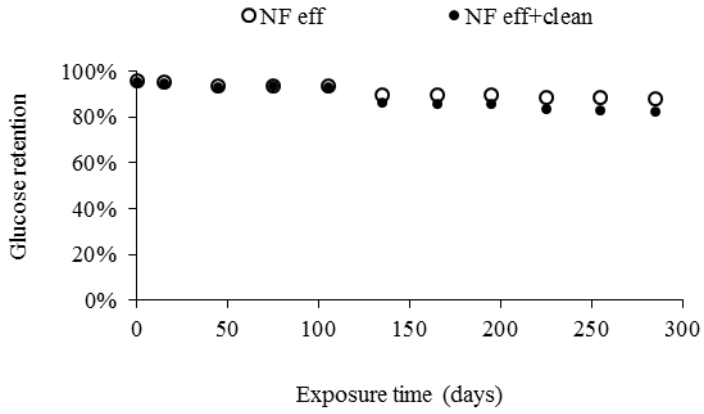

(b)

Figure 3.8 – Retention of (a) magnesium sulfate and (b) glucose as a function of the exposure time for the membrane in contact with effluent (NF_{eff}) and in contact with effluent and cleaning solution ($NF_{eff+clean}$)

Table 3.3 – Contact angle measurements of the virgin membrane and the membrane exposed to the effluent and to the effluent and the cleaning solution

Sample	Virgin NF90	NF_{eff}		$NF_{eff+clean}$	
		105 days	285 days	105 days	285 days
Contact Angle (º)	41.9 ± 2.9	56.0 ± 1.7	58.6 ± 1.9	46.0 ± 2.4	58.5 ± 3.8

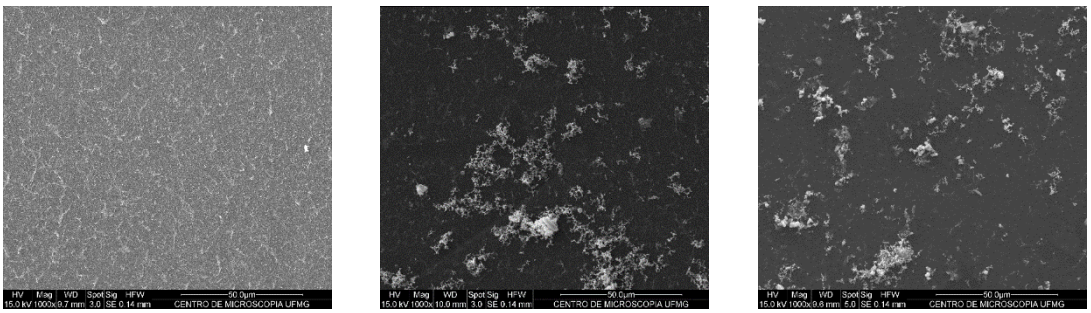

(a) (b) (c)

Figure 3.9 – SEM images of the NF90 membranes: (a) virgin, (b) exposed to the effluent after 285 days, and (c) exposed to the effluent and the cleaning solution after 285 days

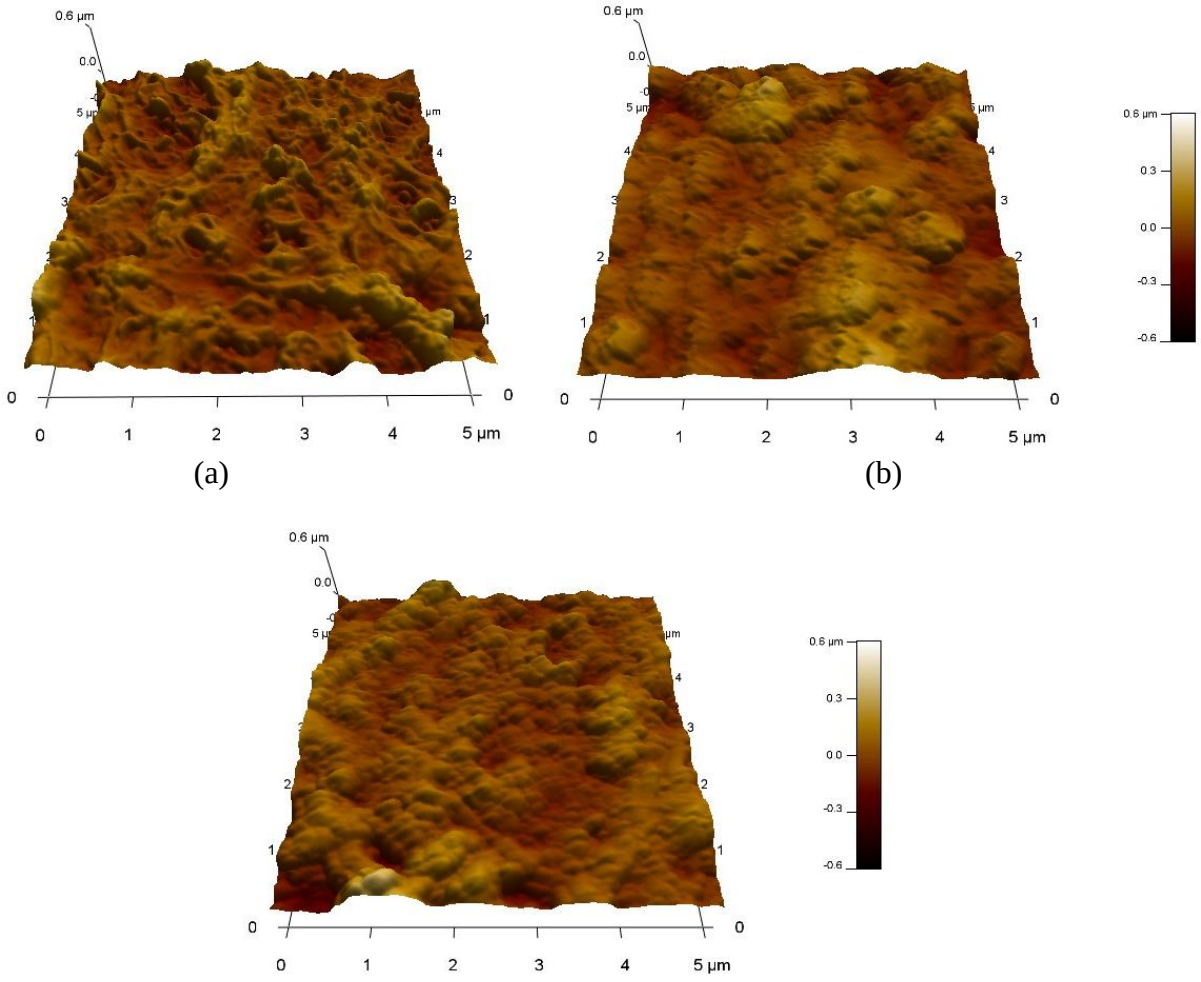

(a) (b)

(c)

Figure 3.10 – AFM images of the NF90 membranes: (a) virgin, (b) exposed to the effluent after 285 days, and (c) exposed to the effluent and the cleaning solution after 285 days

Table 3.4 – Root mean square roughness (RMS) measurements of the NF90 membranes: virgin, exposed to the effluent, and exposed to the effluent and the cleaning solution for 285 days

Sample	NF90 virgin	NF_{eff}	$NF_{eff+clean}$
RMS (nm)	65.1 ± 3.6	52.5 ± 2.2	64.3 ± 2.4

The membranes' effective pore radius were also estimated through methanol retention at several pressures and flux. Figure 3.11 shows the real rejection of methanol as a function of the permeate flux as well as the curve obtained from the nonlinear fit (solid lines) of the Spiegler-Kedem model. As can be observed from Figure 3.11, a good correlation was obtained. Once the σ and P_i parameters were determined by the nonlinear fit of the Spiegler-Kedem model, the pore radius (r_p) was determined (Table 3.5). The pore size was determined for the membranes prior to the immersion process and after 285 days.

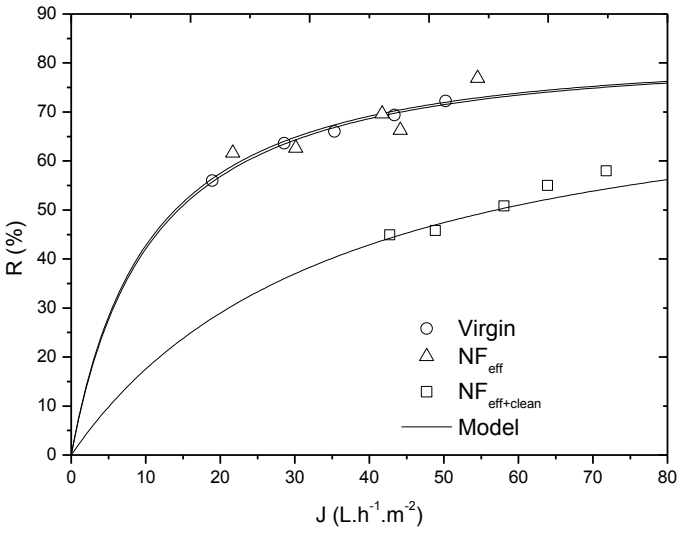

Figure 3.11 – Experimental rejection data for methanol as a function of permeate flux and the curves obtained from the nonlinear fit

Table 3.5 – Reflection coefficient values (σ), solute permeability (P_i), and pore radius (r_p) for methanol

Parameter	σ	P_i (L/h.m².bar)	r_p (nm)
Virgin NF90	0.80	9.91	0.17
NF_{eff}	0.80	9.65	0.17
$NF_{eff+Clean}$	0.72	32.51	0.19

It is evident that contact with the effluent caused an increase in NF_{eff} permeability after approximately 105 days. After this period, the permeability reduced gradually, mainly due to fouling development, demonstrated by SEM (Figure 3.9) and AFM (Figure 3.10) images, and hydrophobicity augmentation (Table 3.3). It is clear that the foulant accumulated in the ridge-and-valley structure of the membranes, reducing the overall surface roughness (Table 3.4). This result is similar to those of Nanda *et al.* (2010), who studied NF fouling through calcium sulfate. Considering the operation's pH, the membrane had a slight negative charge (Chapter 2, Section 2.3.4). As the charge density of the membrane was not too high, calcium sulfate was allowed to approach the membrane surface more closely due to the reduced Donnan's effect (NANDA *et al.*, 2010), causing the roughness modification observed.

On the other hand, the $NF_{eff+clean}$ presented a lower water permeability variation (maximum variation of 20% over the study period). This may have been due to the antagonistic effects of pore size, hydrophobicity, and fouling. While an increase in the pore radius (Table 3.5) tends to lead to an increase in permeability, the elevation of the contact angle (Table 3.3), which indicates an increase in the hydrophobicity, and fouling (Figure 3.9 and Figure 3.10), reduce it. Therefore, the increase in the pore radius was compensated by the increase in hydrophobicity and fouling in such a way that permeability remained approximately constant.

The SEM and AFM images (Figure 3.9 and Figure 3.10) show that the execution of a monthly cleaning procedure reduced the amount of foulants on the membrane. This can also be inferred through the minor reduction of roughness of $NF_{eff+clean}$ in regard to the virgin membrane (Table 3.4). However, the effects of the cleaning procedure were not sufficient to completely avoid the emergence of fouling. As discussed before, the cleaning agents are capable of reducing the interaction of foulant-foulant and foulant-membrane, but it is necessary to optimize the mass transfer conditions so that foulants can be disconnected from the membrane and carried to the bulk of the solution (WEI *et al.*, 2010). Thus, the fouling remaining on the surface of the membrane can be caused by the low efficiency of the cleaning procedure, which consisted of soaking the membrane in the cleaning solution overnight, without recirculation. This is consistent with results shown in Section 3.3.2.

Moreover, although the two membranes acquire similar hydrophobicity at day 285, the contact angle of $NF_{eff+clean}$ was closer to one from the virgin membrane than the NF_{eff} (Table 3.3)

after 105 days. This means that monthly chemical cleaning contributed to reduce the effect of increasing hydrophobicity caused by the continuous contact with the effluent.

There are many mechanisms affecting solute rejection through NF membranes, including steric hindrance, Donnan's effect, and dielectric effects (NGUYEN *et al.*, 2009). In this sense, factors such as the membrane pore size, surface charge, and pore charge directly influence solute retention.

Regarding the magnesium sulfate retention, a small reduction over time was observed for both samples (Figure 3.8a). This can be related to the fouling occurrence (Figure 3.9) and/or changes at the membrane superficial charge. The formation of foulant deposits reduces solute diffusion from the vicinity of the membrane surface back to the bulk solution, resulting in the so-called cake-enhanced concentration polarization effect. This effect causes an increase in the solute concentration at the membrane surface and, as the intrinsic retention of the membrane remains unchanged, the solute transferred to the permeate increases (VOGEL *et al.*, 2010). Vogel and co-authors (2010) observed a reduction in the rejection of both inorganic and organic solutes from an NF270 membrane due to cake composed of humic acid and calcium carbonate.

The superficial charge effect is relevant to the retention of sulfate and magnesium ions, because in this case Donnan and dielectric are the principal effects that determine the membrane's retention. Thus, it is possible that the continued exposure of the membranes to the effluent also altered the superficial charge. As a consequence, the membranes became more neutral and the repulsion of the ions on the solution was reduced. At the effluent pH (5.0), the membrane possessed a small superficial negative charge (Chapter 2, Section 2.3.4). Thus, the observed effect could result from attraction and irreversible adsorption of counter-ions, such as calcium and magnesium, on the surface and membrane pores. This superficial charge reduction can also contribute to roughness modification, as previously discussed.

The statistical test of Mann-Whitney was performed using Matlab R2008a software (The MathWorks, USA) in order to compare the retention of $MgSO_4$ for both membranes after 105 days of exposure. It was concluded that the membrane performances could be considered significantly different to a significance level of 5% (p_{value}= 0.0079), and that the retention of $NF_{eff+clean}$ was the lowest. Thus, the exposure to HCl intensified the neutralization of the superficial charge process, which can be justified by the protonation of the surface's functional

groups of the membrane while in contact with the cleaning solution, and then the membrane became more neutral. As a result of hysteresis effects, a considerable increase in permeability following acid cleaning could be observed, particularly if the membrane had a very thin active skin layer (SIMON *et al.*, 2013).

Glucose retention also diminished slightly with time (Figure 3.8b) and, as previously discussed, membrane fouling can explain this phenomenon. It can be also verified that the decrease in rejection after 105 days of exposure is larger for $NF_{eff+clean}$ (significant difference with p_{value}= 0.0022). As glucose is a neutral solute, its retention is given as a function of steric hindrance. The increase in the pores of the membrane that was subjected to monthly cleanings (Table 3.5) justifies the observed reduction in rejection. With assistance of the positron annihilation technique, Ahmed (2013) noticed that an HCl 1 M (3.65%) solution had a minor effect on the pore size of an NF GE Osmonics DK membrane (reduction of 1%). However, the total exposure of the membrane to HCl in the present study (1.76×10^6 ppm·h) is much larger than that of Ahmed (2013) (0.66×10^6 ppm·h), and the cleaning solution most likely has a cumulative effect on the membrane.

It is worth noting that, although there have been changes in the rejection of membranes over time, the reduction has not been very intense. NF membranes still showed good performance even after 285 days of exposure to the effluent and to the cleaning solution. Final retentions of $MgSO_4$ and glucose were 87-74% and 88-82%, respectively. This is partly due to the use of a good pre-treatment. The pre-treatment included a pH adjustment of the effluent, which in its original pH is very acidic and may cause polymer degradation, and the UF retention of suspended and colloidal solids, which can result in fouling and physical damage of the membranes.

The effect of continuous exposure to the effluent and the combination effluent and cleaning agent on the chemical composition of the NF90 membrane was evaluated through attenuated total reflectance Fourier transform infrared spectroscopy (ATR-FTIR). The spectrums are presented in Figure 3.12.

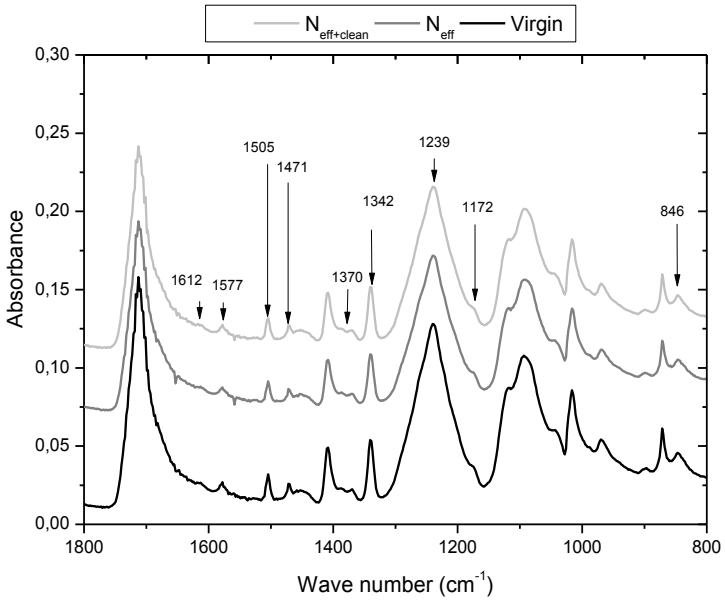

Figure 3.12 – Infrared spectrums in the region between 1800 to 400 cm^{-1} to NF 90 membrane exposed only to the effluent and to the combination of effluent and cleaning agent

In the infrared spectroscopy for attenuated total reflectance, the selective and intermediate layers are analyzed, and all results consist in an overlapping of spectrums from each layer (TANG *et al.*, 2009). Thus, bands of the selective layer, whose base polymer is polyamide, and also from the support layer, whose polymer is polysulfone, were verified on the spectrums obtained for NF90. The main detected bands, specific for the mentioned polymers, can be found in Table 3.6.

Appearance or disappearance of the characteristic bands was not verified during the evaluation period, as it can be seen through a comparison of the spectrums presented in Figure 3.12. Therefore, the results obtained suggest that the degradation of the polymer polyamide did not occur, or it happened on a very small scale, which corroborate the results obtained in this study.

Table 3.6 – Main IR bands of polysulfone (PSF) and polyamide (PA) components of NF90 membrane in the region between 1800 and 800 cm^{-1}

Assignment	Reported peaks (cm^{-1})[a]	Observed peaks (cm^{-1})	Vibration	Intensity
PA	1609	1612	Aromatic amide (N-H deformation vibration or C=C ring stretching vibration)	Weak
PSF	~1587, 1504,1488	1577, 1505, 1471	Aromatic in-plane ring bend stretching vibration	Middle
	~1245	1239	C-O-C asymmetric stretching vibration of the aryl-O-aryl group	Strong
	1385-1365	1370	C-H symmetric deformation vibration of $-C(CH_3)_2$	Weak
	1350-1280	1342	Asymmetric SO_2 stretching vibration	Middle
	1180-1145	1172	Symmetric SO_2 stretching vibration	Strong
	~830	846	In-phase out-of-plane hydrogen deformation of para-substituted phenyl group	Weak

[a] Peak values of PA and PSU were reported by Tang *et al.* (2009)

3.4 CONCLUSIONS

With this Chapter it was concluded that the NF process is a suitable treatment for gold mining effluent, allowing for a high conductivity and ion retention efficiency. However, the effects of concentration polarization and fouling cause a reduction of approximately 80% of the permeate flux when the permeate recovery rate is 70%.

SEM and EDS analysis showed that fouling is mainly made up of calcium, magnesium, sodium, zinc, copper, aluminum, iron, arsenic, and silica. The supersaturation index over membrane surface (SI_m) for calcium sulfate was larger than 1 even at the beginning of NF (SI_m = 1.68 at permeate recovery rate of ~ 0%) and increased with the concentration of the effluent (SI_m = 2.94 at permeate recovery rate of 70%). Thus, calcium sulfate was found precipitated in the form of bassanite (hydrated calcium sulfate $CaSO_4.0.5H_2O$) on the membrane.

To control fouling and ensure process sustainability, chemical cleaning was studied. It was observed that the basic (NaOH) and chelator (EDTA) cleaning agents did not demonstrate good cleaning efficiency. Among the acids tested, HCl was the most efficient, and thus was chosen

as the best for the studied application. The most efficient cleaning procedure was 90-minute recirculation cleaning, without soak.

It is known that the constant contact of the membrane with effluent and cleaning solution can lead to changes in its performance, structure, and morphology. To study these effects, the NF membrane was exposed to the effluent and to the combined effluent and HCl solution for 285 days. Alterations in hydrophobicity and occurrence of fouling caused the permeability of the membrane exposed only to the effluent to increase in the first 105 days and then decrease to the initial point again. On the other hand, an antagonistic effect on pore enlargement, fouling, and increased hydrophobicity caused the permeability of the membrane exposed to the effluent and the cleaning solution to remain substantially constant. Fouling, surface charge changes, and an increased pore radius led to a decrease in retention salts (magnesium sulfate) and neutral solutes (glucose) by the two membranes. The retention of the membrane exposed to the cleaning solution was statistically lower, reinforcing the importance of optimizing the cleaning condition to maximize cleaning efficiency with the least exposure. Positively, the infrared spectroscopy results showed no indication of degradation of the polymeric material of the membrane.

It was concluded that several factors influence the permeability and rejection of NF membranes, such as pore size, hydrophobicity, fouling, and surface charge, and that joint analysis is a complex task. Although there were changes in the rejection of the membranes over time, the reduction was not very intense, and NF membranes still showed good performance even after 285 days of exposure to the effluent and the cleaning solution. Thus, it can be said that the results of this study are promising and demonstrate the robustness of NF technology for gold mining effluent treatment.

4 CHAPTER

COMPREHENSIVE BENCH AND PILOT SCALE INVESTIGATION OF NF FOR GOLD MINING EFFLUENT TREATMENT: MEMBRANE PERFORMANCE AND FOULING CONTROL STRATEGIES

4.1 INTRODUCTION

Gold mining is an industrial sector of significant economic importance. However, it is also responsible for many adverse impacts on water resources such as water cycle changes and deterioration of the water quality of receiving water bodies (LOBO *et al.*, 2015). The effluents from ore processing have low pH and high concentrations of heavy metals and metalloids, such as Cd, Cr, Hg, and As, since these elements are often associated with valuable components in ores and concentrates (CHAN and DUDENEY, 2008; LANGSCH *et al.*, 2012).

Nowadays, many countries are facing a significant water scarcity problem. Over the last decade, the acceptance of water reclamation and reuse has increased, which is an effective approach for reducing fresh water consumption and wastewater discharge. Moreover, because of the high consumption of fresh water and high effluent generation, mining is one of the industrial sectors with the highest potential for water reuse. However, further studies focused on the application of advanced treatment technologies on mining effluents, aimed at meeting the quality requirements for reclaimed water, are still needed.

Nanofiltration (NF) process can efficiently retain salts and metals from aqueous medium (AL-RASHDI *et al.*, 2013; PAGES *et al.*, 2013). Therefore, it presents high potential to treat mining effluents. Although some authors have studied the NF of mining effluents (AL-THYABAT and AL-ZOUBI, 2012; AL-ZOUBI *et al.*, 2010 b; HÄYRYNEN *et al.*, 2009; HOYER *et al.*, 2014; RICCI *et al.*, 2015; SIERRA *et al.*, 2013), the literature is still small and does not reflect the full potential of this process. It lacks advanced studies of the application of membrane separation processes for mining effluents; especially, studies aimed at optimizing the operating conditions and ensuring a viable process in both technical and economic terms.

Fouling is a major limitation of NF. Membrane fouling increases the chemical cleaning requirement and ultimately results in water production loss, membrane integrity loss, poorer water quality and shorter membrane lifetime; which consequently impose a heavy economic weight on the plant operation (WILF, 2010). Fouling is related to operating conditions and feed stream composition (BEYER *et al.*, 2010). Both, fouling tendency and NF permeate quality, are strongly influenced by operating conditions such as: feed pre-treatment (PETRINIC *et al.*, 2015); feed pH (CAPAR *et al.*, 2006; CHANG *et al.*, 2014; KAYA *et al.*, 2010; WANG *et al.*, 2007); concentration of solutes on the feed solution (CHANG *et al.*, 2014; SEMIÃO and SCHÄFER, 2011); permeate recovery rate (KAYA *et al.*, 2009; PATIL *et al.*, 2015);

temperature (AMAR *et al.*, 2009; DANG *et al.*, 2014; KAYA *et al.*, 2009; NILSSON *et al.*, 2008); and hydrodynamic conditions imposed by different transmembrane pressures (BELKHOUCHE *et al.*, 2009; KAYA *et al.*, 2009; KAYA, Y *et al.*, 2010) and by different cross-flow velocities (GHERASIM and MIKULÁŠEK, 2014; MUKHERJEE *et al.*, 2016).

Antiscalant dosage is often necessary in membrane separation process when the effluent has significant concentration of cations and anions of sparingly soluble salts because of the inherent increase in concentrate concentration (PLOTTU-PECHEUX *et al.*, 2002). Some sparingly soluble salts reported in the literature include calcium sulfate, carbonate and fluoride; barium sulfate; and strontium sulfate (ANTONY *et al.*, 2011). Commonly used antiscalants in membrane separation processes include polyacrylic acid, polyacrylamide, polymaleic anhydride, and polyphosphates (AL-ROOMI and HUSSAIN, 2015). Antiscalant is used to complex the metal involved in the formation of the salt or to inhibit the crystal growth (VAN PAASSEN *et al.*, 1998). Many mechanisms were proposed for antiscalant influence on crystallization. Rahardianto *et al.* (2008) suggested that antiscalants can adsorb onto newly formed crystal facets, causing defects and thereby retarding or halting further crystal growth or weakening the mechanical strength of the scale. It has also been hypothesized that antiscalants increase the surface energy of crystal nuclei, effectively slowing the rate of crystal nucleation (LYSTER *et al.*, 2010; OH *et al.*, 2009) and/or that antiscalants cause a negative electrostatic potential on the antiscalant modified scale surface, which can prevent not only the agglomeration of scale nuclei in the concentrate but also the precipitation of scale nuclei on the membrane surface (YUAN *et al.*, 2009).

Even with the optimization of operating conditions and antiscalant dosage, fouling can develop on the membrane surface or inside the membrane pores. Therefore, membrane cleaning methods aimed at fouling removal are mandatory for membrane separation processes (SCHÄFER *et al.*, 2005). Membrane cleaning methods are classified into physical, chemical and physico-chemical. Chemical cleaning is the most studied membrane cleaning method, especially in NF and RO systems. Although physical cleaning methods can be economically attractive (AL-AMOUDI and LOVITT, 2007), they have not been given much attention. As a result, more investigation is needed in order to evaluate their effectiveness.

The most frequently used physical cleaning method for microfiltration (MF) and ultrafiltration (UF) is backwashing. However, the pressure necessary to perform backwashing on NF and RO

membranes with sufficient flux would be very high because of the high resistance of the membrane. As this could loosen the membrane layer from its support layer, backwashing is not commonly used in these processes (RIETMAN, 2013). Therefore, others physical cleaning methods should be used for NF and RO, which include, for example, hydrodynamic forward or reverse flush, air spurge and automatic sponge ball cleaning (AL-AMOUDI and LOVITT, 2007). Among these, forward flux is of special interest as no substantial changes in the NF/RO unit are needed for its application. During forward flush, the cross-flow velocity in the feed stream is maintained while the transmembrane pressure is removed. This stops the permeate flux and reduces the concentration polarization.

The best operating conditions, antiscalant dosage and cleaning processes must be carefully selected for each specific application to achieve the best overall performance. This line of research has received the attention of researchers throughout the world. However, these parameters are usually evaluated through bench scale tests. Bench scale tests use a flat sheet membrane cell with a small area in the order of tens of cm^2. Bench scale units are practical and inexpensive, and require only a small volume of effluent for operation. While these studies are useful to improve our fundamental knowledge of the membrane process, the scaling-up of their results remains an issue due to differences in filtration-time and hydraulic conditions in bench scale membrane cell and actual spiral wound modules (AYACHE *et al.*, 2013). As a result, although some important conclusions of the NF performance can be obtained from bench scale tests, these results cannot be directly applied to long term fouling of large-scale systems (SHETTY and CHELLAM, 2003). Moreover, some operating conditions can only be evaluated in pilot systems. Examples include the hydrodynamic flow conditions and the factors that influence it; and the monitoring of process performance and permeate flux over long periods of time. So, these pilot experiments provide more reliable information about fouling rates, cleaning methods and long-term membrane stability (FRANK *et al.*, 2002).

In previous studies, bench scale integrated UF-NF was evaluated and proved to be a favorable treatment for the gold mining industry effluent. As reported in Chapter 2, the UF-NF of the effluent allowed for high rejections of sulfate, calcium and magnesium. In Chapter 3, the NF membrane stability over effluent and acid cleaning solution was assessed. It was concluded that even long-term exposure did not significantly impact membrane rejection and permeability. Thus, due to the good results observed in bench scale, this Chapter aims to evaluate the integrated UF-NF system on pilot scale trials.

Consequently, the goal of this Chapter was to evaluate different NF membrane fouling control strategies in a UF and NF pilot plant applied to the treatment of gold mining effluent. This work focused on the factors that influence the hydrodynamic flow conditions (operating pressure and feed cross-flow velocity in the module), the evaluation of antiscalant application, and the membrane cleaning efficiency by physical cleaning (forward flush) and chemical cleaning.

4.2 MATERIALS AND METHODS

4.2.1 Effluents from gold mining and description of the effluent treatment process

Two effluents from a gold mining, i.e., the effluent from the sulfuric acid production plant and the water from the calcined dam, were mixed at a 1:1 ratio and, in this study, this mixture is referred to as "effluent from gold mining". Further information on the mining production process, the collection points of the effluent and their characterization can be found in Chapter 2 (Section 2.2.1).

As discussed in Chapter 2, the treatment process proposed for the effluent consisted of a pH adjustment to 5.0 with a NaOH solution, ultrafiltration, and nanofiltration (Figure 3.1).

4.2.2 Experimental setup

Tests were conducted in bench and pilot scale units using ultra and nanofiltration membranes ZeeWeed and NF90. Both tests conditions are described below.

4.2.2.1 Bench scale integrated UF-NF

Figure 4.1 shows a schematic diagram of the UF and NF bench scale unit. More informations about the unit, including membrane area and pumps maximum pressures and flow rates, may be found in Chapter 2, Section 2.2.2.

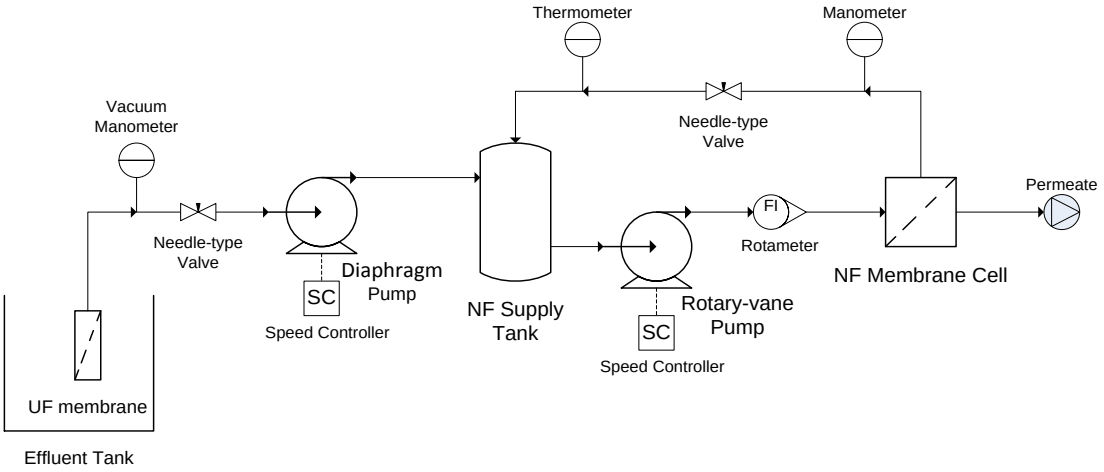

Figure 4.1 – Schematic of UF and NF bench-scale unit

4.2.2.2 Pilot scale integrated UF-NF

Figure 4.2 shows a schematic diagram of the pilot scale integrated UF-NF unit. The mixed effluent was sent to an effluent tank with a volume of 250 L. The pH was manually adjusted in this tank to 5.0 with 10% NaOH solution. Then, a centrifugal pump with maximum flow of 40 L/h trasfered the effluent to a submerged UF tank with a volume of 77 L. The submerged UF module had a membrane area of 0.9 m². The UF permeate was connected to a vacuum tank with a volume of 20 L. Vacuum was generated by a vacuum diaphragm pump with a maximum flow of 60 L/h. The pressure was measured by a manometer and adjusted by a needle-type valve. The permeate flux was monitored by measuring the time required to fill the vacuum tank. The UF concentrate was manually removed daily.

Once the vacuum tank was full, the UF stopped and a solenoid valve opened to discharge the UF permeate to the NF supply tank. The NF supply tank had a volume of 450 L. A second diaphragm pump equipped a with speed controller and a maximum flow of 324 L/h was used for the NF system. A manometer and a needle-type valve at the concentrate stream were used to adjust the operating conditions of this process. Permeate and concentrate flow rates were measured by a rotameter. A commercial spiral wound NF module (NF90-2540 - DowFilmtec) with a membrane area of 2.6 m² was applied.

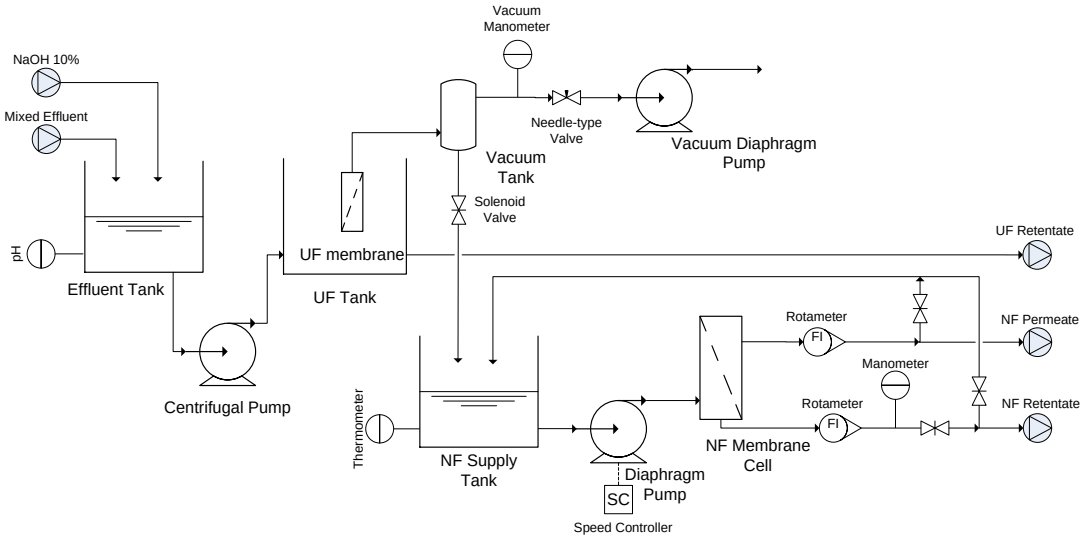

Figure 4.2 – Schematic of UF and NF pilot-scale unit

4.2.3 Experimental procedure

The experimental procedure followed in both bench and pilot scale tests are described in this Section. In this Chapter, the retention efficiencies of the UF and NF (E_{UF} and E_{NF}) were calculated according to Equation 4.1 and Equation 4.2.

$$E_{UF} = {(C_{effluent} - C_{pUF})}/{C_{effluent}}\, x100\% \qquad \text{Equation 4.1}$$

$$E_{NF} = {(C_{pUF} - C_{pNF})}/{C_{pUF}}\; x100\% \qquad \text{Equation 4.2}$$

where $C_{effluent}$, C_{pUF} and C_{pNF} are the conductivities, ion concentrations or arsenic concentrations in the effluent after pH adjustment, UF permeate and NF permeate, respectively. As shown in Equation 4.1, the E_{UF} comprises the retention efficiency of the UF, excluding the removal by precipitation caused by the pH adjustment.

4.2.3.1 Bench scale UF and NF experimental procedure

Firstly, UF membrane was cleaned with a 200 ppm NaClO solution in an ultrasound bath for 20 min. The membrane was then flushed with distilled water. The UF tests were carried out with 4 liters of mining effluent at pH 5.0. UF was carried out at a constant pressure of 0.3 bar. Permeate flux was measured every 15 minutes. Samples of the effluent after pH adjustment and UF permeate were collected and analyzed as described in Chapter 2, Section 2.2.5.

In all bench scale NF tests, the pressure and feed flow rate were set at 10 bar and 144 L/h respectively. This gives a cross-flow velocity of 1.9 m/s and a Reynolds number of 847 (for details about calculation, please see in Section 2.2.4 the Equation 2.1, Equation 2.2 and Equation 2.3).

Before each experiment, the NF membrane was cleaned by soaking in citric acid solution at pH 2.5 followed by 0.1% NaOH solution in an ultrasound bath for 20 min. After that, the membrane was flushed and compacted with distilled water. The permeate flux was periodically measured by collecting the volume of permeate produced in 60 seconds in a measuring cylinder. The feed temperature was monitored and maintained at approximately 25°C. Permeate flux was normalized to 25°C by means of a viscosity correction factor (DRAK *et al.*, 2000).

To evaluate the system behavior with increasing feed concentration and permeate recovery rate (RR), 10 liters of ultrafiltered effluent at pH 5.0 was fed into the NF system. The NF unit was operated with continuous permeate removal and concentrate recycle to NF supply tank. NF was carried out until RR of 72%. Samples of the feed effluent and NF permeate were collected and analyzed for conductivity.

To evaluate the long-term operation of the bench scale unit, NF was carried out in semi batch form. Initially, 2 L of the UF permeate were added to the NF supply tank. The NF permeate was continuously collected, whereas the concentrate was returned to the supply tank. Then, once the RR reached 40%, every time 200 mL of permeate were collected, 500 mL of the UF permeate were added to the supply tank, so that the RR remained close to 40%. The test was conducted for 1,500 minutes (after RR stabilization) and a total of 18.5 L of the UF permeate were used. The permeate flux was monitored regularly and feed and permeate were separated for physico-chemical analysis.

4.2.3.2 Pilot scale UF and NF experimental procedure

UF was continuously performed in the pilot scale plant. The pH of the effluent was adjusted to 5.0 and, subsequently, it was ultrafiltered at a pressure of 0.25 bar. Samples of the effluent after pH adjustment and UF permeate were collected periodically and the removal retentions were calculated by Equations 4.1 and 4.2.

Tests were carried out in the NF pilot scale unit to evaluate the effects of pressure, cross-flow velocity, concentration, antiscalant usage, and physical and chemical cleaning on membrane

performance. Before each test, tap water was recirculated through the module at a flow rate of 144 L/h for 30 minutes and the water flux was measured at 6 bar. If it was close to the flux of the virgin membrane (which was around 42 L/h.m² at 6 bar), the module was considered clean and the next test was started. Otherwise, a chemical cleaning procedure was performed. This cleaning consisted of recirculating 0.2% HCl solution for 90 minutes. After cleaning, the membrane was compacted with tap water for 60 minutes. The water flux was again measured at 6 bar and compared to that of the virgin membrane.

In all tests, the feed temperature was monitored and the permeate flux was measured periodically. Permeate flux was normalized to 25°C using the viscosity correction factor. Feed and permeate samples were collected and analyzed for conductivity, pH, sulfate, calcium, magnesium, and arsenic (as described in Chapter 2, Section 2.2.5). A summary of the operating conditions for each test is found in Table 4.1.

Table 4.1 – Operating conditions of the pilot scale tests

Test	Operation	Initial feed volume (L)	Feed flow rate (L/h)	Operating pressure (bar)	Total filtration time (min)	Antiscalant usage	Physical cleaning
Effect of operating pressure	Batch [a]	200	144	4, 6, 8 and 10	240	No	No
Effect of feed cross-flow velocity	Batch [a]	200	90, 96, 120, 144, 168, 384	6	240	No	No
Concentration test (without antiscalant)	Semi-batch [b]	180	90	6	360	No	No
Concentration test (with antiscalant)	Semi-batch [b]	180	90	6	360	Yes	No
Physical cleaning	Continuous [c]	75	90	6	3,540	Yes	Yes
Chemical cleaning	Continuous [c]	75	90	6	19,100	Yes	No

[a] The concentrate and permeate were returned to the NF supply tank.

[b] The concentrate was returned to the NF supply tank and the permeate was continuously collected.

[c] The concentrate and permeate were partially removed and partially returned to the supply tank to maintain the volume of effluent in the NF supply tank constant.

The commercial antiscalant agent Acumer 4300 (Dow Filmtec) at a dosage of 10 ppm was used for antiscalant evaluation. According to the manufacturer, the product consists of maleic multipolymer and was developed to prevent both calcium carbonate and calcium sulfate salt deposition in water systems (DOWFILMTEC™, 2012).

Forward flush was evaluated as a physical cleaning procedure. During forward flush, the system was depressurized while maintaining the same feed flow rate (equal 90 L/h). The physical cleaning frequency assessed was two minutes per hour. Chemical cleaning with 90-minute 0.2% HCl solution recirculation was evaluated after continuous operation for intervals of 100 and 215 hours (600 and 1290 minutes). Water flux at 6 bar was measured before and after the cleanings.

4.2.3.3 Calculations

The Reynolds number and mass transfer coefficient were calculated for each pilot test to determine the effects of feed flow rate and cross-flow velocity on the NF performance. According to Van Gauwbergen and Baeyens (1997), cross flow velocity of a spiral wound membrane module (v, in m/s), can be calculated as a function of the feed flow rate (Q_{feed}, in m^3/s), and effective flow area of the feed channel (A_{eff}, in m^2), by Equation 4.3:

$$v = \frac{Q_{feed}}{A_{eff}} \qquad \text{Equation 4.3}$$

and A_{eff} can be obtained from Equation 4.4:

$$A_{eff} = B.d_{sp}.\varepsilon \qquad \text{Equation 4.4}$$

where d_{sp} is the thickness of the channel (m), which is assumed to be twice the average filament thickness of the feed spacer (d_F); B is the module width (m); and ε is the porosity (Equation 4.5, Equation 4.6 and Equation 4.7).

$$\varepsilon = 1 - \left(\frac{V_{sp}}{V_t}\right) \qquad \text{Equation 4.5}$$

$$V_{sp} = 0.5.\Pi.d_F^2.l_m \qquad \text{Equation 4.6}$$

$$V_t = l_m^2.d_{sp} \qquad \text{Equation 4.7}$$

where l_m is the mesh size of the feed spacer (m). In order to calculate Re, the hydraulic diameter (d_h) must be determined by Equation 4.8

$$d_H = \frac{4\varepsilon}{\left(\frac{2}{d_{sp}}\right)+(1-\varepsilon)a_{sp}} \quad \text{Equation 4.8}$$

where:

$$a_{sp} = \frac{A_{sp}}{V_{sp}} \quad \text{Equation 4.9}$$

$$A_{sp} = 2.\pi.l_m.d_{sp} \quad \text{Equation 4.10}$$

Thus, the Re can be calculated by Equation 4.11.

$$Re = \frac{\rho.v.d_h}{\mu} \quad \text{Equation 4.11}$$

The mass transfer coefficient can be calculated using the dimensionless Sherwood number (Sh) which, in spiral wound modules, is associated with the dimensionless numbers of Reynolds and Schmidt (Sc) as shown by Equation 4.12 (SALGADO *et al.*, 2015).

$$Sh = 0.14\, Re^{0.64}\, Sc^{0.42} = \frac{k_i.d_h}{D} \quad \text{Equation 4.12}$$

$$Sc = \frac{\mu}{\rho.D_i} \quad \text{Equation 4.13}$$

where k_i is the mass transfer coefficient (m/s) and D_i diffusivity (m²/s) of a certain component 'i' (WANG *et al.*, 2005).

In order to evaluate the salt precipitation on membrane surface, the calcium sulfate supersaturation index on the membrane surface (SI_m) was determined for the feed concentration test. Detailed procedure for calculation is presented at Chapter 2, Section 2.2.4.7. Calcium sulfate was chosen as representative of salt precipitation as it has a low solubility and a high concentration in effluent from gold mining (Table 2.1) presenting, therefore, a greater precipitation potential.

The concentration polarization factor (CP) was also calculated by Equation 4.14.

$$CP = \frac{C_{im}}{C_{ib}}$$ Equation 4.14

where C_{im} and C_{ib} are the concentrations of the specie i on membrane/solution interface and bulk solution.

The resistance in series concept was used to evaluate the chemical cleaning. The total resistance (R_{total}) was divided into membrane resistance ($R_{membrane}$), physically reversible fouling resistance ($R_{physic-rev}$) and physically irreversible fouling resistance ($R_{physic-irrev}$). $R_{physic-irrev}$ in turn was divided into chemically reversible fouling ($R_{chem-rev}$) and irreversible fouling (R_{irrev}) resistances. Physically reversible fouling resistance comprises the concentration polarization resistance and the resistance from fouling removable by physical cleaning. On the other hand, chemically reversible fouling resistance is the one removable by cleaning procedure with HCl solution. Finally, irreversible fouling resistance comprises the resistances which cannot be removed by physical nor chemical cleanings (Equation 4.15 and Equation 4.16).

$$R_{total} = R_{membrane} + R_{physic-rev} + R_{physic-irrev}$$ Equation 4.15

$$R_{physic-irrev} = R_{chem-rev} + R_{irrev}$$ Equation 4.16

Based on the virgin membrane water flux, the intrinsic membrane resistance to filtration ($R_{membrane}$) was calculated according to Equation 4.17:

$$R_{membrane} = \frac{P}{J_{virgin} \times \mu}$$ Equation 4.17

where J_{virgin} is the water flux at 25°C in m³/s.m² measured before the beginning of the tests, P is the operating feed pressure (600 kPa) and μ is the permeate viscosity in N.s/m², assumed to be equal to water viscosity.

Equation 4.18 was used to calculate the total resistance:

$$R_{total} = \frac{P - \sigma \Delta \pi}{\mu \times J_{effluent}}$$ Equation 4.18

where σ is the reflection coefficient, estimated by the averaged membrane rejection of the major con stituents of the effluent (MATTARAJ *et al.*, 2008), and Δπ is the difference in the osmotic pressure of the solution at the membrane surface and permeate. The osmotic pressure at membrane surface was estimated to be equal to that in concentrate stream. $J_{effluent}$ is the permeate flux in m³/s.m² obtained right before the cleaning procedure.

The osmotic pressure difference between the NF concentrate and the permeate was estimated by the Van't Hoff Equation (Equation 4.19):

$$\Delta\pi = RT\Sigma\Delta C \qquad \text{Equation 4.19}$$

where R is the universal gas constant (L.Pa/K.mol), T is the permeation temperature (K), and ΣΔC is the sum of the difference in molar concentrations of the main dissolved species present in concentrate and permeate (sulfate, calcium, magnesium and arsenic) (mol/L).

The physically irreversible fouling resistance can be calculated by the water flux after 30 min of water recirculation ($J_{physic-clean}$, in m³/s.m²) (Equation 4.20).

$$R_{physic-irrev} = \frac{P}{J_{physic-clean} \times \mu} - R_{membrane} \qquad \text{Equation 4.20}$$

On the other hand, the physically reversible fouling resistance can be calculated by Equation 4.21.

$$R_{physic-rev} = R_{total} - R_{membrane} - R_{physic-irrev} \qquad \text{Equation 4.21}$$

Based on water flux after chemical cleaning ($J_{chem-clean}$), the irreversible fouling resistance can be found (Equation 4.22).

$$R_{irrev} = \frac{P}{J_{chem-clean} \times \mu} - R_{membrane} \qquad \text{Equation 4.22}$$

Finally, chemically reversible fouling resistance was calculated using Equation 4.23.

$$R_{chem-rev} = R_{physic-irrev} - R_{irrev} \qquad \text{Equation 4.23}$$

4.2.4 Economic aspects

A cost estimate of the UF-NF membrane system to treat the gold mining effluent was conducted. The variables considered in this estimate were: the system capital expenditure (CapEx); membrane replacement costs; power consumption costs; system maintenance; chemical products for membrane cleaning; alkalizing agent for pH adjustment; and personnel costs. All calculations were based on a designed system capacity (Q_{des}) of 280 m³/h, which is the gold mining effluent flow rate mentioned by the mining company. The dollar quotation was considered R$ 4.00/US$ 1.00.

The UF-NF CapEx was US$ 2,450,000. The replacement costs of NF and UF membranes were US$ 50 and US$ 75 dollars per square meter, respectively. These prices were provided by a large commercial membrane supplier. The required membrane area was calculated considering stabilized pilot scale permeate flux (10 L/h.m² for NF and 22 L/h.m² for UF). The membrane lifetime was considered to be 5 years (LIIKANEN *et al.*, 2006). Also according to membrane supplier, system maintenance charges were equivalent to 5% of the initial investment.

To estimate the CapEx per cubic meter of effluent, the capital cost was annualized using the amortization factor (*A/P*) as presented in Equation 4.24 (SETHI and WIESNER, 2000).

$$A/P = \frac{i_c(1+i_c)^{DL}}{(1+i_c)^{DL}-1} \qquad \text{Equation 4.24}$$

where i_c is the investment rate, considered equal to 12% in Brazil, and DL is the design life of the plant, taken as 15 years. The capital cost per cubic meter of effluent (C_{cap/m^3}) was obtained from Equation 4.25:

$$C_{cap/m^3} = \frac{CapEx.A/P}{Q_{des}} \qquad \text{Equation 4.25}$$

The NF power consumption, estimated by ROSA 9.1 software (DowFilmtec), was 0.61 kWh/m³ while UF power consumption was 0.22 kWh/m³ (CHEW *et al.*, 2016). The electricity tariff was US$ 0.04/kWh, which is the actual tariff paid by this mining company.

The alkalizing agent used for pH adjustment was NaOH. The volume of NaOH solution used to adjust the effluent pH was measured and used to determine the amount of neutralizing agent required (0.96 $kg_{NaOH}/m^3_{effuent}$). The price of NaOH was US$ 1.00/kg. The cost of cleaning

agents was calculated by considering one chemical cleaning with HCl 0.2% solution every two weeks and HCl 35% solution at the rate of US$ 0.38/L.

Personnel costs included payroll for hiring four technicians/operators and 13 annual salaries plus 100% corresponding to labor costs (payroll taxes and benefits).

4.3 RESULTS AND DISCUSSION

4.3.1 Evaluation of NF at different operating pressures

Figure 4.3 shows the permeate flux and the ratio of permeate flux by initial permeate flux (J/J_0) for the NF at different feed pressures.

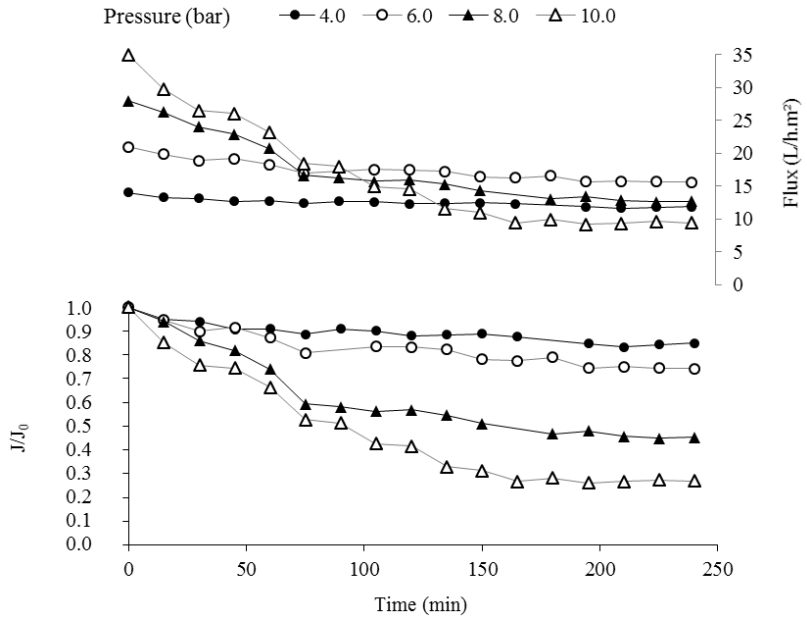

Figure 4.3 – Permeate flux and ratio of permeate flux to initial flux (J/J_0) for different NF pressures. Operating conditions: pilot-scale plant, feed flow rate 144 L/h, without antiscalant.

One may note that the higher the pressure, the greater is the initial flux, but the faster is the flux decay and the lower is J/J_0 after 4 hours of filtration. This is because driving force is enhanced at higher pressures and both solvent and solutes are more convected towards the membrane surface, leading to augmented concentration polarization and fouling and sharp flux decline (KAYA *et al.*, 2010; MUKHERJEE *et al.*, 2016). The concentration polarization factor (CP) was calculated for calcium and sulfate ions for each condition considering the average permeate flux observed between 0 and 15 minute filtration (Table 4.2). The growth in CP caused by

increase in pressure was significant, which resulted in higher filtration resistance. Consequently, the largest flows at the end of the experiment were observed for lower pressures.

Table 4.2 – Concentration polarization factor calculated for each operating pressure

Pressure (bar)	4	6	8	10
$CP_{Ca^{2+}}$	1.87	2.02	2.33	2.62
$CP_{SO_4{}^{2-}}$	1.67	1.78	2.03	2.27

With regard to ions retention, it is observed that, contrary to the findings reported by other authors (KAYA *et al.,* 2009), retention decreased with increasing pressure (Figure 4.4). This can be explained by two factors. On the one hand, it was observed that higher final solvent fluxes were obtained for the lower pressures, which causes a dilution of solutes in the permeate. On the other hand, the higher concentration polarization cause an increase in solute concentration at the membrane surface and, as the intrinsic retention of the membrane remains unchanged, the solute transferred to the permeate increases.

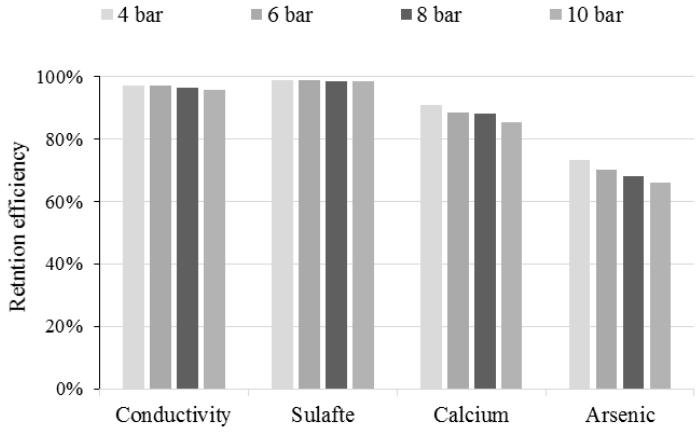

Figure 4.4 – Retention efficiencies of conductivity, sulfate, calcium, and arsenic at different NF pressures

Thus, increasing pressure should be avoided because it leads to higher energy expenditure, but no benefits either in terms of concentration polarization control or in terms of solute retention.

4.3.2 Evaluation of NF at different cross-flow velocities

Figure 4.5 shows the ratio of permeate flux by initial permeate flux for the NF at different feed cross-flow velocities.

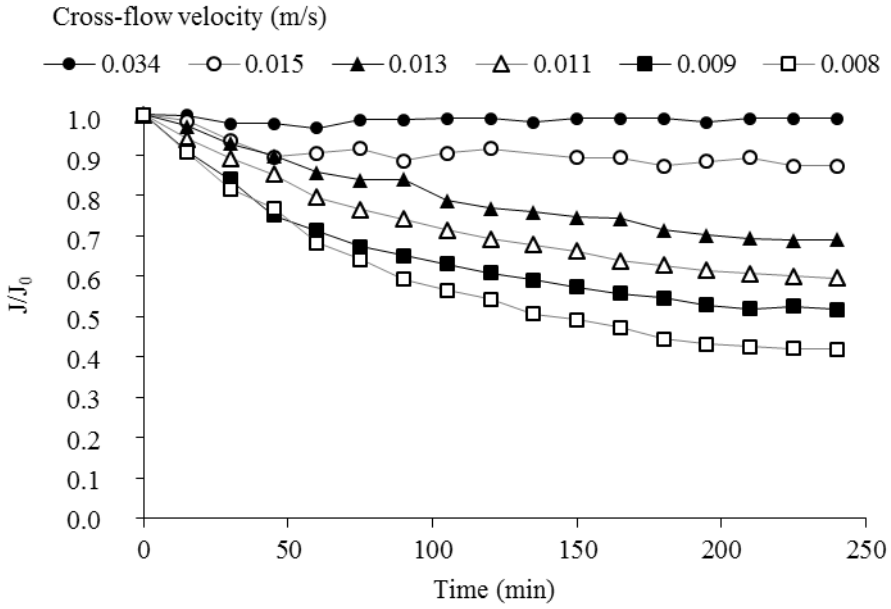

Figure 4.5 – Ratio of permeate flux by initial permeate flux for the NF of gold mining effluent at different cross-flow velocities. Operating conditions: pilot-scale plant, operating pressure 6 bar, without antiscalant.

By increasing the feed flow rate, the cross-flow velocity growths and, consequently, the Reynolds number increases. This leads to a more turbulent flow and improves the mass transfer conditions (Table 4.3), facilitating the back diffusion of solutes retained by the membrane to the bulk solution and reducing the concentration polarization. Consequently, the permeate flux increases for two reasons: reduction of the membrane fouling and reduction of osmotic pressure on the membrane surface, which increases the effective filtration pressure. All the feed flow-rates tested are considered laminar conditions. The transition from laminar to turbulent flow in spiral wound modules occurs between Re numbers of 150 and 300 and depends on the feed spacer features (GERALDES *et al.*, 2002).

Table 4.3 - Flow conditions tested

Feed flow rate (L/h)	Cross-flow velocity (m/s)	Reynolds number	Effective SO_4^{2-} mass transfer coefficient ($x10^5$ m/s)	Effective Ca^{2+} mass transfer coefficient ($x10^5$ m/s)
90	0.008	8	1.08	0.86
96	0.009	8	1.13	0.90
120	0.011	11	1.30	1.04
140	0.013	13	1.46	1.16
168	0.015	15	1.61	1.28
384	0.034	34	2.74	2.18

At higher feed flow rates, since back transport from the membrane surface to the solution bulk is increased, fewer solutes enters the permeate channels (ROY *et al.*, 2015). This can be seen in Figure 4.6, which shows the increase in solutes retention efficiencies at higher cross-flow velocities.

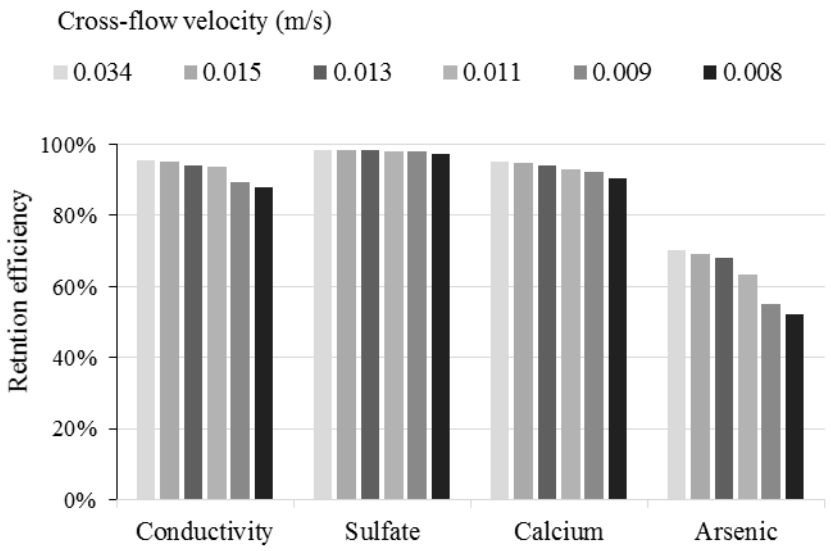

Figure 4.6 – Retention efficiencies of conductivity, sulfate, calcium, and arsenic at different cross-flow velocities

On the other hand, higher feed flow rates require pumps with higher power, which consumes more energy. According to Sethi and Wiesner (2000), the feed pump power requirement (E_f, in W) can be estimated by Equation 4.26:

$$E_f = \frac{P \times Q_{feed}}{\eta}$$ Equation 4.26

where Q_{feed} is the feed flow rate (m³/s), P is the pressure (Pa), and η is the pump efficiency, estimated as 70%. Figure 4.7 shows the nanofiltration permeate flux after 4 hours filtration and the required feed pump power calculated by Equation 4.26 for a single-vessel NF unit (considering a 2.6 m² module) for each cross-flow velocity tested.

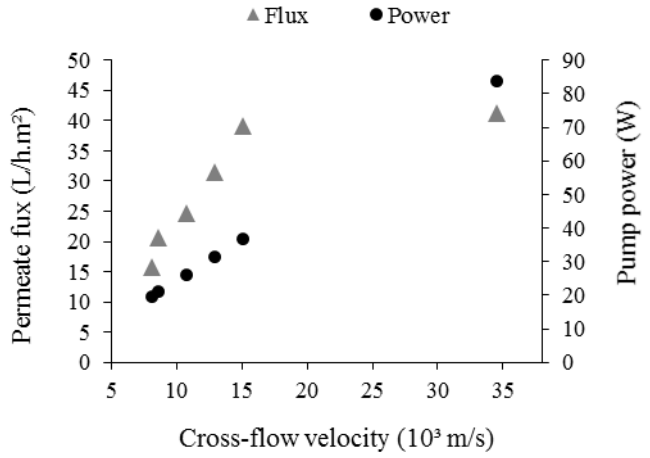

Figure 4.7 – Nanofiltration permeate flux after 4 hours filtration and respective required pump power

It can be seen that 15 x 10^{-3} m/s cross-flow velocity (feed flow rate of 168 L/h) can be regarded as a threshold value. From this point on, little variation was observed on permeate flux. The 4-hour NF fluxes for cross-flow velocities of 15 and 34 x 10^{-3} m/s were 39 and 41 L/h.m², respectively, and they were close to the water permeability (42 L/h.m² at 6 bar). This shows that fouling can be effectively controlled through the improvement of hydrodynamic and mass transfer conditions. Since the required feed pump power is a linear function of the feed flow rate, cross-flow velocities above 15 x 10^{-3} m/s increase the energy expenditure without providing benefits in terms of permeate flux, and, therefore, are is not recommended.

4.3.3 Concentration test with and without antiscalant

Sulfate and calcium concentrations in the effluent were close to 3,700 and 560 mg/L respectively. The calcium sulfate supersaturation index was 1.52, which means that the effluent was already saturated. Although precipitation may be expected when SI >1, a significantly

higher value of supersaturation index must be reached to result in scaling because of kinetics and metastability effects (SCHÄFER *et al.*, 2005). The presence of other cations in the effluent, such as Mg^{2+}, can also hinder the calcium sulfate precipitation when the SI is slightly larger than 1, since the availability of sulfate ions for gypsum incipient nuclei formation is reduced because of the competition from $MgSO_4$ complexation (LE GOUELLEC and ELIMELECH, 2002). According to Dydo *et al.* (2004), scaling can be prevented if SI_{CaSO_4} < 1.62 to 2.02.

On the other hand, once the nanofiltration begins, the formation of the boundary layer and concentration polarization starts. This increases the concentration of solutes on the membrane surface and the SI_m (Table 4.4). It can be seen that, even for a permeate recovery rate as low as 10%, the solution SI_m was above 2.8. Moreover, as the RR increases, the ionic concentrations on the concentrate increases, consequently increasing the SI_m. This suggests the importance of antiscalant usage to minimize membrane fouling.

Table 4.4 – $CaSO_4$ supersaturation index at the membrane surface (SI_m) for different permeate recovery rates during effluent nanofiltration without antiscalant. Operating conditions: pilot-scale plant, feed flow rate 90 L/h, operating pressure 6 bar, without antiscalant.

RR	10%	20%	30%	40%	50%	60%	70%	80%	90%
SI_m	2.86	2.96	2.96	3.29	3.27	3.45	4.07	5.38	10.68

Figure 4.8 shows the NF permeate conductivity and the ratio of permeate flux by initial flux for different RR values with and without antiscalant dosage. It is noted that, until a RR of approximately 40%, permeate flux with and without antiscalant is similar. After that RR, the permeate flux without antiscalant is always lower, indicating higher membrane fouling.

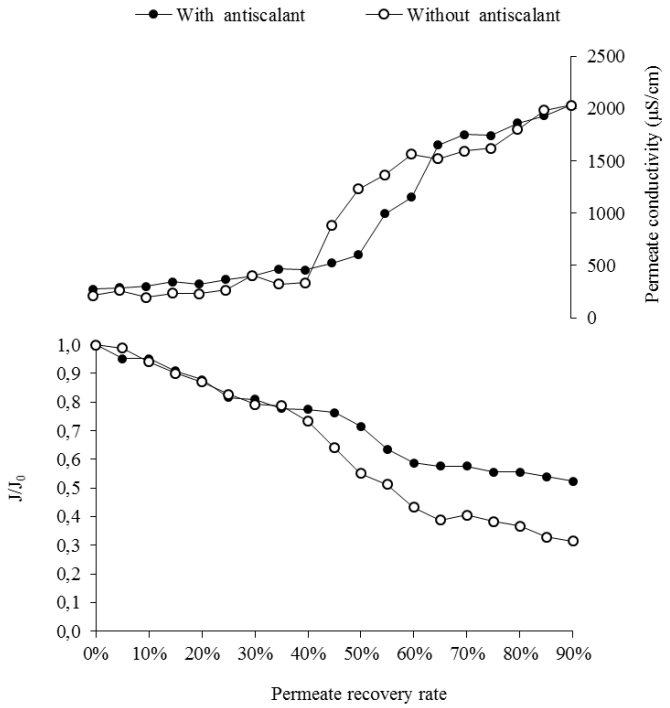

Figure 4.8 – Conductivity retention efficiency and ratio of permeate flux by initial permeate flux for different permeate recovery rates with and without antiscalant dosage. Operating conditions: pilot-scale plant, feed flow rate 144 L/h, operating pressure 6 bar.

According to the supplier, the antiscalant Acumer 4300 acts through at least three mechanisms: solubility enhancement or threshold effect, which reduces precipitation of low solubility inorganic salts; crystal modification, which deforms the growing inorganic salt crystals to give small, irregular, readily fractured crystal that do not adhere well to surfaces; and dispersing activity, which prevents precipitated crystals or other inorganic particles from agglomerating (DOWFILMTEC™, 2012). Al-Roomi and Hussain (2015) concluded that maleic anhydride based polymers can adsorb on both seeds, inhibiting the nucleation phase, and microcrystals. In the second case, the polymer may convey a higher negative charge to the crystals, which slows agglomeration, settling and deposition. The presence of antiscalant agents can also interfere with the regular crystal structure and thereby increase the internal stress and prevent the deposition of microcrystals.

Therefore, the global effect of antiscalant dosage is to reduce the formation of precipitates that can deposit at the membrane surface. At permeate recovery rates below 40%, NF performance with and without antiscalant was almost identical, which suggests that the deposition of $CaSO_4$ or other salts at the membrane surface was low. With the increase in the RR, the supersaturation index of calcium sulfate became higher than 3.0 (Table 4.4) and, consequently, fouling was

expected when antiscalant was not used. This explains the higher permeate flux observed with antiscalant usage.

The permeate conductivity with and without antiscalant dosage tends to increase with the increment of the RR and the concentration of ions in the concentrate stream. The increase of ionic concentration in the concentrate solution causes elevation in solute concentration at the membrane-solution interface, and, as the intrinsic retention of the membrane remains unchanged, the solute flux to the permeate increases. The permeate conductivity follows a similar patter to that of the permeate flux. Up to a RR of approximately 40%, the conductivity of permeates with and without antiscalant dosage were similar. At RR higher than 40%, the values for NF with antiscalant were lower. This can be related to the deposition of precipitates at the membrane surface of NF without antiscalant. The formation of such deposits reduces solute diffusion from the vicinity of the membrane surface back to the bulk solution, resulting in the cake-enhanced concentration polarization effect (VOGEL *et al.*, 2010). This causes the concentration of ions in the membrane-solution interface to be higher, promoting a higher solutes concentration in the permeate.

Therefore, it can be seen that, for the effluent studied, antiscalant is an important asset to minimize fouling, as it increases permeate flux by 13 to 36% for RR of 45 to 90%. Moreover, antiscalant dosage decreased solutes flux and improved the final permeate quality.

Figure 4.9 shows the permeate conductivity and flux as a function of permeate RR in bench and pilot scale tests without antiscalant dosage. The fouling tendency, observed by the decrease of permeate flux (Figure 4.9 a), was considerably higher in the bench scale unit. This difference is attributed to three factors. First, the pressure applied at bench scale test was higher, which leads to higher permeate flux. It caused increased concentration polarization and fouling. Secondly, the hydrodynamic condition of the bench unit (Re = 850) is theoretically much favored over the pilot unit (Re = 8). However, membrane cells traditionally used in laboratory experiments have a very bad flow distribution, presenting short circuiting of the feed stream and recirculation areas where the flow velocity is very low (CORTÉS-JUAN *et al.*, 2011). Finally, due to the low filtration area of the bench scale membrane cell, more than 57 hours of filtration were required to concentrate 10 L of effluent to a RR of 70%, which caused an excessive recirculation of the concentrate to the supply tank. On the other hand, in the pilot scale unit, less than 6 hours were required to concentrate 180 L of effluent to a RR of 90%.

Since salts precipitation and fouling formation are time-dependant (LYSTER *et al.*, 2010), extending the bench scale test duration may have caused an overestimation of the fouling formation. According to Gorzalski and Coronell (2014), bench scale fouling tests produced foulant layers that were different in composition from those generated at full scale units. The dissimilarities between bench and full scale results were likely caused by the various challenges in reproducing full scale conditions at bench scale units, particularly the use a one pass filtration scheme.

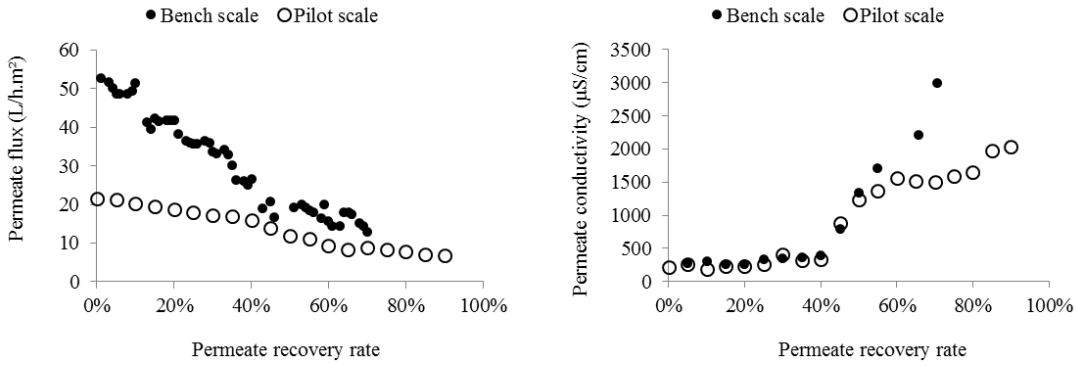

Figure 4.9 – (a) Permeate flux, and (b) permeate conductivity for the concentration test on bench and pilot scale without antiscalant

However, up to a RR of approximately 45%, no difference was observed in the permeate conductivity between bench and pilot scale tests (Figure 4.9 b). At RR higher than 50%, the conductivity of the pilot scale permeate was increasingly lower than the one obtained at bench scale. This can also be related to the overestimation of the membrane fouling in the bench scale tests and consequent cake-enhanced concentration polarization effect. These results corroborate the importance of evaluating the nanofiltration in a pilot scale unit in order to collect data for scale up.

It must be emphasized that the permeate conductivity remained low (< 400 µS/cm) and almost constant up to a RR of 40% for both cases, bench and pilot scale. From this RR onwards there was a significant increase in the permeate conductivity. Therefore, in order to maintain a high permeate quality and generate a treated effluent fit for industrial reuse, the pilot test indicated a maximum RR of 40%, which validated the results obtained in the bench scale unit (Chapter 2).

4.3.4 Evaluation of physical cleaning

In order to evaluate the effectiveness of physical cleaning to control membrane fouling, nanofiltration permeate flux was monitored for operation with and without periodic forward flush (forward flush was carried out for 2 min every 58 min of nanofiltration). The dashed line in Figure 4.10 indicates the chemical cleaning processed after the operation without physical cleaning, and subsequent change to operation with periodic forward flush.

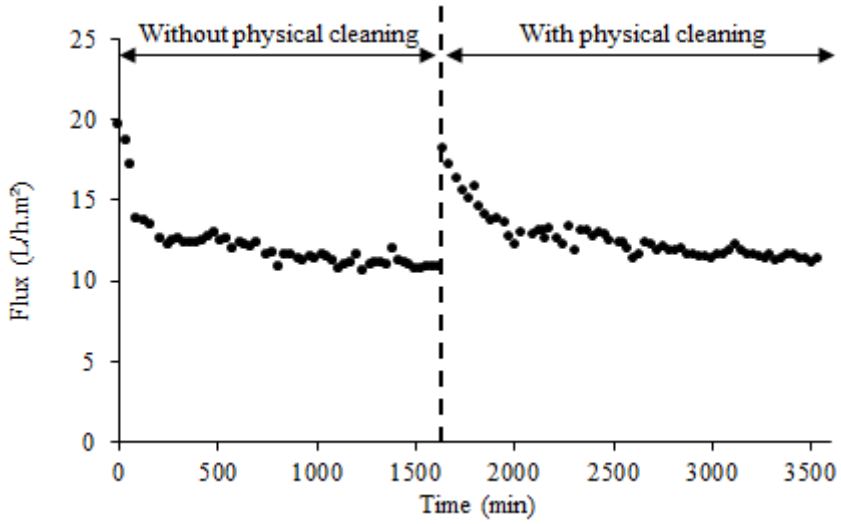

Figure 4.10 – NF permeate flux with and without forward flush physical cleaning. Operating conditions: pilot-scale plant, feed flow rate 90 L/h, operating pressure 6 bar, with antiscalant.

From Figure 4.10 it is observed that the flux pattern followed a typical flux decline kinetic: at the beginning there is a remarkable decrease of flow followed by a less-sharp progressive decay, which can be assumed to tend to zero (SALGADO *et al.*, 2015). Physical cleaning reduced the rate of the first stage flux decay. In the initial 210 minutes of operation, the average variation rate of the permeate flux without physical cleaning was -0.034 L/h.m².min; while with physical cleaning this variation was 45% lower, corresponding to -0.018 L/h.m².min. However, after the initial transient period, semi-steady state was achieved and the permeate flux tended to a constant value in both cases due to the presence of forced convection by the concentrate stream in the axial direction (MUKHERJEE *et al.*, 2016). The final fluxes of the two operating conditions were similar, respectively 10.8 and 11.3 L/h.m² for the processes with and without physical cleaning. Although the stabilized flux with physical cleaning was 4% higher, the productivities in both cases were almost the same. Since with physical cleaning the

nanofiltration was carried out for 58 min per hour, and in the remaining 2 min there was no permeate generation, the system productivity with physical cleansing was 10.9 L/h.m².

During NF, mass transfer of solutes from the solution bulk to the membrane surface occurs because of the convective flux of permeate. The retained solutes, which are concentrated in the membrane-solution interface and create a concentration gradient, are transported back to the bulk of the solution by diffusion (BHATTACHARYA and HWANG, 1997). Since with forward flux the recirculation of the feed stream is maintained in the absence of permeate flux, the convective flux of solutes towards the membrane stops and the foulants returns to the solution bulk. As a result, physical cleaning can contribute to slowing the fouling process by removing part of the accumulated material at the membrane surface and delaying the consolidation of the boundary layer. However, once the salts begin to precipitate, deposit or adsorb on the membrane, physical cleaning by forward flush alone is unable to remove them. This would explain why the initial permeate flux decay with physical cleaning was lower than without physical cleaning, but the steady flux was similar in both conditions.

The retention efficiencies of operation with and without physical cleaning are shown in Table 4.5. The results shown here are the averages of three samplings. It can be seen that there is no major difference between these two conditions.

Table 4.5 – Retention efficiencies of conductivity, sulfate, calcium, and arsenic during operation with and without forward flush

Physical cleaning	NF retention efficiency				
	Conductivity	Sulfate	Calcium	Magnesium	Arsenic
No	95%	98%	88%	83%	54%
Yes	95%	99%	90%	84%	52%

In conclusion, for long-term continuous operation physical cleaning has little impact on fouling control and on the maintenance of the membrane permeability. Moreover, it did not alter NF retention efficiencies. Similar results were found by Bonné *et al.* (2003) who evaluated periodical air flush (15 s air and 45 s water flush), and by Kramer *et al.* (2015) who evaluated 5 min of forward flush every 24 h of filtration. Finally, the use of these methods usually results in a more complex system control and equipment design (AL-AMOUDI and LOVITT, 2007),

and reduces the system productivity. Therefore, it was not an effective fouling control strategy for the mining effluent.

4.3.5 Evaluation of chemical cleaning

Chemical cleaning was applied after 100 and 215 hours of continuous NF (Figure 4.11). The flux pattern was similar to the one observed in Figure 4.10, which comprised an initial sharp flux decline, related to concentration polarization development, followed by slow permeate flux decay. The resistances to filtration measured after 100 and 215 hour-NF are shown in Figure 4.12.

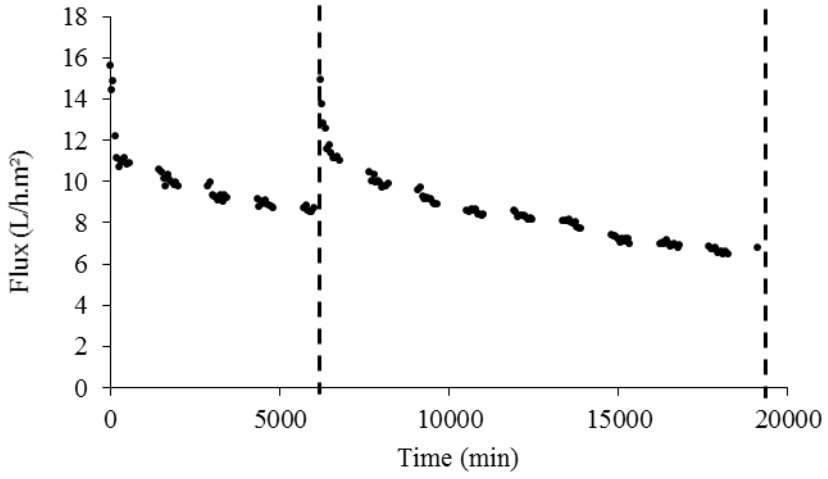

Figure 4.11 – NF permeate flux as function of time. The dashed line indicates the chemical cleaning. Operating conditions: pilot-scale plant, feed flow rate 90 L/h, operating pressure 6 bar, with antiscalant, no application of forward flush.

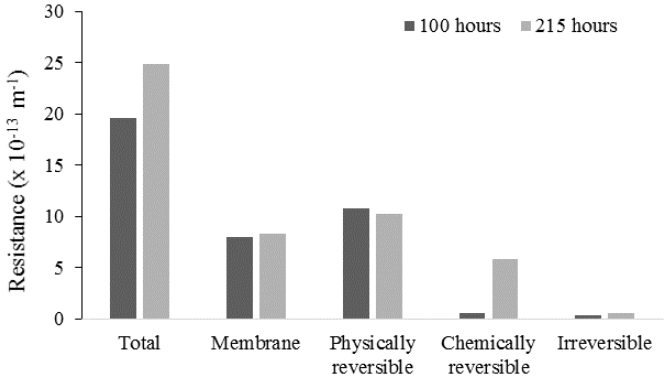

Figure 4.12 – Resistances to filtration after 100 and 215-hour continuous NF

The increase in filtration time from 100 to 215 hours increased the total resistance by almost 30%. This growth is mainly due to increased strongly attached fouling, which cannot be removed by physical methods but only by chemical cleaning. This reinforces the importance of choosing the best cleaning procedure so that fouling can be effectively removed and does not became irreversible.

On the other hand, the physically reversible fouling resistance was substantially similar in both cases (variation of only 5%). This resistance is mainly related to concentration polarization. Therefore it was concluded that the development of the polarized layer occurred rapidly, and thereafter there was no increase in its influence on the filtration process. This is consistent with the flux profile from Figure 4.11.

Irreversible fouling, although minor contributor to the total resistance, experienced an increment of 70% with increasing filtration time. Thus, in order not to cause irreversible loss of permeability over time, the best chemical cleaning frequency must be assessed.

The characterization of UF feed, UF permeate and NF permeate obtained during different filtration tests (with or without physical cleaning and at different chemical cleaning frequency) is shown in Figure 4.13. The dashed lines represented the application of NF chemical cleaning procedure. It is clear that there was a progressively loss of permeate quality after the chemical cleanings, with increase in permeate concentrations of sulfate, arsenic, calcium and magnesium. It was attributed to both permeate flux reduction and solutes accumulation over membrane surface. Thus, evaluation of the optimum chemical cleaning frequency is also needed in order to maintain the high quality of the permeate.

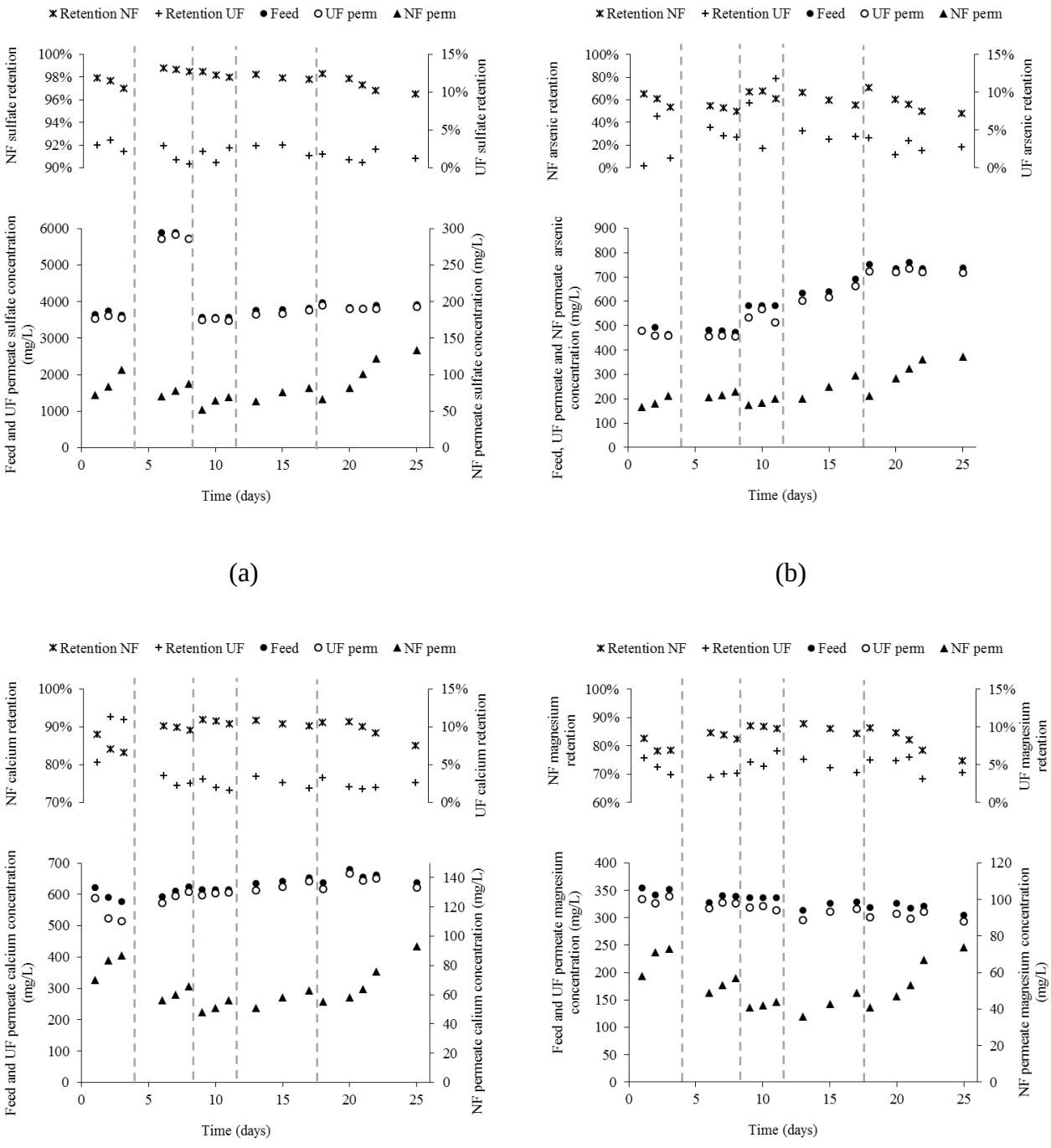

Figure 4.13 – Characterization of UF feed, UF permeate and NF permeate in terms of (a) sulfate, (b) arsenic, (c) calcium and (d) magnesium. Dashed lines represented NF chemical cleanings.

4.3.6 Bench and pilot scale integrated UF-NF performance

Table 4.6 presents the UF average retention and permeate flux in both bench and pilot scale tests. The UF had low retention efficiencies (below 7%) for all evaluated parameters. This result is consistent with the effluent characterization (Table 2.1) since most of the contaminants are dissolved inorganic solids which are not efficiently removed by the UF membrane. The small observed retention of sulfate, calcium, magnesium and arsenic is due to electrostatic interactions between the solutes and the membrane surface and pores (ALVENTOSA-DELARA *et al.*, 2014) or ion adsorption on membrane or cake (TANHAEI *et al.*, 2014). Moreover, the retention efficiencies in bench and pilot scales were similar. Since the same membrane was used in both tests and operating conditions do not influence significantly ion retention by UF (ALVENTOSA-DELARA *et al.*, 2014), this similarity was expected. In relation to fouling, the bench scale UF showed better performance. Differences in hydrodynamic conditions and total filtration time may have caused this.

Table 4.6 – Average physico-chemical characteristics and operating parameters of the UF of mixed gold mining effluent

Sample		Sulfate	Calcium	Magnesium	Arsenic	Permeate flux	Pressure	Permeability
Bench scale [a]	Gold mining effluent at pH 5.0 (mg/L)	3,694	532	468	524	-	-	-
	UF permeate (mg/L)	3,582	511	437	516	-	-	-
	UF removal efficiency	3%	4%	7%	1%	-	-	-
	Filtration parameters	-	-	-	-	71 L/h.m²	0.3 bar	238 L/h.m².bar
Pilot scale [b]	Gold mining effluent at pH 5.0 (mg/L)	4,190	607	341	596	-	-	-
	UF permeate (mg/L)	4,114	579	325	571	-	-	-
	UF removal efficiency	2%	5%	5%	4%	-	-	-
	Filtration parameters	-	-	-	-	22 L/h.m²	0.25 bar	89 L/h.m².bar

[a] average of 5 samples

[b] average of 14 samples

Permeate flux and permeability measured in 1500-1800 minute-nanofiltration are shown in Figure 4.14. Bench and pilot scale tests were conducted at 10 and 6 bar and permeate RR of 36-

40% and 30-43%, respectively. Permeability ($K_{effluent}$, in L/h.m².bar) was calculated according to Equation 4.27.

$$K_{effluent} = \frac{J_{effluent}}{\Delta P - \sigma \Delta \pi} \qquad \text{Equation 4.27}$$

The membranes have similar initial permeability. Due to the higher pressure applied, the permeate flux at the bench scale test was higher. However, the greater convective flow of solutes towards membrane causes higher concentration polarization and fouling, leading to a more pronounced permeability decay. Difference in hydrodynamic conditions, discussed in Section 4.3.3, may also have caused this discrepancy.

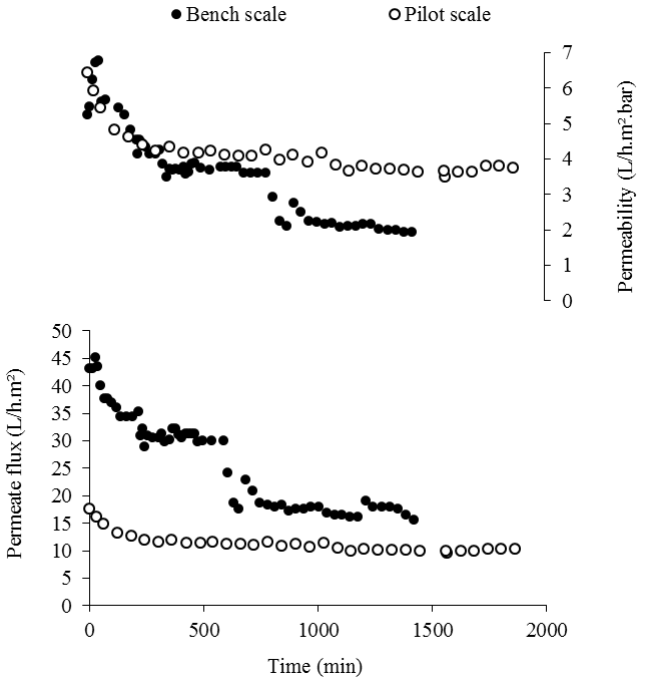

Figure 4.14 – Permeate flux and permeability measured for bench and pilot NF

Regarding solutes retention (Table 4.7), it is possible to note that pilot sulfate retention is slightly higher and calcium, magnesium and arsenic retentions are lower than the bench scale's. This may be due to differences in concentrations levels of the raw effluents, since different samples were used in each test.

Table 4.7 – Physico-chemical parameters of bench and pilot scale NF feed and permeate

Scale	Sample	Conductivity (µS/cm)	Sulfate (mg/L)	Calcium (mg/L)	Magnesium (mg/L)	Arsenic (mg/L)
Bench scale [a]	NF feed	3970	2553	426	110	506
	NF permeate	238	126	24	6	161
	Retention	94%	95%	94%	95%	68%
Pilot scale [a]	NF feed	4649	4040	605	315	581
	NF permeate	265	83	64	53	239
	Retention	94%	98%	89%	83%	59%

[a] average of 17 samples

4.3.7 Economic aspects

Table 4.8 shows the treatment cost by UF and NF of the mining effluent in US$/m^3. The highest cost is associated with pH adjustment (alkalizing agent). However, as the effluent has an acidic pH, neutralization is necessary even for conventional treatments, like precipitation and sedimentation, and effluent discharge in water bodies. Capital cost amortization is the second highest cost. This reflects the high cost of equipment initial purchase. Although the cost with cleaning agent is almost negligible, the high cost of membrane replacement reinforces the importance of establishing the best chemical cleaning conditions and operation, aiming at increasing the membrane lifetime.

Table 4.8 – Mining effluent treatment costs by UF and NF

Item	Cost (US$/m³)	Cost (%)
Membrane replacement	0.117	9%
Capital cost amortization	0.147	11%
Alkalizing agent	0.960	72%
Cleaning agent	0.004	0.3%
Energy	0.034	3%
Maintenance	0.050	4%
Labor	0.027	2%
TOTAL	1.338	100%

The total cost of treatment was US$ 1.34/m³, and this value can be considered low. The cost of the actual wastewater treatment current installed on the gold mining industry, based on precipitation and sedimentation, is US$ 1.60/m³. The current cost of fresh water is US$ 0.18/m³. Since the permeate has quality for industrial reuse, the treatment of this effluent with UF-NF would reduce water consumption by approximately 932,000 m³ per year (considering a UF and

NF permeate recovery rate of 95% and 40%, respectively), representing a saving of more than US$ 165,000.00/year.

4.4 CONCLUSIONS

In Chapter 4, a UF-NF pilot-scale unit was used to evaluate fouling control strategies, aiming at reproducing the filtration time and hydrodynamic conditions of full scale plants.

The changes in flow conditions provided by operating pressure increase were not favorable to the system. The increase of permeate flux increases the concentration polarization and enhances the permeate flux decay. In addition, there were no improvements in retention efficiencies.

On the other hand, the improvement in mass transfer by increasing the feed flow rate and cross-flow velocity can effectively reduce the concentration polarization and fouling tendency. The cross-flow velocity threshold was identified as $15x10^{-3}$ m/s; after this point there was an elevation in energy expenditure, but no benefits in terms of membrane fouling tendency.

Antiscalant usage reduced the permeate flux decay for recovery rates higher than 40%. Since the antiscalant works minimizing the nucleation, growth or deposition of precipitated crystals at the membrane surface, it was conclude that the precipitation of this effluent becomes imperative after 40% of RR.

Physical cleaning by forward flush was not effective for this system. Operation with periodical forward flush showed lower permeate flux decay rate during the initial transient period, however at semi-steady state the system productivity was similar to that of the operation without physical cleaning.

The increase in continuous filtration time from 100 to 215 hours increased the total resistance by almost 30%, which was mainly due to increase in chemically reversible fouling. On the other hand, the physically reversible fouling resistance was similar in both cases (variation of only 5%), indicating no variation in concentration polarization during time after the development of the polarized layer.

The importance of evaluating these operating parameters in a pilot scale unit must be highlighted. It was observed significant differences in the results of permeate flux and retention

efficiencies from the bench and pilot scale tests. These differences were attributed to longer concentrate recirculation and different flow conditions.

The total cost of treatment was US$ 1.34/m³, which is smaller than the actual wastewater treatment current installed on the gold mining industry. It was observed that the highest cost fraction was associated with pH adjustment. Capital cost amortization was the second highest cost.

5 CHAPTER

TREATMENT OF GOLD MINING EFFLUENT BY A TWO-STAGE NANOFILTRATION PROCESS: ARSENIC AND CALCIUM INTERMEDIATE CHEMICAL PRECIPITATION

5.1 INTRODUCTION

Nanofiltration process (NF) can retain efficiently salts and metals cations from aqueous medium (AL-RASHDI *et al.*, 2013; PAGES *et al.*, 2013), and, as a result, present high potential to treat effluents aiming at water reuse. The literature shows the use of NF process to treat different types of effluents, generating a permeate that could be reused for irrigation (AZAÏS *et al.*, 2014; OCHANDO-PULIDO and FÉREZ, 2015), groundwater recharge (AZAÏS *et al.*, 2014), industrial purposes (ANDRADE *et al.*, 2014; KURT *et al.*, 2012; LIU *et al.*, 2011; RIERA *et al.*, 2013), and as potable water (BELLONA *et al.*, 2012; KAPPEL *et al.*, 2014). Moreover, the use of this process has been increasing, mainly because of advantages such as reliability, ease of operation, low power consumption and high efficiency (FU and WANG, 2011).

The permeate recovery rate (RR) is one of the main design parameters of the pressure-driven membrane separation processes (GREENLEE *et al.*, 2009). These are the most well-established membrane technologies and include: microfiltration (MF); ultrafiltration (UF); nanofiltration (NF); and reverse osmosis (RO). While MF and UF usually operate at RR of 90-96%, for NF and RO these values are substantially lower (BI *et al.*, 2014). Since NF and RO membranes are much more permeable to water than to solutes, increasing the permeate RR induces an increase in salt concentration in the bulk solution; which consequently increases the fouling-potential and the precipitation of sparingly soluble salts (PÉREZ-GONZÁLEZ *et al.*, 2012). Although inorganic fouling (or scaling) may be partially inhibited by antiscalants dosage, antiscalant is not recommended if the salt supersaturation index is very high (HYDRANAUTICS, 2008). Consequently, membrane scaling reduces the NF permeate productivity by forcing an operation at recovery rates lower than optimal; and, at the same time, increases the concentrate volume, which is an unwanted product of this process (SUBRAMANI *et al.*, 2012).

For many inland locations, the management and disposal of the concentrate represents a limiting step for the implementation of NF and RO technologies. For example, desalination plants usually operate with water recoveries rates ranging from 35 to 85%. This implies in huge volumes of concentrate solute-rich, which are frequently discharged into the water bodies and constitute a serious threat to marine ecosystems. Accordingly, there is an urgent need for environment-friendly management options for the concentrate (PÉREZ-GONZÁLEZ *et al.*, 2012).

The integration of NF and/or RO with intermediate chemical demineralization was shown to be a promising technique for concentrate minimization in brackish water desalination (GABELICH *et al.*, 2011; QU *et al.*, 2009; RAHARDIANTO *et al.*, 2007; SUBRAMANI *et al.*, 2012). It consists of removing mineral scale cations (e.g., calcium, barium, strontium, etc.) as solid precipitates from the concentrate of the first-stage membrane process. This allows subsequent water recovery in a second-stage membrane process (GABELICH *et al.*, 2011). The removal of scale cations is mostly accomplished through chemical softening (COMSTOCK *et al.*, 2011; GABELICH *et al.*, 2011; GREENLEE *et al.*, 2010; RAHARDIANTO *et al.*, 2007; SUBRAMANI *et al.*, 2012) or seeded precipitation (MCCOOL *et al.*, 2013; QU *et al.*, 2009; RAHARDIANTO *et al.*, 2010). This work will focus on chemical softening.

Gold mining effluents are characterized by high concentrations of species with high fouling tendency, such as sulfate, calcium, and magnesium (RICCI *et al.*, 2015; SIMATE and NDLOVU, 2014; VISSER *et al.*, 2001); especially when the processed ore is rich in sulfide (SÁNCHEZ-ANDREA *et al.*, 2014). Moreover, gold ores are frequently associated with toxic elements (GONZÁLEZ *et al.*, 2012), and, as a result, gold ore processing may generate an effluent with toxic metal cations and oxy-anions, including mercury, selenium, molybdenum, cadmium, chromium, lead, barium, zinc, aluminum, and arsenic (LANGSCH *et al.*, 2012; MYAGKAYA *et al.*, 2016). Therefore, the gold mining effluent can contaminate surface and groundwater (LUSILAO-MAKIESE *et al.*, 2013; NING *et al.*, 2011).

Arsenic is a persistent, bio-accumulative, toxic element, often found in effluents from the mineral-processing industries. It is derived from extraction of metals by oxidation and acid dissolution of the arsenic-containing minerals such as arsenopyrite or Ni–Co–Fe arsenides and sulfarsenides presented in many gold and uranium ores (JIA and DEMOPOULOS, 2008). Among the available technologies, effluent neutralization accompanied by arsenic coprecipitation with ferric iron is the industrial method of choice when it comes to the removal of arsenic from acidic mineral-processing effluents (JIA and DEMOPOULOS, 2008).

The efficiency of arsenic removal by coprecipitation is influenced by several factors, including the molar ratio of iron/arsenic and the pH (TWIDWELL and MCCLOSKEY, 2011). The arsenic may be removed from the aqueous solution by adsorption or complexation on the surface of the amorphous ferrihydrite, or by precipitation as ferric arsenate, a poorly crystalline material, or as crystalline scorodite. Among these species, scorodite is the most stable form at

low pH values, approximately below 1.7; above this pH, ferrihydrite and arsenical ferrihydrite predominate. The formation of ferric arsenate is especially significant in reactions at low pH and high concentrations of arsenic; whereas high concentration of iron favors the formation of ferrihydrite (DE KLERK *et al.*, 2012; RICHMOND *et al.*, 2004; TWIDWELL and MCCLOSKEY, 2011). In industrial practice, the arsenic is removed and stabilized using a Fe/As molar ratio of 3-4. In these conditions, the precipitated solids are most likely a mixture of ferric arsenate and arsenical ferrihydrite (TWIDWELL and MCCLOSKEY, 2011).

Additionally, the presence of other ions in the effluent solution may have an effect on the coprecipitation of arsenic. Aluminum and calcium can improve arsenic removal (DE KLERK *et al.*, 2012; JIA and DEMOPOULOS, 2008), while nickel had no impact on it (DE KLERK *et al.*, 2012). Although the increase in sulfate concentration have led to an increase in the arsenic concentration of the treated effluent (PAPASSIOPI *et al.*, 1996); the presence of this and other anions, such as phosphate and carbonate, as well as the presence of some cations, such as copper, lead, and zinc, can positively influence the long term stability of the precipitates (TWIDWELL and MCCLOSKEY, 2011). Because of the various inorganic species present in gold mining effluents, the slurry generated in the precipitation process may include calcium, sulfate, and aluminum, amongst many others species besides arsenic and iron. This results in the generation of large amounts of waste material, which may be difficult to filter (TWIDWELL and MCCLOSKEY, 2011). Moreover, the costs for disposing this slurry in specially designed waste storage ponds is high.

Based on the discussion presented here, this Chapter aimed to evaluate an innovative treatment route for recycling gold mining effluents based on integration of two stage NF and intermediate arsenic and calcium chemical precipitation. In a previous study, the operating conditions for NF were evaluated (Chapters 2, 3 and 4). Although the results shown the great performance of NF to treat gold mining effluent for water reuse, the water recovery rate was limited to 40% because of the risk of calcium sulfate precipitation and the decrease of the permeate quality. Thus, in this Chapter a two-step intermediate chemical precipitation was integrated to NF process for the treatment of the NF concentrate and the increase of overall water recovery. The first precipitation step aimed at the removal of arsenic from the aqueous solution by coprecipitation with ferric sulfate. This process generated slurry with high concentration of arsenic, which facilitates slurry disposal due to volume reduction. The second precipitation step aimed at the removal of calcium from the aqueous solution as calcium carbonate. This process

reduced the supersaturation degree of calcium sulfate, and allowed higher water recovery in a second NF stage.

No similar studies could be found in the literature. The majority of papers evaluating intermediate chemical demineralization used this process after membrane demineralization of fresh, brackish or sea water. A few studies on seeded precipitation applied to mining effluents were found, however the design of the system proposed was quite different. Harries (1985), Pulles *et al.* (1992) and Juby *et al.* (1996) added $CaSO_4$ seeds in the feed solution of a tubular RO module, to serve as preferential sites for the growth of additional crystals of calcium sulfate, silica and other salts, and prevent the formation of scale on the membrane surface. The intermediate precipitation of arsenic is also poorly discussed. Xu and co-authors (2013) evaluated the removal of arsenic from a groundwater RO concentrate by precipitation/coagulation with iron prior to a second stage of salts removal by electrodialysis. However, studies with similar focus are scarce. Moreover, to the best knowledge of the authors, the two-step intermediate chemical precipitation of the first-stage NF concentrate followed by a second-stage NF, as proposed in this study, has not yet been presented in any other study, and, because of its potential to treat effluents rich in arsenic and calcium, it is worth attention.

5.2 MATERIALS AND METHODS

5.2.1 Effluents from gold mining and description of the effluent treatment process

Two effluents from a gold mining, i.e., the effluent from the sulfuric acid production plant and the water from the calcined dam, were mixed at a 1:1 ratio and, in this study, this mixture is referred to as "effluent from gold mining". Further information on the mining production process, the collection points of the effluent and their characterization can be found in Chapter 2 (Section 2.2.1).

The first-stage of effluent NF treatment was evaluated in both bench and pilot scale tests (Chapters 2 and 4). This Chapter focused on the evaluation of a two-step intermediate chemical precipitation, as shown in the block diagram presented in Figure 5.1.

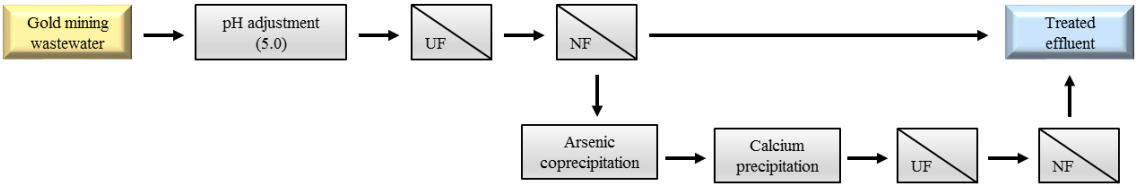

Figure 5.1 – Proposed treatment system for gold-mining effluent

5.2.2 Experimental setup

Figure 5.2 shows a scheme of the UF and NF bench scale unit. UF was conducted on a commercial submerged membrane module (ZeeWeed), polyvinylidenefluoride (PVDF)-based polymer composition with average pore diameter of 0.04 µm, and a filtration area of 0.9 m^2.

Nanofiltration was carried out with the membrane NF90 (Dow Filmtec). The NF90 membrane is a thin film composite membrane composed of three layers: (1) a polyester support web, (2) a microporous polysulfone inter layer and (3) an ultrathin aromatic polyamide active layer.

For concentrate generation, which was subsequently applied in precipitation tests, the first-stage NF was performed using the commercial module NF90-2540 with a filtration area of 2.6 m^2. On the other hand, the evaluations of the first and second-stage NF flux and fouling were conducted in a stainless steel membrane cell with 9.8 cm diameter and filtration area of 75 cm^2. In this experiments, the flat-sheet commercial membranes were properly cut to fit the membrane cell, and a feed spacer of 28 mil (25.4 µm) was placed over the membrane to promote flow distribution.

More informations about the experimental unit, including pumps specification, maximum pressures, and flow rates, may be found in Chapter 2, Section 2.2.2.

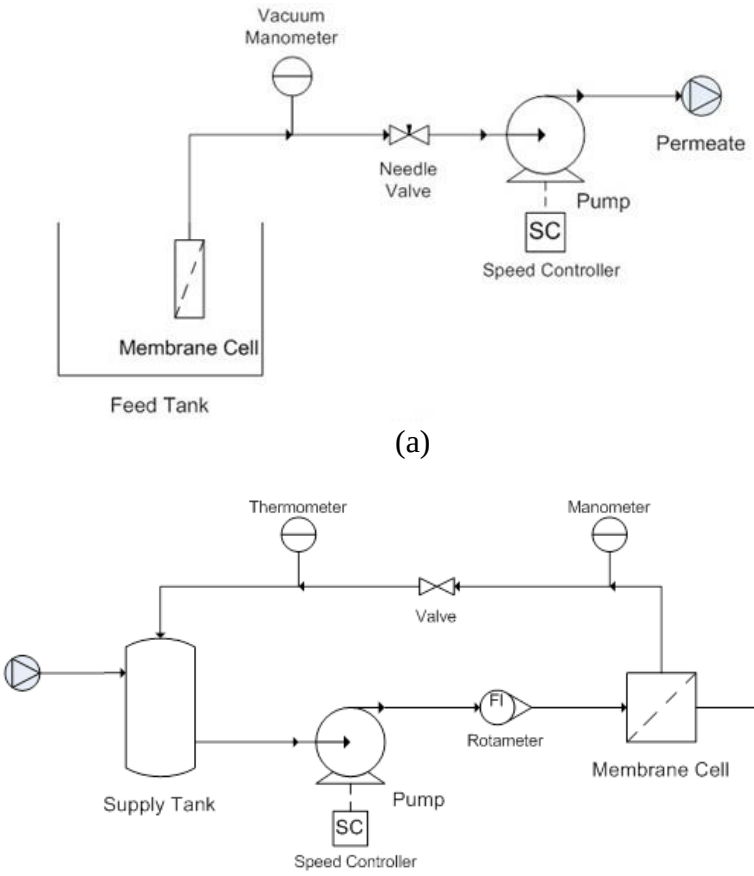

Figure 5.2 - Schematic illustration of (a) UF and (b) NF units

5.2.3 Nanofiltration experimental procedure

In all NF tests, before effluent filtration, the NF membrane was cleaned by soaking in citric acid solution at pH 2.5 followed by 0.1% NaOH solution in an ultrasound bath for 20 min. After that, the membrane was flushed and compacted with distilled water at 10 bar. The water temperature was also monitored and kept at approximately 25 °C. The permeate flux was normalized to a temperature of 25°C by means of a correction factor calculated by the ratio of water viscosity at the temperature of permeation by the water viscosity at 25°C (DRAK *et al.*, 2000). After permeate flux stabilization, the water permeability was measured by the linearization of the stabilized permeate fluxes of distilled water at a pressures of 10.0, 7.5, 5.0, and 2.5 bar.

5.2.3.1 First-stage NF

The first-stage NF was carried out with the purpose to: 1) study membrane fouling; and 2) produce concentrate for intermediate precipitation tests. In the first case, a stainless-steel NF cell, with 0.0075 m², was used.

The NF of pretreated effluent (after pH adjustment to 5.0 and UF at 0.3 bar) was performed at constant pressure of 10 bar, permeate RR between 36 and 40% and feed flow rate of 144 L/h. This resulted in a cross-flow velocity of 1.9 m/s, and a Reynolds number of 847 (detailed calculation may be found in Section 2.2.4). Initially, 2 L of the UF permeate were added to the NF supply tank. The NF permeate was continuously collected, whereas the concentrate was returned to the supply tank. Then, when the RR reached 40%, every time 200 mL of permeate were collected, 500 mL of the UF permeate were added to the NF supply tank, so that the RR remained close to 40%. The test lasted 1,500 minutes (after RR stabilization) and a total of 18.5 L of the UF permeate were used. The permeate flux was monitored regularly.

Physico-chemical analysis of the raw effluent, UF permeate, first-stage NF permeate, and first-stage NF concentrate were carried out as described in Section 5.2.6; moreover, the supersaturation index of the solutions was calculated as describe in Chapter 2, Section 2.2.4.7.

After calculating the concentration of the specie i on membrane/solution interface (C_{im}), the real rejections of the membrane (R_{real}) to Ca^{2+} and SO_4^{2-} were also estimated by Equation 5.1.

$$R_{real} = \frac{C_{im} - C_{ip}}{C_{im}} x100\% \qquad \text{Equation 5.1}$$

In contrast, for generation of effluent for precipitation tests, NF commercial module with 2.6m² was used. The appropriate volume of UF permeate was fed into the NF unit. NF was performed with 10 bar and 144 L/h feed flow rate, which resulted in Re of 13 (detailed calculations on Section 4.2.3.3). The NF permeate was continuously collected, whereas the concentrate was recycled to the supply tank until RR reached 40%.

5.2.3.2 Second-stage NF: Evaluation of feed pH

The influence of the feed pH on the permeate flux, and on the retention of sulfate, conductivity and arsenic of the second-stage NF was assessed. The feed pH values of the experiments were 11.5, 10.0, 8.5 and 7.0; and a 2.0 M HCl solution was applied for pH adjustment. The 0.0075 m²-filtration area NF cell was used.

Intermediate arsenic coprecipitation and calcium precipitation were carried out using the optimal conditions (Sections 5.2.4 and 5.2.5). The supernatant from the calcium precipitation was ultrafiltrated at constant pressure of 0.3 bar (second-stage UF). 4 L of this permeate were pH-adjusted and then nanofiltered for 240 min at a constant pressure of 10 bar and feed flow rate of 144 L/h. The permeate was collected for analysis, while the concentrate was returned to the supply tank.

5.2.3.3 Second-stage NF: Evaluation of permeate recovery rate

To study the effect of permeate RR on the second-stage NF performance, the pH of 3.5 L of the second-stage UF permeate was adjusted to the pre-set value and then were transferred to NF unit. The NF was carried out for 9,900 min, at 10 bar and feed flow rate of 144L/h. The permeate was continuously collected, while the concentrate was recycled to the supply tank. At the end of the experiment, the second-stage NF reached a permeate recovery rate of 60%.

The permeate flux and conductivity were measured at each 1% of increase in the permeate RR; and at each 10% of increase, a NF permeate sample was collected and analyzed according to the parameters of sulfate, calcium, sodium and arsenic (Section 5.2.6).

The fouling resistance ($R_{fouling}$) was calculated based on permeate flux ($J_{effluent}$, in $m^3/s.m^2$) and the membrane resistance ($R_{membrane}$) (Equation 5.2 and Equation 5.3)

$$R_{fouling} = \frac{P - \sigma \Delta\pi}{\mu . J_{effluent}} - R_{membrane} \qquad \text{Equation 5.2}$$

$$\mathrm{R_{membrane}} = \frac{1}{\mathrm{K_{virgin} \times \mu}} \qquad \text{Equation 5.3}$$

where P is the applied transmembrane pressure (Pa); σ is the reflection coefficient estimated by the averaged membrane rejection of sulfate and sodium; $\Delta\pi$ is the difference in osmotic pressure between concentrate and permeate (Pa); μ is the viscosity of permeate ($N.s/m^2$); and K_{virgin} is the water permeability at 25°C ($m^3/s.m^2.Pa$).

The difference in osmotic pressure between NF concentrates and permeates obtained with different permeate recovery rates were estimated by the Van't Hoff equation, as described in Equation 5.4:

$$\Delta\pi = RT\Sigma\Delta C \quad \text{Equation 5.4}$$

where R is the universal gas constant (L.Pa/K.mol), T is the permeation temperature (K), and $\Sigma\Delta C$ is the sum of the difference in molar concentrations of the main dissolved species present in the concentrate and the permeate. Osmotic pressures were calculated using concentrations of sulfate and sodium analyzed for RR 10, 20, 30, 40, 50 and 60% and were mathematically adjusted for other RR values.

After the concentration test, the membrane was physically cleaned inside the NF unit through the recirculation of distilled water at 144 L/h for 30 minutes. After physical cleaning, the water permeability was measured (K_{irrev}, in m³/s.m².Pa) and the resistance of the irreversible fouling was determined (Equation 5.5)

$$R_{firrev} = \frac{1}{K_{irrev} \times \mu} - R_{membrane} \quad \text{Equation 5.5}$$

The reversible fouling resistance could be then calculated by Equation 5.6.

$$R_{frev} = R_{fouling} - R_{firrev} \quad \text{Equation 5.6}$$

5.2.4 Arsenic coprecipitation

Arsenic intermediate coprecipitation experiments were carried out with the concentrate from the first-stage NF at 40% recovery rate (as described in Section 5.2.3.1). Ferric sulfate ($Fe_2(SO_4)_3.5H_2O$) was added and pH adjustment was accomplished with NaOH solution (5 M).

The experiments were conducted in a standard 2 L square Jar Test (Nova Ética) at stirring speed of 40 rpm. For each test, the designed mass of ferric sulfate was dissolved in 50 mL of the concentrate and added to 950 mL of concentrate; therefore, 1 L of concentrate was used in each test. Because of the different amounts of ferric sulfate in each test condition, the effluent pH reduced from 5.0 to 2.2 - 3.6. The effluent pH was adjusted to the designed condition, and the required volume of NaOH solution for this adjustment was measured. The time for precipitation was 30 min, after that a sample was collected for suspended solids and total arsenic analyses (Section 5.2.6).

The rotational central composite design was used to optimize the independent variables molar ratio of ferric iron (Fe^{3+}) to total arsenic (As_{total}) (or simply Fe/As), and reaction pH. Table 5.1 shows the variable level, and the design matrix for the experiment.

Table 5.1 - Rotational central composite design of arsenic coprecipitation

Test	Fe/As		pH	
	Level	Value	Level	Value
1	+	5.0	+	8.0
2	-	1.0	+	8.0
3	+	5.0	-	4.0
4	-	1.0	-	4.0
5	0	3.0	0	6.0
6	0	3.0	0	6.0
7	0	3.0	0	6.0
8	0	3.0	0	6.0
9	+1.41	5.8	0	6.0
10	-1.41	0.2	0	6.0
11	0	3.0	+1.41	8.8
12	0	3.0	-1.41	3.2

The responses variables assessed were the arsenic removal efficiency, arsenic theoretical concentration in the dry slurry, and coprecipitation cost. The coprecipitation cost was calculated by using only the costs with the reagents $Fe_2(SO_4)_3.5H_2O$ (US$0.14/kg) and NaOH (US$1.00/kg). The theoretical concentration of arsenic in the slurry (As_{slurry}, g_{As}/g_{SS}) was estimated by Equation 5.7.

$$As_{slurry} = \frac{C_i - C_f}{SS} x100\% \qquad \text{Equation 5.7}$$

where C_i and C_f are the arsenic concentrations before and after the intermediate coprecipitation, respectively, and SS is the concentration of suspended solids after the coprecipitation, all measured in g/L.

A second-order polynomial model was built for each response, its general equation is shown in Equation 5.8 (CANDIOTI *et al.*, 2014):

$$y = \beta_0 + \sum_{i=1}^{k} \beta_i x_i + \sum_{i=1}^{k} \beta_{ii} x_i^2 + \sum_{1 \le i \le j}^{k} \beta_{ij} x_i x_j + \varepsilon \qquad \text{Equation 5.8}$$

where y is the observation or response, x_i and x_j are the factors studied, β_0 is the constant term or intercept; β_i, β_{ii} and β_{ij} represent the coefficients of the first order, quadratic and interaction terms, respectively; and ε is the residual associated with the experiments.

Statistica 8.0 software (Statsoft, USA) was used to fit a quadratic polynomial model and create a response surface for each dependent variable. The significance of the model equations and the model terms were evaluated in term of p value with a 95% confidence level.

Finally, the coprecipitation process was repeated under the optimum Fe/As and pH conditions. The slurry decanted for 16 hours. The supernatant was used for the second-step intermediate precipitation experiments (calcium carbonate precipitation).

5.2.5 Calcium precipitation

The precipitation of calcium from the arsenic coprecipitation supernatant was evaluated. The experimental procedure was similar to that described in Section 5.2.4. Sodium carbonate (Na_2CO_3) was used to precipitate calcium as $CaCO_3$. The carbonate addition increased the effluent pH to values between 10.0 and 10.9; therefore, the reaction pH was adjusted to the designed condition with NaOH solution (5 M) or HCl solution (2 M).

Once more, the rotational central composite design was used to optimize the independent variables molar ratio of carbonate anion (CO_3^{2-}) to calcium cation (Ca^{2+}) (or simply CO_3/Ca), and reaction pH. The design matrix for the experiment is shown in Table 5.2. The responses evaluated were the Ca^{2+} removal efficiency, and precipitation cost. The precipitation cost took into account only the costs with the reagents Na_2CO_3 (US$0.47/kg), NaOH (US$1.00/kg), and HCl (US$1.07/kg).

Table 5.2 - Rotational central composite design of calcium precipitation

Test	CO_3/Ca		pH	
	Level	Value	Level	Value
1	+	4.0	+	12.0
2	-	1.0	+	12.0
3	+	4.0	-	8.0
4	-	1.0	-	8.0
5	0	2.5	0	10.0
6	0	2.5	0	10.0
7	0	2.5	0	10.0
8	0	2.5	0	10.0
9	+1.41	4.6	0	10.0
10	-1.41	0.4	0	10.0
11	0	2.5	+1.41	12.8
12	0	2.5	-1.41	7.2

5.2.6 Analytical methods

The aqueous samples collected in different stages of the treatment system were analyzed for conductivity, pH, sulfate, magnesium, total arsenic, and metals aluminum, iron, manganese, potassium, according to the methodology presented in Chapter 2, Section 2.2.5. Calcium was analyzed by atomic absorption (Spectrophotometer GBC 932), sodium was analyzed by ion chromatograph (Dionex ICS-1000 equipped with AS-22 and ICS 12-A columns), and slurry suspended solids was analyzed according to *Standard Methods* (APPA, 2005).

5.2.7 Economic aspects

A cost estimate of the two-stage UF-NF membrane system associated to intermediate arsenic and calcium chemical precipitation was conducted. The variables considered in this estimate were: the system capital expenditure (CapEx); membrane replacement costs; power consumption costs; system maintenance; chemical products for membrane cleaning; alkalizing and acidifying agent for pH adjustment; chemical reagents for intermediate precipitation of arsenic and calcium; arsenic slurry disposal; second-stage NF concentrate treatment; and personnel costs. All calculations were based on a designed system capacity (Q_{des}) of 280 m³/h, which is the gold mining effluent flow rate informed by the mining company. The dollar quotation was considered to be R$ 4.00/US$ 1.00.

The first- and second-stage total UF-NF CapEx was US$ 3,200,000.00. NF and UF membranes replacement costs were US$ 50 and US$ 75 dollars per square meter, respectively. These prices were provided by a large commercial membrane supplier. The required membrane area was calculated considering 10 L/h.m² for NF and 22 L/h.m² for UF. Permeate recovery rates of 95% for first- and second-stage UF, 40% for first-stage NF and 85% for second-stage NF were also considered. The membrane lifetime was 5 years (LIIKANEN *et al.*, 2006). Also according to membrane supplier, system maintenance charges corresponded to 5% of the initial investment.

To estimate the CapEx per cubic meter of effluent, the capital cost was annualized by means of amortization factor (*A/P*) as presented in Equation 5.9 (SETHI and WIESNER, 2000).

$$A/P = \frac{i_c(1+i_c)^{DL}}{(1+i_c)^{DL}-1} \qquad \text{Equation 5.9}$$

where i_c is the investment rate, considered equal 12% in Brazil, and DL is the design life of the plant, 15 years. The capital cost per cubic meter of effluent (C_{cap/m^3}) was obtained from Equation 5.10:

$$C_{cap/m^3} = \frac{CapEx.A/P}{Q_{des}} \qquad \text{Equation 5.10}$$

The NF power consumption, estimated by ROSA 9.1 software, was 0.61 kWh/m³ while UF power consumption was 0.22 kWh/m³ (CHEW *et al.*, 2016). The electricity tariff was US$ 0.04/kWh, which is the actual tariff paid by the mining company.

The alkalizing agent NaOH was used for pH adjustment of raw effluent, arsenic coprecipitation and calcium coprecipitation. The volumes of NaOH 5 M solution used in each case were experimentally measured and used to determine the neutralizing agent demand. Ferric sulfate and sodium carbonate were used for chemical precipitation steps. Dosage of these reagents were calculated according to the optimized molar ratio Fe/As and CO_3/Ca. HCl total consumption was calculated considering the amount of acidifying agent applied for both membrane cleaning and pH adjustment of the calcium precipitation supernatant before second-stage membrane processes. Cleaning cost was calculated considering one chemical cleaning with HCl 0.2% solution every two weeks. Chemical reagents prices were US$ 1.00, US$ 0.14, US$ 1.07 and US$ 0.47 per kg of NaOH, $Fe_2(SO_4)_3.5H_2O$, HCl and Na_2CO_3, respectively.

According to the mining industry, the disposal of slurries contaminated with arsenic is US$ 58.20/ton. The (conventional) treatment of concentrates from first-stage UF, second-stage UF and second-stage NF was estimated at US$ 1.53/m³, which is the actual cost of effluent treatment at the mining industry.

Personnel costs included payroll for hiring four technicians/operators and 13 annual salaries plus 100% corresponding to labor costs (payroll taxes and benefits).

5.3 RESULTS AND DISCUSSION

5.3.1 Advantages of using a two-step intermediate chemical precipitation

Previous studies have shown that the maximum RR of the first-stage nanofiltration of the gold mining effluent is 40%. An increase in the RR above 40% causes an increase in solutes concentration in the bulk solution and in the membrane-solution interface, which consequently leads to higher membrane scaling tendency and loss of permeate quality (Chapter 2).

Therefore, the first-stage NF of the pretreated gold mining effluent was carried out until a RR of approximately 40%, for a total of 1,500 minutes. Table 5.3 shows the main characteristics of the raw effluent, pretreated effluent (after pH adjustment and UF), and the first-stage NF permeate and concentrate. The first-stage NF process efficiently retained all species analyzed, except for arsenic, sodium and chloride. Because of this high retention, the concentrate generated is rich in numerous inorganic species. In particular, the high concentration of arsenic makes it a hazardous waste, which requires an appropriate treatment before final disposal.

Table 5.3 - Characteristics of the effluents at different points of the first-stage NF treatment of the gold-mining effluent

Parameters	Raw effluent	Pre-treated effluent	NF permeate	NF concentrate	NF retention efficiency
pH	2.08	5.00	4.96	5.09	-
Conductivity (µS/cm)	4,550	3,250	398	8,050	88%
Sulfate (mg/L)	2,625	2,553	126	4,942	95%
Chloride (mg/L)	196	192	25	258	87%
Aluminum (mg/L)	68	2	0.05	3	98%
Arsenic (mg/L)	534	506	161	514	70%
Calcium (mg/L)	550	539	6	666	99%
Iron (mg/L)	34	2	0.03	3	99%
Magnesium (mg/L)	247	243	3	278	99%
Manganese (mg/L)	22	19	0.2	21	99%
Potassium (mg/L)	44	50	2	58	96%
Sodium (mg/L)	77	76	23	81	70%
Zinc (mg/L)	64	37	1	46	97%

Figure 5.3 shows the theoretical calcium sulfate SI_m versus the RR of the second-stage NF, for a scenario where the first-stage NF concentrate has not undergone any intermediate treatment. This calculus considered that the steady state permeate flux of the second-stage NF was equal to that of the first-stage NF (i.e.18 L/h.m²). The real rejection of the membrane ($R_{real,Ca^{2+}}$ = 98.0%, and $R_{real,SO_4^{2-}}$ = 97.6%) was also considered equal in both processes, and it was used to estimate the ionic concentrations in the permeate and concentrate through an interactive process. To this purpose, a permeate concentration ($C_{i,p}$) was arbitrated for each RR and the bulk concentration ($C_{i,b}$) was calculated based on the feed solution concentration (the first-stage NF concentrate at 40% of RR) ($C_{i,f}$), as shown by Equation 2.16. With $C_{i,p}$, $C_{i,b}$ and the permeate flux, $C_{i,m}$ can be obtained from 2.15, and R_{real} from Equation 5.1. A new value of $C_{i,p}$ was then selected until the values of the real rejections were equal those of the first-stage NF.

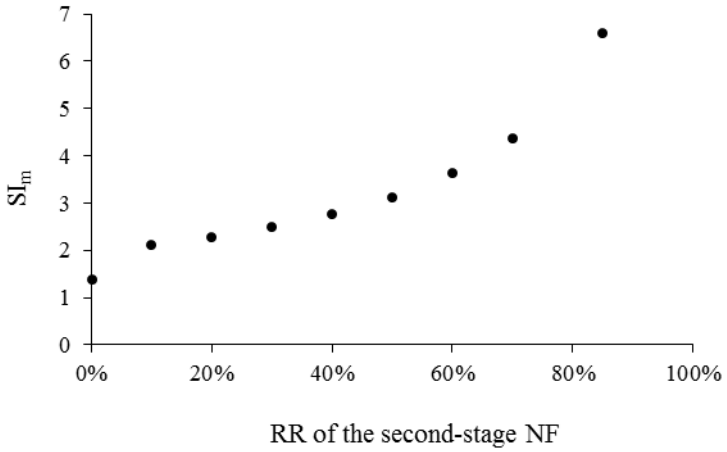

Figure 5.3 – Calcium sulfate SI_m versus RR of the second-stage NF, when no intermediate treatment of the first-stage NF concentrate was used

The literature suggests that $CaSO_4$ precipitation can occur when the SI is higher than 1.62 to 2.02 (DYDO *et al.*, 2004); or 2.3 (HYDRANAUTICS, 2008; RAHARDIANTO *et al.*, 2008) and 2.5 (MCCOOL *et al.*, 2013) if antiscalants are used. From Figure 5.3 it can be seen that the estimated SI_m of second-stage NF is similar or higher than the threshold values for any RR. Therefore, it cannot be operated without $CaSO_4$ precipitation and membrane scaling. As a result, an intermediate precipitation is mandatory prior to the second-stage NF, and should be performed in two steps. The first step aim at the removal of arsenic and the treatment of the concentrate, which is a hazardous waste. The second step aim at the removal of calcium and to increase the overall water RR. Arsenic removal from an aqueous phase is commonly performed by coprecipitation with Fe^{3+} salts. On the other hand, Ca^{2+} removal can be accomplished by precipitation with CO_3^{2-}.

Figure 5.4 shows the equilibrium concentrations of the cations Ca^{2+} and Mg^{2+} with the anions SO_4^{2-}, CO_3^{2-} and OH^-, versus solution pH. In the calculations, it was considered a sulfate concentration equal to the value calculated for the bulk solution of the second-stage NF at 85% of RR, and a molar ratio of CO_3/Ca = 1.0.

As can be seen, calcium hydroxide ($Ca(OH)_2$) precipitation is only significant at high pHs (pH > 12); and only at pHs higher than 13.4 the equilibrium concentration of Ca^{2+} with OH^- is lower than that of Ca^{2+} with SO_4^{2-}, which is a necessary condition to prevent scaling. Consequently, the removal of Ca^{2+} through chemical precipitation with CO_3^{2-} is more

attractive, especially since it is possible to obtain low concentrations of Ca^{2+} at moderate pH values.

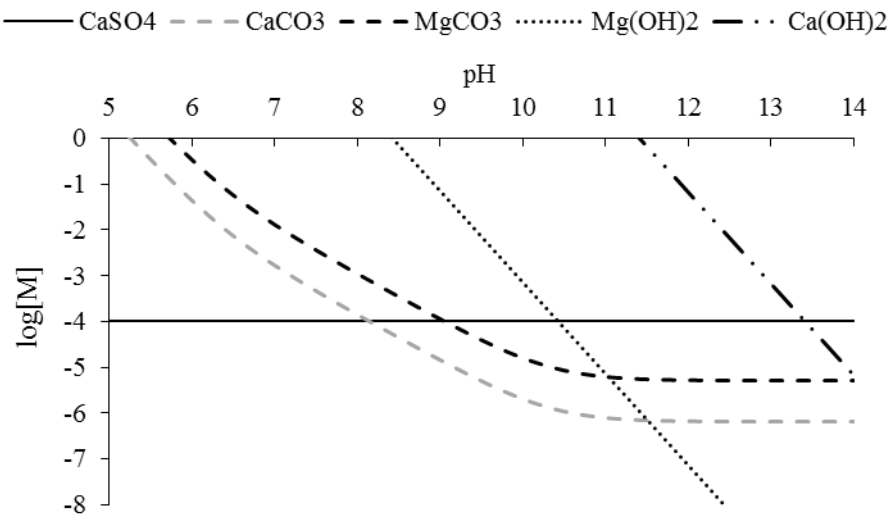

Figure 5.4 – Equilibrium concentrations of the cations Ca^{2+} and Mg^{2+} with the anions SO_4^{2-}, CO_3^{2-} and OH^-, versus solution pH.

5.3.2 Arsenic coprecipitation

The influence of the molar ratio of Fe/As and reaction pH on the arsenic coprecipitation of the first-stage NF concentrate was evaluated by means of an experimental design.

The response surfaces are shown in Figure 5.5. All the coefficients of first and second order and interaction terms were considered statistically significant for arsenic removal at a 5% significance level. For the response arsenic concentration in the dry slurry, the quadratic coefficient of the reaction pH, and that of the interaction of reaction pH and molar ratio Fe/As were not significant. Lastly, no coefficient was considered statistically significant for the coprecipitation cost at a 5% significance level.

(a)

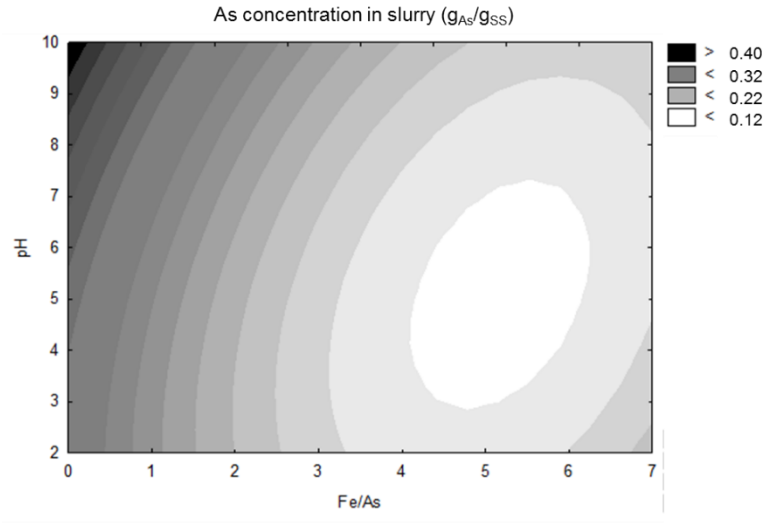

(b)

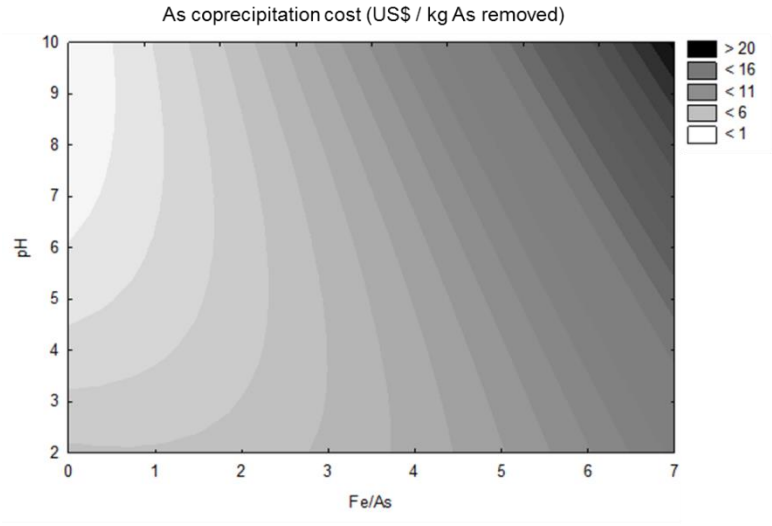

(c)

Figure 5.5 – Response surface of: (a) arsenic removal efficiency; (b) arsenic concentration in the dry slurry; and (c) coprecipitation cost, versus molar ratio of Fe/As and reaction pH

The maximum arsenic removal efficiency was observed at reaction pH between 5 and 9, and molar ratio of Fe/As between 2.5 and 5.5 (Figure 5.5 a). For this response, the maximum critical point occurred at reaction pH of 7.0 and Fe/As equal to 4.0.

The optimum reaction pH found is consistent with that reported in the literature. According to Nishimura and Umetsu (2000), the optimal pH for arsenate removal lies in a mildly acidic region (i.e. 3.5–5.5). However, for mining effluents with relevant concentration of elements such as Al, Ni, Fe, Ca and SO_4, this range can increase to 5.0 – 7.3 (MOLDOVAN and HENDRY, 2005). Moreover, pH 7.0 is close to pH of minimum solubility of both ferrihydrite and ferric arsenate (DE KLERK *et al.*, 2012; LANGMUIR *et al.*, 2006); therefore, the low solubility and increased precipitation of this compounds increases the arsenic removal. A high reaction pH is not beneficial, since above pH 7.8 the ferrihydrite has a negative surface charge, which repels arsenite and arsenate (RICHMOND *et al.*, 2004).

The optimum molar ratio of Fe/As is also close to those used in large-scale treatment systems of mining effluents (TWIDWELL and MCCLOSKEY, 2011). According to Richmond *et al.* (2004), under high concentrations of iron, a rapid hydrolysis provides the ferrihydrite with a high surface area; and, as a result, it has a higher arsenate adsorption capacity. Moreover, in the pH range from 4 to 7, the minimum molar ratio of Fe/As required for formation of stable arsenical ferrihydrite precipitate is 3 (RICHMOND *et al.*, 2004).

The arsenic concentration on the slurry is an important parameter of the precipitation, as it is directly related to the cost of slurry disposal. The most concentrated slurries were generated at low Fe/As molar ratio and high reaction pH. At low concentrations of Fe^{3+}, the formation of ferric arsenate is favored; and since it is an equimolar compound of Fe and As, it results in a high concentration of As in the solid.

It is clear from Figure 5.5 (b) that, on the optimized conditions for As removal (pH 7.0 and 4.0 Fe/As molar ratio), the arsenic concentration on the slurry is low. The mathematical model fitted to the data provides a theoretical concentration for this condition equal to 0.14 g_{As}/g_{SS}. Although this is not one of the highest values observed in the surface response, it is still considered viable. Currently, the mining company where the effluent was collected uses a large-scale treatment system with ferric sulfate and lime addition for arsenic coprecipitation. The

slurry generated during this process has a arsenic concentration of 5%. This difference may be a result of an adequacy of the operating conditions, applying the coprecipitation in a more concentrated effluent (the first-stage NF concentrate), and the use of soda instead of lime as a neutralizing agent.

Higher Fe/As molar ratio increased the treatment cost as more reagent ferric sulfate was required (Figure 5.5 c). Interestingly, for lower Fe/As molar ratio the cost per kg of arsenic removed decreased with increasing pH, because of higher As removal efficiency, as observed in Figure 5.5 (a). On the other hand, for higher Fe/As molar ratio, the pH increase led to an increase in the coprecipitation cost. This occurs because the costs with alkalizing agent are increased, however, there is no proportional increase in As removal since the removal efficiency is already high.

Finally, since arsenic is a toxic element, extremely dangerous to the environment, its removal was prioritized. Accordingly, the conditions that provided optimum arsenic removal were selected as the most favorable for the coprecipitation, and were used for the subsequent tests.

5.3.3 Calcium precipitation

The simulation of the second-stage NF was carried out similarly to that shown in Section 5.3.1. However, here the iterative process was performed so that, for each RR, a treated feed concentration (after the precipitation process) ($C_{i,f_{treated}}$) was estimated. This allowed that, with a constant R_{real} value, the SI_m was also constant and equal to 2.0. The literature reports that for SI values of $CaSO_4$ larger than 1.62 - 2.5 there is scaling on the membrane surface (DYDO *et al.*, 2004; HYDRANAUTICS, 2008; MCCOOL *et al.*, 2013; RAHARDIANTO *et al.*, 2008). In this study, a SI_m equal to 2.0 was selected as a threshold value. Then, it was possible to calculate the theoretical calcium removal efficiency required to avoid excessive risk of scaling for each potential RR value of the second-stage NF (Figure 5.6).

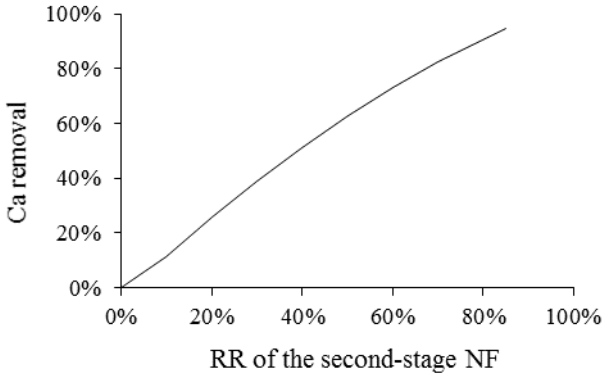

Figure 5.6 – Theoretical calcium removal efficiency for each potential RR value of the second-stage NF to maintain the SI_m equal to 2.0

As the membrane rejection is high, the salt concentration at the solution bulk is progressively higher with the RR increase. On the other hand, the ionic product of Ca^{2+} and SO_4^{2-} cannot exceed 2 x K'_{sp} to avoid $CaSO_4$ precipitation. As the increase in sulfate concentration with RR is inevitable, the calcium concentration must be lower in the feed solution of the second-stage NF, and, consequently, the efficiency of the calcium precipitation process must be higher.

The optimization of calcium precipitation was performed by experimental design considering two responses: calcium removal efficiency, and precipitation cost per m^3 of permeate of the second-stage NF. A second order function was fitted to the curve shown in Figure 5.6 to allow the estimation of the acceptable RR (namely m^3 of permeate per m^3 of feed solution) for each calcium removal efficiency obtained experimentally.

Again, the second-order mathematical model was built for each response. The response surfaces are shown in Figure 5.7. All the coefficients of the second order polynomial function were considered statistically significant for the precipitation cost; while for calcium removal, only the coefficient of the interaction term was not statistically significant.

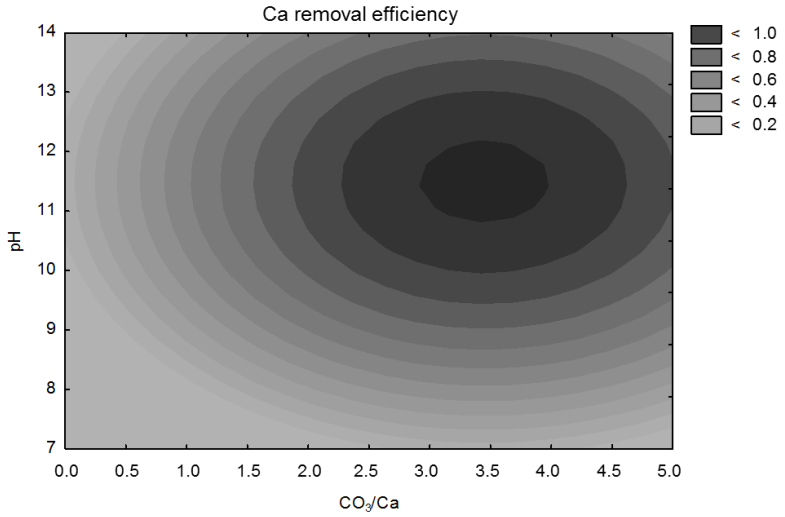

(a)

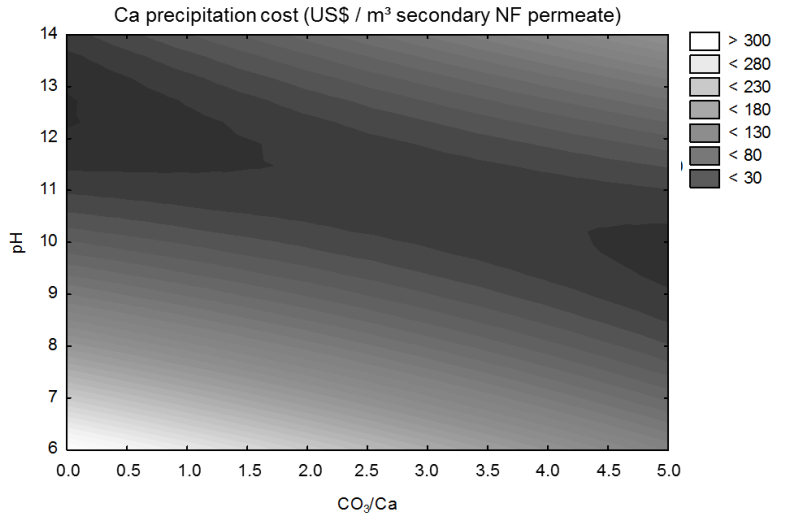

(b)

Figure 5.7 – Response surface of: (a) calcium removal efficiency; and (b) precipitation cost, versus molar ratio of CO_3/Ca and reaction pH

It can be seen that higher reaction pH increased the calcium removal efficiency (Figure 5.7 a). The species carbonic acid, bicarbonate, and carbonate are in equilibrium in the aqueous solution, and the predominant specie depends on the solution pH as shown by Equation 5.11.

$$H_2CO_3 \underset{pKa=6.3}{\Longleftrightarrow} H^+ + HCO_3^- \underset{pKa=10.3}{\Longleftrightarrow} H^+ + CO_3^{2-} \qquad \text{Equation 5.11}$$

As the pH increases, the concentration of CO_3^{2-} also increases, and at pH values higher than 10.3, this becomes the predominant specie. In saturated solutions, the ionic product of Ca^{2+}

and CO_3^{2-} is constant and, consequently, the increase in CO_3^{2-} concentration leads to a decrease in Ca^{2+} concentration at equilibrium (Figure 5.4).

The increase in reaction pH also favors the Mg^{2+} removal through the precipitation of $Mg(OH)_2$, especially at pH values higher than 10.5 (Figure 5.4). This, in turn, favors the coprecipitation of silica (HEIJMAN *et al.*, 2009). As Mg^{2+} and silica are also fouling components for the NF membranes (HEIJMAN *et al.*, 2009; JARUSUTTHIRAK *et al.*, 2007), its removal in conjunction with Ca^{2+} is beneficial.

Calcium removal also increased with the increase in CO_3/Ca molar ratio. At low CO_3/Ca molar ratio, the CO_3^{2-} consumption for the precipitation of other metal cations, such as Mg^{2+} (Figure 5.4), led to a reduction in Ca^{2+} removal (GABELICH *et al.*, 2007). Therefore, because of the various metals present in the mining effluent, a CO_3/Ca molar ratio higher than the stoichiometric relationship should be used.

Also, ionic sulfate can influence the $CaCO_3$ precipitation. According to Zarga *et al.* (2013), an increase of sulfate ion concentration affects the $CaCO_3$ induction time evolution. Moreover, $CaSO_4$ precipitation may be induced by $CaCO_3$ precipitation, as it provides mineral seeds for sulfate crystallization (GABELICH *et al.*, 2007). In this work, $CaSO_4$ precipitation was not observed during $CaCO_3$ precipitation. SO_4^{2-} concentrations were measured at the beginning and the end of the 12 tests of the experimental design, and the all the results differed by less than 8%.

Regarding the precipitation cost, it was observed that the optimum pH range was between 8.5 and 14.0, depending on the CO_3/Ca molar ratio used. Operation at lower pHs leads to higher cost because of higher HCl requirement for the solution acidification after the addition of Na_2CO_3, and lower Ca^{2+} removal, which limited the RR of the second-stage NF and reduced the m^3 of permeate produced in that process. On the other hand, very high pHs increased the reagents cost because alkalizing agent (NaOH) was needed to adjust the pH.

The highest calcium removal occurred at reaction pH between 11 and 12, and molar ratios of CO_3/Ca between 3 and 4. The optimal point for calcium removal was observed at pH 11.5 and CO_3/Ca equal to 3.5. This condition is within the range of lower precipitation cost, which suggests that the costs with reagents is compensated by the permeate production increased in

the second-stage NF. Consequently, the reaction pH equal to 11.5 and the CO_3/Ca molar ratio equal to 3.5 were selected as the best operating condition for the intermediate precipitation of the Ca^{2+}.

5.3.4 Intermediate precipitation at optimum conditions

First- and second-step precipitations of arsenic and calcium were accomplished using 30 L of first-stage NF concentrate and the optimum conditions found previously. Table 5.4 shows the results regarding the main physico-chemical parameters.

Table 5.4 – Characteristics of the effluent before and after chemical intermediate precipitation

Parameter	Raw gold mining effluent	First-stage UF permeate	First-stage NF permeate	First-stage NF concentrate	Supernatant of As precipitation	Supernatant of Ca precipitation
Sulfate (mg/L)	3622	3567	77	4023	9214	9145
Calcium (mg/L)	613	596	34	755	719	5
Arsenic (mg/L)	1075	672	362	711	1.5	1.3
Sodium (mg/L)	113	884	27	1354	4170	8058

The pretreatment with pH adjustment and UF was slightly removed calcium and sulfate from the raw effluent, due to precipitation and/or electrostatic repulsion by the UF membrane (for details, see Section 4.3.6). The arsenic removal efficiency is higher because it can coprecipitate with the iron present in the raw effluent (Table 5.3) when the pH is raised to 5.0. Sodium concentration was noticeably increased because of NaOH dosing for pH adjustment.

As discussed previously, solute retention by NF was high, yielding a concentrate rich in sulfate, calcium and arsenic. At optimum conditions, the intermediate arsenic precipitation removed 99.8% of this pollutant, generating a supernatant with only 1.5 mg/L of arsenic. Moreover, because iron was dosed as ferric sulfate salt and NaOH was used for pH adjustment, there was a significant increase in sulfate and sodium concentrations.

In the next intermediate precipitation step, there was 99.3% removal efficiency of calcium. In addition, 13% of the residual arsenic was removed due to coprecipitation with calcium (JIA and DEMOPOULOS, 2008). Again, the pH adjustment using NaOH was responsible for 93% increase in the sodium concentration.

Therefore, the second-stage NF feed is characterized by low concentrations of arsenic and calcium, and high concentrations of sodium and sulfate.

5.3.5 Evaluation of pH on second-stage NF

According to the membrane supplier, NF90 should not be constantly operated at pH higher than 11.0 (DOWFILMTEC™ b). Since the intermediate precipitation of Ca was performed at pH 11.5, effluent acidification is necessary before the membrane treatment. Thus, second-stage NF was performed using the supernatant from intermediate chemical precipitation at pHs of 11.5, 10.0, 8.5 and 7.0. The relation between instant permeate flux and initial permeate flux (J/J_0) is shown in Figure 5.8 for each condition.

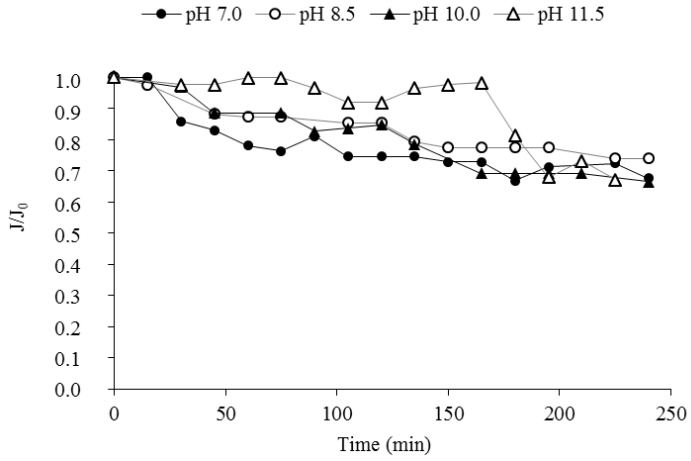

Figure 5.8 – Relation between flux and initial flux for the second-stage NF at different pH

The flux profile in relation to time is similar for the operation with pHs 7.0, 8.5 and 10.0; however, pH 8.5 was the one that showed the best performance. Flux decay after 4-hour filtration was 32%, 26% and 32% for pHs 7.0, 8.5 and 10.0, respectively. NF at pH 11.5 presented stable flux until 165 min, thereafter there was a decay of 33%. At basic pH, NF90 has a negative zeta potential (Chapter 2, Section 2.3.4). Thus, the flux decrease observed might have been caused by concentration polarization and electrostatic interaction between the negative charged membrane and the cations in the bulk solution.

The retention efficiency of conductivity and sulfate is similar for the milder conditions (Figure 5.9), while at pH 11.5 the retention is smaller. Studying a thin film composite NF membrane, Dalwani *et al.* (2011) found that the molecular weight cut-off of the membrane was practically

constant in acidic and neutral conditions. Conversely, at extremely alkaline conditions (pH > 11) an increase in molecular weight cut-off and effective average pore size were observed. At this condition, the zeta potential of pores walls is highly negative, and the electrostatic repulsion may cause pore enlargement. This would explain the results found in this work.

On the other hand, arsenic retention was lower at neutral pH. At this condition, while As(V) is found in both forms $H_2AsO_4^-$ and $HAsO_4^{2-}$, As(III) is mainly presented as H_3AsO_3. Because it is in neutral form, As (III) does not suffer electrostatic repulsion by the negative charged membrane and is only retained by steric hindrance, justifying the low retention. Once pH is increased, the negative forms $HAsO_4^{2-}$ and $H_2AsO_3^-$ begin to dominate, which leads to improved NF retention. The increase in effective average pore size at pH 11.5 may have caused the decreased in retention observed in this point.

Feed pH 8.5 was selected as the most adequate for the second-stage NF. It showed high retention efficiency for the species analyzed and the higher permeate flux. Moreover, it is suitable for continuous operation and require less acid for pH adjustment than pH 7.0.

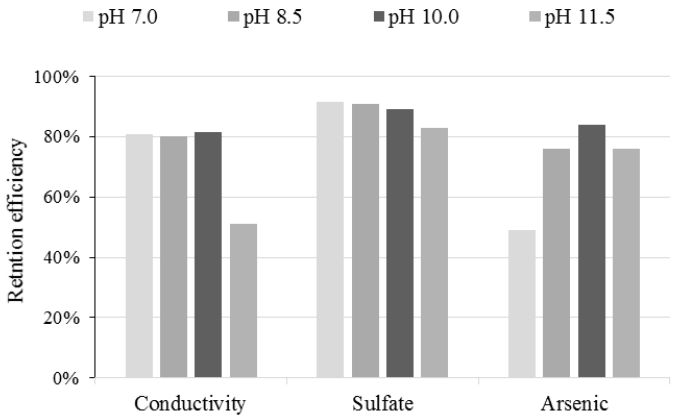

Figure 5.9 – Retention efficiency of conductivity, sulfate and arsenic for the second-stage NF at different pH

5.3.6 Evaluation of permeate recovery rate of second-stage NF

A concentration test of second-stage NF was performed up to 60% permeate recovery rate (RR). Higher RR could not be achieved because of the low volume of concentrate remained and operating limitations of the bench system used. Figure 5.10 shows the permeate flux, osmotic pressure and fouling resistance versus RR.

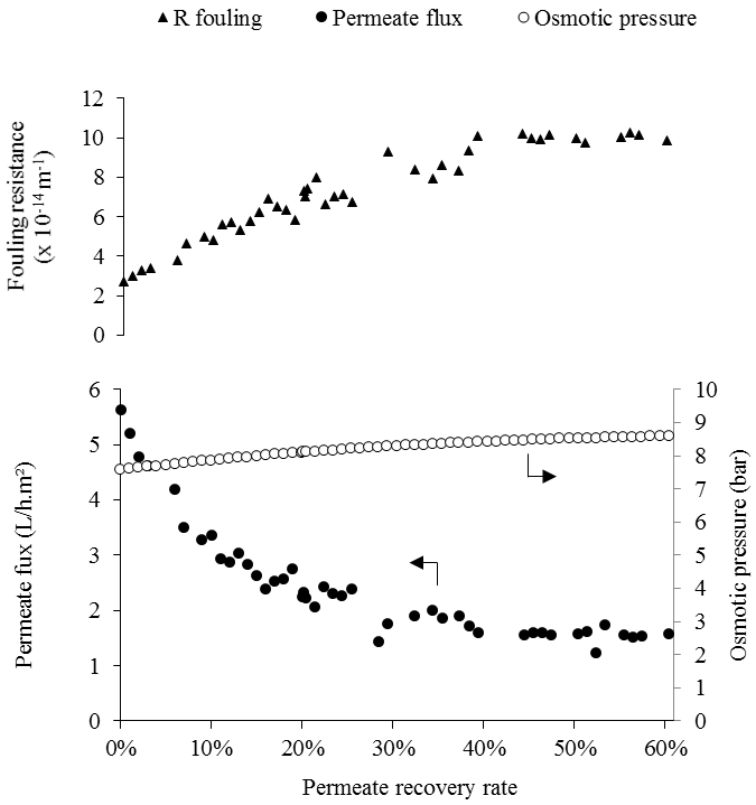

Figure 5.10 – Permeate flux, osmotic pressure and fouling resistance as a function of second-stage NF permeate recovery rate

Since the applied pressure was 10 bar, the permeate fluxes (5.2 – 1.5 L/h.m²) may be considered relatively low; however, it was related to the high osmotic pressure and consequent low driving force $\Delta P - \sigma\Delta\pi$. There was a significant decrease in permeate flux with increasing RR, achieving a final flux about 70% lower than the initial one. It occurred partly because the increase in RR elevates the concentration of solutes in bulk solution (Figure 5.11). This caused both permeate conductivity and osmotic pressure increase, reducing even more the effective pressure. There was a 14% increase in osmotic pressure throughout the concentration process.

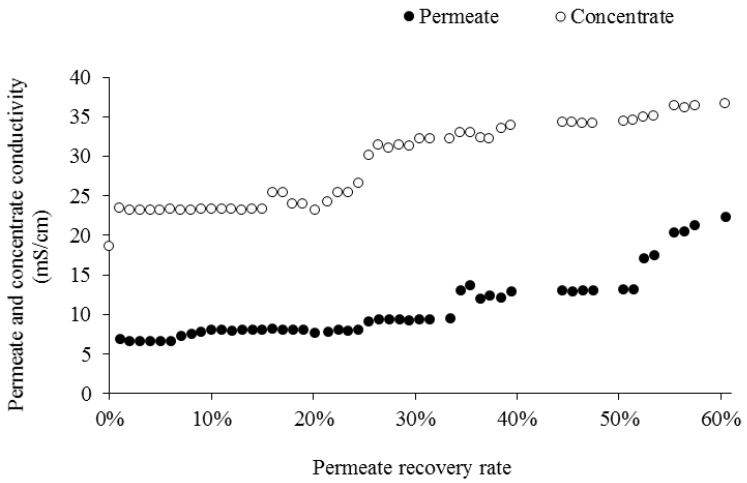

Figure 5.11 – Permeate and concentrate conductivity as a function of permeate recovery rate

Moreover, a gradual growth in fouling resistance also occurred until 38% RR; and from this point onwards there was a tendency for stabilization. This fouling resistance included the individual resistances from concentration polarization, solutes weakly attacked to the membrane polymeric structure and sticky precipitates deposited over membrane surface. To understand which one of these were the most relevant, the resistances of reversible and irreversible fouling were determined (Table 5.5). The largest portion was the one related to reversible fouling (90% from total resistance), which comprised the concentration polarization resistance and the resistance from fouling loosely attacked to the membrane and removable by physical cleaning.

Table 5.5 – Resistances determined after the concentration test of the second-stage NF

Resistance	Value (x 10^{-14} m^{-1})
Membrane	7.7
Reversible fouling	107.0
Irreversible fouling	4.5

The supersaturation index of calcium sulfate over membrane surface (SI_m) was calculated for different RRs (Table 5.6). The SI_m is comfortably smaller than 1.0 for all the conditions, indicating that there was no risk of scaling.

Table 5.6 – $CaSO_4$ supersaturation index at the membrane surface (SI_m) for different permeate recovery rates of second-stage NF

RR	0%	10%	20%	30%	40%	50%	60%
SI_m	0.15	0.16	0.17	0.18	0.20	0.22	0.25

These results showed that, despite the significant permeate flux decay observed for increased RR, the flux could be recovered by simple physical cleaning method and the fouling did not cause loss of hydraulic membrane permeability. Thus, it is possible to operate the second-stage NF with high RR, ensuring higher production of reuse water.

5.3.7 Economic aspects

The flowchart of the global process, including the flow rates of the different streams and concentrations of the major solutes is shown in Figure 5.12. It was constructed considering 85% RR at second-stage NF. In this condition, global RR is 67%. Permeate and concentrate second-stage NF concentrations of sulfate, sodium, calcium and arsenic were estimated so that the real membrane rejections were similar to those measured between RR of 10 and 60%.

The flow rates and reagents dosages shown in Figure 5.12 were used to calculated the treatment cost.

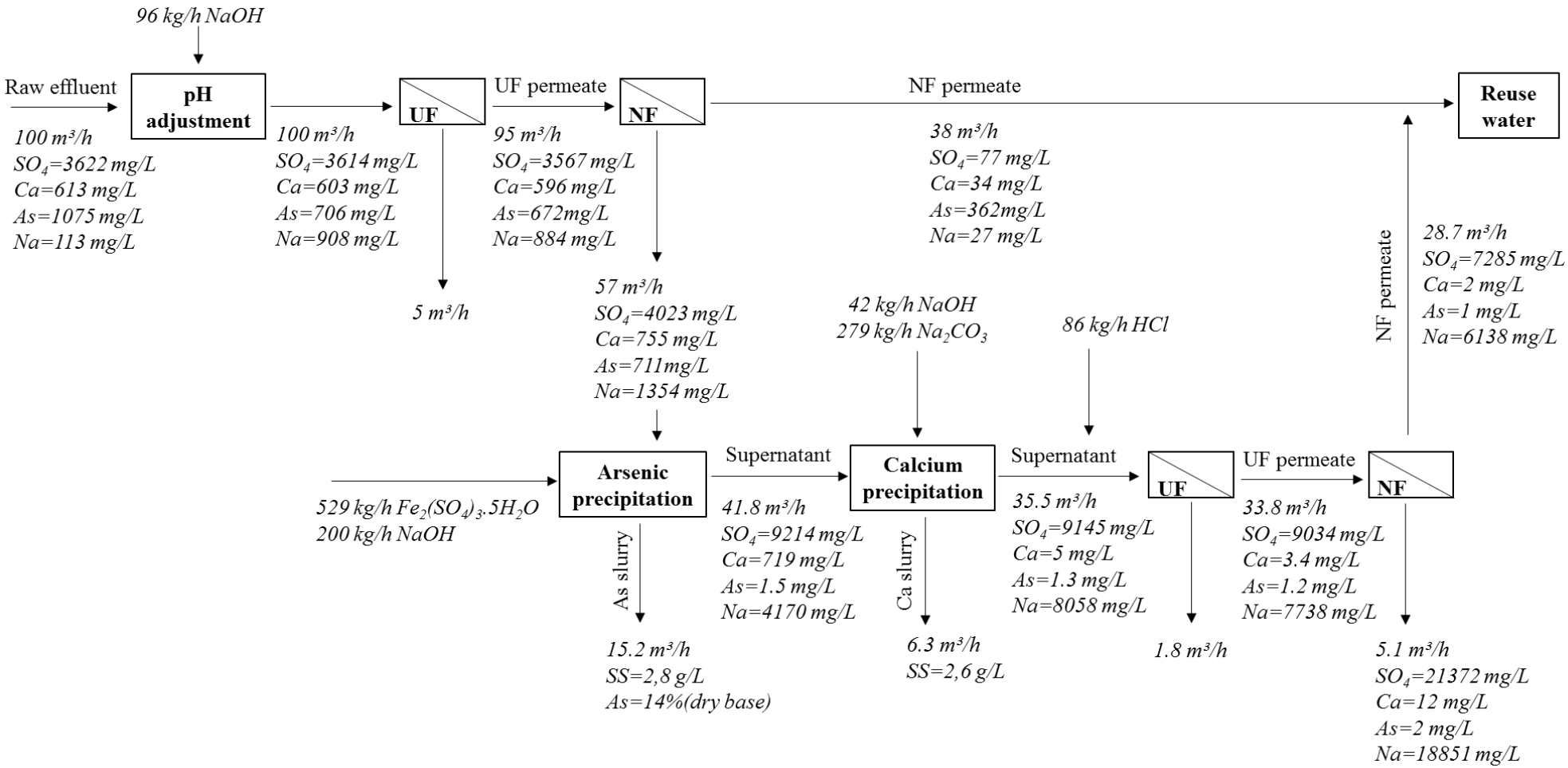

Figure 5.12 – Flowchart of the global treatment process

The largest share of the treatment cost is due to the chemical treatment stages (Table 5.7), which include arsenic coprecipitation (39% of total cost), calcium precipitation (18%), alkalizing agent for raw effluent pH adjustment to 5.0 (16%) and acidifying agent for pH adjustment of the precipitation supernatant to 8.5, before the second-stage membrane process (14%). Costs related to membrane separation processes (capital cost, NF and UF membrane replacement, energy, cleaning agent and maintenance) account for only 8% of the total.

The total cost of the complete treatment is US$ 6.28/m³, which is considered high when compared with the current treatment cost performed by the company, US$ 1.60/m³. However, unlike the conventional treatment, the system proposed here allows the generation of 187 m³/h of reuse water. Since the current cost of fresh water is US$ 0.18/m³, it represents a saving of almost US$ 295,000.00/year. Moreover, the proposed system produces an arsenic slurry more concentrated than the currently generated by the mining company. This allows for cost reduction and increase in lifetime of tailings reserved for special slurry disposal.

Table 5.7 – Mining effluent treatment costs by two-stage UF and NF associated with intermediate precipitation

Item	Cost (US$/m³)
Capital cost amortization	0.20
NF and UF membrane replacement	0.17
Energy	0.04
Cleaning agent	0.01
Alkalizing agent for gold mining pH adjustment	0.96
Acidifying agent for calcium precipitation supernatant pH adjustment	0.87
Intermediate arsenic coprecipitation	2.43
Intermediate calcium precipitation	1.14
Arsenic slurry disposition	0.19
UF and NF concentrates treatment	0.18
Maintenance	0.07
Labor	0.03
TOTAL	6.28

5.4 CONCLUSIONS

The integrated two-stage UF-NF and intermediate precipitation system is an efficient process for the retention of the main species contaminants of gold mining effluent. The first step aimed

at the treatment of the concentrate by removing arsenic with ferric coprecipitation; while in the second-step, calcium carbonate was precipitated in order to allow increased permeate recovery rate in a second-stage UF-NF.

Factorial design was used to optimize the conditions for coprecipitation of arsenic. The optimum conditions were molar ratio Fe/As of 4.0 and pH of 7.0, which were consistent with the literature.

For the precipitation of calcium, the optimum conditions were molar ratio CO_3/Ca 3.5 and pH 11.5. The higher pH increased the process efficiency since it favors carbonate species in relation to bicarbonate and carbonic acid. The stoichiometric excess of carbonate was necessary due to the competition of Ca^{2+} with other metal cations such as Mg^{2+}.

Once the precipitation occurred at high pH, neutralization of the supernatant was necessary. Very high pHs are unsuitable for membrane continuous operation and also cause an increase in membrane pore size and a reduce in solute rejection. The pH 8.5 was the one that provided jointly high conductivity, sulfate and arsenic retention and higher permeate flux.

The permeate flux at permeate recovery rate of 60% was 70% lower than the initial one. This reduction was attributed to both osmotic pressure increase and fouling resistance growth. The fouling resistance was mainly related to reversible fouling (90% from total resistance), which comprised the concentration polarization resistance and the resistance from fouling loosely attacked to the membrane and removable by physical cleaning. SI_m calculation confirmed that no scaling could be deposited over membrane surface. Thus, it was concluded that it is possible to operate the second-stage NF with high RR, ensuring higher production of reuse water.

The process cost is US$ 6.28/m³. However, the largest share of the treatment cost is due to the chemical treatment stages, which include arsenic coprecipitation (39% of total cost), calcium precipitation (18%), alkalizing agent for raw effluent pH adjustment to 5.0 (16%) and acidifying agent for pH adjustment of the precipitation supernatant to 8.5 (14%). Costs related to membrane separation processes (capital cost, NF and UF membrane replacement, energy, cleaning agent and maintenance) account for only 8% of the total.

6 CHAPTER

GENERAL CONCLUSIONS

Integrated UF-NF has proven to be an efficient system to treat gold mining effluent. The permeate has the required quality to be reused as process water in the mining industry and the concentrate can be treated by intermediate chemical precipitation, allowing arsenic removal and further water recovery at a second-stage membrane processes.

The operating conditions were evaluated in both bench and pilot scale. The main conclusions regarding this evaluation were:

- Feed pH of 5.0 was chosen as ideal for UF and NF treatment of gold mining effluent, since it provides benefits in terms of lower fouling potential and higher pollutant retention efficiency.

- Ambient temperature should be used. The increase in temperature leads to reduction of concentration polarization and fouling due to increased mass transfer of solutes; however, the increase in pore size leads to significant reduction in solutes retention efficiency.

- Permeate recovery rate of first-stage NF is limited to 40% because of significant increase in permeate conductivity and risk of scaling. However, antiscalant dosage reduced the permeate flux decay for recovery rates higher than 40%.

- The changes in flow conditions provided by operating pressure increase were not favorable to the system, as well as application of physical cleaning by forward flush

- The improvement in mass transfer by increasing the cross-flow velocity can effectively reduce the concentration polarization and fouling tendency. The cross-flow velocity threshold was identified as $15x10^{-3}$ m/s; after this velocity there is an increase in energy expenditure, but no benefits in terms of lower membrane fouling tendency.

- The most efficient cleaning procedure was 90-minute recirculation of HCl 0.2% solution, without soak.

The membrane fouling and stability when in contact with effluent and cleaning solution were also studied. Although there were changes in the rejection of the membranes over time, the reduction was not intense, and NF membranes still showed good performance even after 285

days of exposure, what demonstrated the robustness of NF technology for gold mining effluent treatment. It was also concluded that:

- Fouling was mainly made up of calcium, magnesium, sodium, zinc, copper, aluminum, iron, arsenic, and silica. The supersaturation index over membrane surface (SI_m) for calcium sulfate was always larger than 1. Thus, calcium sulfate was found precipitated in the form of bassanite (hydrated calcium sulfate $CaSO_4.0.5H_2O$) on the membrane.

- Fouling, surface charge changes, and an increased pore radius led to a decrease in retention of salts (magnesium sulfate) and neutral solutes (glucose) by membranes over time. The retention of the membrane exposed to the cleaning solution was statistically lower, reinforcing the importance of optimizing the cleaning condition to maximize cleaning efficiency with the least exposure.

Because concentrate from first-stage NF was rich in arsenic and supersaturated in calcium sulfate, a two-step intermediate chemical precipitation was studied. The first step aimed at the treatment of the concentrate by removing arsenic with ferric coprecipitation; while in the second-step, calcium carbonate was precipitated in order to allow increased permeate recovery rate in a second-stage UF-NF. The main conclusions were:

- Factorial design was used to optimize the conditions for coprecipitation of arsenic and precipitation of calcium. The optimum conditions for arsenic removal were molar ratio Fe/As 4.0 and pH 7.0. For the precipitation of calcium, the optimum conditions were molar ratio CO_3/Ca 3.5 and pH 11.5.

- Both osmotic pressure and fouling resistance increase were responsible for decreasing the permeate flux at second-stage NF. However, the fouling resistance was mainly related to reversible fouling. Thus, it was concluded that it is possible to operate the second-stage NF with high RR, ensuring higher production of reuse water.

Additionally, other important conclusions of this thesis include:

- There were significantly differences in NF90 membrane surface zeta potential measured with standard KCl solution (electrolyte solution) and synthetic effluent (solution with salt concentration similar to gold mining effluent). This proves that, to understand

retention mechanisms and to accurately model membrane processes, analysis of surface charge must be carried out using solutions similar to the solution of interest.

- When using the NF90 membrane to treat gold mining effluent, the retention of high-valence counter-ions to balance the charge of retained co-ions charge, together with steric hindrance, were the strongest retention mechanisms.

- The importance of evaluating operating parameters in a pilot scale unit was highlighted. We observed significant differences in the results of permeate flux and retention efficiencies from the bench and pilot scale tests. These differences are attributed to longer concentrate recirculation at bench scale tests and different flow conditions.

- The first-stage cost of treatment was US$ 1.34/m³, which is smaller than the actual wastewater treatment current installed on the gold mining industry.

- The cost of the complete process, including fist- and second-stage UF-NF and intermediate chemical precipitation of arsenic and calcium, is US$ 6.28/m³. However, the largest share of the treatment cost is due to the chemical treatment stages. Costs related to membrane separation processes (capital cost, NF and UF membrane replacement, energy, cleaning agent and maintenance) account for only 8% of the total.

Despite the high cost, the complete process proposed allows the generation of 187 m³/h of reuse water, which may represent a saving of almost US$ 295,000.00/year. Moreover, the proposed route produces an arsenic slurry more concentrated than the currently generated by the mining company. This allows for cost reduction and increase in lifetime of tailings reserved for special slurry disposal. From an environmental perspective, the proposed treatment system contributes to a reduction in natural water capitation and a decrease in wastewater discharge, which reduces the environmental impacts of industrial sector.

7 CHAPTER

BIBLIOGRAPHIC REFERENCES

Bibliographic References

ABDESSEMED, D.; NEZZAL, G. Coupling softening—ultrafiltration like pretreatment of sea water case study of the Corso plant desalination (Algiers). *Desalination***,** v. 221, n. 1, p. 107-113, 2008.

ACERO, J. L.; BENITEZ, F. J.; LEAL, A. I.; REAL, F. J.; TEVA, F. Membrane filtration technologies applied to municipal secondary effluents for potential reuse. *Journal of Hazardous Materials***,** v. 177, n. 1, p. 390-398, 2010a.

ACERO, J. L.; BENITEZ, F. J.; TEVA, F.; LEAL, A. I. Retention of emerging micropollutants from UP water and a municipal secondary effluent by ultrafiltration and nanofiltration. *Chemical Engineering Journal***,** v. 163, n. 3, p. 264-272, 2010b.

ACHEAMPONG, M. A.; LENS, P. N. L. Treatment of gold mining effluent in pilot fixed bed sorption system. *Hydrometallurgy***,** v. 141, p. 1-7, 2014.

AHMED, A.-A. Effect of chemical cleaning agents on virgin nanofiltration membrane as characterized by positron annihilation spectroscopy. *Separation and Purification Technology***,** v. 110, p. 51-56, 2013.

AKCIL, A.; KOLDAS, S. Acid Mine Drainage (AMD): causes, treatment and case studies. *Journal of Cleaner Production***,** v. 14, n. 12-13, p. 1139-1145, 2006.

AL-AMOUDI, A.; LOVITT, R. W. Fouling strategies and the cleaning system of NF membranes and factors affecting cleaning efficiency. *Journal of Membrane Science***,** v. 303, n. 1, p. 4-28, 2007.

AL-AMOUDI, A.; WILLIAMS, P.; MANDALE, S.; LOVITT, R. W. Cleaning results of new and fouled nanofiltration membrane characterized by zeta potential and permeability. *Separation and Purification Technology***,** v. 54, n. 2, p. 234-240, 2007.

AL-RASHDI, B.; JOHNSON, D.; HILAL, N. Removal of heavy metal ions by nanofiltration. *Desalination***,** v. 315, p. 2-17, 2013.

AL-ROOMI, Y. M.; HUSSAIN, K. F. Potential kinetic model for scaling and scale inhibition mechanism. *Desalination*, 2015.

AL-THYABAT, S.; AL-ZOUBI, H. Purification of phosphate beneficiation wastewater: Separation of phosphate from Eshydia Mine (Jordan) by column-DAF flotation process. *International Journal of Mineral Processing***,** v. 110, p. 18-24, 2012.

AL-ZOUBI, H.; RIEGER, A.; STEINBERGER, P.; PELZ, W.; HASENEDER, R.; HÄRTEL, G. Optimization study for treatment of acid mine drainage using membrane technology. *Separation Science and Technology***,** v. 45, n. 14, p. 2004-2016, 2010 a.

AL-ZOUBI, H.; RIEGER, A.; STEINBERGER, P.; PELZ, W.; HASENEDER, R.; HÄRTEL, G. Nanofiltration of acid mine drainage. *Desalination and Water Treatment***,** v. 21, n. 1-3, p. 148-161, 2010 b.

AL-ZOUBI, H. S.; AL-THYABAT, S. S. Treatment of a Jordanian Phosphate Mine Wastewater by Hybrid Dissolved Air Flotation and Nanofiltration. *Mine Water and the Environment***,** v. 31, n. 3, p. 214-224, 2012.

ALVENTOSA-DELARA, E.; BARREDO-DAMAS, S.; ZURIAGA-AGUSTÍ, E.; ALCAINA-MIRANDA, M. I.; IBORRA-CLAR, M. I. Ultrafiltration ceramic membrane performance during the treatment of model solutions containing dye and salt. *Separation and Purification Technology***,** v. 129, p. 96-105, 2014.

ALZAHRANI, S.; MOHAMMAD, A.; HILAL, N.; ABDULLAH, P.; JAAFAR, O. Comparative study of NF and RO membranes in the treatment of produced water—Part I: Assessing water quality. *Desalination***,** v. 315, p. 18-26, 2013.

AMAR, N. B.; SAIDANI, H.; PALMERI, J.; DERATANI, A. Effect of temperature on the rejection of neutral and charged solutes by Desal 5 DK nanofiltration membrane. *Desalination***,** v. 246, n. 1, p. 294-303, 2009.

ANA. Região enfrenta sérios problemas por causa da escassez de água. 2014. Disponível em: < http://www2.ana.gov.br/Paginas/portais/bacias/AtlanticoSudeste.aspx >. Acesso em: 23/05/2015.

ANDRADE, L.; MENDES, F.; ESPINDOLA, J.; AMARAL, M. Nanofiltration as tertiary treatment for the reuse of dairy wastewater treated by membrane bioreactor. *Separation and Purification Technology***,** v. 126, p. 21-29, 2014.

ANTONY, A.; LOW, J. H.; GRAY, S.; CHILDRESS, A. E.; LE-CLECH, P.; LESLIE, G. Scale formation and control in high pressure membrane water treatment systems: A review. *Journal of Membrane Science***,** v. 383, n. 1, p. 1-16, 2011.

APPA; AWWA; WEF. Standard methods for the examination of water and wastewater. 21. ed.. Washington: APHA,2005.

ARNAL, J. M.; GARCÍA-FAYOS, B.; SANCHO, M. Membrane Cleaning. In: NING, R. Y. (Ed.). *Expanding issues in desalination*: InTech, 2011. p.63-83. ISBN 978-953-307-624-9.

ASANO, T.; BURTON, F.; LEVERENZ, H.; TSUCHIHASHI, R.; TCHOBANOGLOUS, G. *Water reuse: issues, technologies, and applications*. 1. McGraw-Hill, 2007. 1570

AYACHE, C.; PIDOU, M.; CROUÉ, J.; LABANOWSKI, J.; POUSSADE, Y.; TAZI-PAIN, A.; KELLER, J.; GERNJAK, W. Impact of effluent organic matter on low-pressure membrane fouling in tertiary treatment. *Water Research***,** v. 47, n. 8, p. 2633-2642, 2013.

AZAÏS, A.; MENDRET, J.; GASSARA, S.; PETIT, E.; DERATANI, A.; BROSILLON, S. Nanofiltration for wastewater reuse: Counteractive effects of fouling and matrice on the rejection of pharmaceutical active compounds. *Separation and Purification Technology***,** v. 133, p. 313-327, 2014.

BAKER, R. W. *Membrane Technology and Applications*. Chichester: John Wiley & Sons Ltd., 2004.

BALANNEC, B.; VOURCH, M.; RABILLER-BAUDRY, M.; CHAUFER, B. Comparative study of different nanofiltration and reverse osmosis membranes for dairy effluent treatment by dead-end filtration. *Separation and Purification Technology***,** v. 42, n. 2, p. 195-200, 2005.

BARGEMAN, G.; STEENSMA, M.; TEN KATE, A.; WESTERINK, J.; DEMMER, R.; BAKKENES, H.; MANUHUTU, C. Nanofiltration as energy-efficient solution for sulfate waste in vacuum salt production. *Desalination***,** v. 245, n. 1, p. 460-468, 2009.

BELKHOUCHE, N.-E.; DIDI, M. A.; TAHA, S.; FARÈS, N. B. Zinc rejection from leachate solutions of industrial solid waste—effects of pressure and concentration on nanofiltration membrane performance. *Desalination***,** v. 239, n. 1, p. 58-65, 2009.

BELLONA, C.; DREWES, J. E. The role of membrane surface charge and solute physico-chemical properties in the rejection of organic acids by NF membranes. *Journal of Membrane Science***,** v. 249, n. 1, p. 227-234, 2005.

BELLONA, C.; HEIL, D.; YU, C.; FU, P.; DREWES, J. E. The pros and cons of using nanofiltration in lieu of reverse osmosis for indirect potable reuse applications. *Separation and Purification Technology***,** v. 85, p. 69-76, 2012.

BELLONA, C.; MARTS, M.; DREWES, J. E. The effect of organic membrane fouling on the properties and rejection characteristics of nanofiltration membranes. *Separation and Purification Technology***,** v. 74, n. 1, p. 44-54, 2010.

BEYER, M.; LOHRENGEL, B.; NGHIEM, L. D. Membrane fouling and chemical cleaning in water recycling applications. *Desalination***,** v. 250, n. 3, p. 977-981, 2010.

BHATTACHARYA, S.; HWANG, S.-T. Concentration polarization, separation factor, and Peclet number in membrane processes. *Journal of Membrane Science***,** v. 132, n. 1, p. 73-90, 1997.

BI, F.; ZHAO, H.; ZHANG, L.; YE, Q.; CHEN, H.; GAO, C. Discussion on calculation of maximum water recovery in nanofiltration system. *Desalination***,** v. 332, n. 1, p. 142-146, 2014.

BONNÉ, P.; HIEMSTRA, P.; VAN DER HOEK, J.; HOFMAN, J. Is direct nanofiltration with air fluxh an alternative for household water production for Amsterdam? *Desalination***,** v. 152, n. 1, p. 263-269, 2003.

BUZZI, D. C.; VIEGAS, L. S.; SILVAS, F. P. C.; ESPINOSA, D. C. R.; RODRIGUES, M. A. S.; BERNARDES, A. M.; TENÓRIO, J. A. S. The use of microfiltration and electrodialysis for treatment of acid mine drainage. In: INTERNATIONAL MINE WATER ASSOCIATION ANNUAL CONFERENCE, 2011, Aachen. *Proceedings…* Aachen: 2011.

CANDIOTI, L. V.; DE ZAN, M. M.; CAMARA, M. S.; GOICOECHEA, H. C. Experimental design and multiple response optimization. Using the desirability function in analytical methods development. *Talanta***,** v. 124, p. 123-138, 2014.

CAPAR, G.; YILMAZ, L.; YETIS, U. Reclamation of acid dye bath wastewater: Effect of pH on nanofiltration performance. *Journal of Membrane Science***,** v. 281, n. 1-2, p. 560-569, 2006.

CHAN, B. K. C.; DUDENEY, A. W. L. Reverse osmosis removal of arsenic residues from bioleaching of refractory gold concentrates. *Minerals Engineering***,** v. 21, n. 4, p. 272-278, 2008.

CHANG, F.-F.; LIU, W.-J.; WANG, X.-M. Comparison of polyamide nanofiltration and low-pressure reverse osmosis membranes on As (III) rejection under various operational conditions. *Desalination***,** v. 334, n. 1, p. 10-16, 2014.

CHEW, C. M.; AROUA, M. K.; HUSSAIN, M. A.; ISMAIL, W. M. Z. W. Evaluation of ultrafiltration and conventional water treatment systems for sustainable development: an industrial scale case study. *Journal of Cleaner Production***,** v. 112, p. 3152-3163, 2016.

CHILDRESS, A. E.; ELIMELECH, M. Effect of solution chemistry on the surface charge of polymeric reverse osmosis and nanofiltration membranes. *Journal of Membrane Science***,** v. 119, n. 2, p. 253-268, 1996.

CHILDRESS, A. E.; ELIMELECH, M. Relating nanofiltration membrane performance to membrane charge (electrokinetic) characteristics. *Environmental science & technology***,** v. 34, n. 17, p. 3710-3716, 2000.

COMSTOCK, S. E.; BOYER, T. H.; GRAF, K. C. Treatment of nanofiltration and reverse osmosis concentrates: comparison of precipitative softening, coagulation, and anion exchange. *Water Research***,** v. 45, n. 16, p. 4855-4865, 2011.

CORREIA, C. S. H. Contribuição para a análise da presença de arsénio em águas de abastecimento e sua remoção por precipitação química (*Contribution to the analysis of the presence of arsenic in drinking water and its removal by chemical precipitation*). 2008. Thesis (Masters in Environmental Engineering) - Universidade Nova de Lisboa, Lisboa. 2008.

CORTÉS-JUAN, F.; BALANNEC, B.; RENOUARD, T. CFD-assisted design improvement of a bench-scale nanofiltration cell. *Separation and Purification Technology***,** v. 82, p. 177-184, 2011.

CURCIO, E.; JI, X.; QUAZI, A. M.; BARGHI, S.; DI PROFIO, G.; FONTANANOVA, E.; MACLEOD, T.; DRIOLI, E. Hybrid nanofiltration–membrane crystallization system for the treatment of sulfate wastes. *Journal of Membrane Science***,** v. 360, n. 1, p. 493-498, 2010.

DA SILVA, M. K.; AMBROSI, A.; DOS RAMOS, G. M.; TESSARO, I. C. Rejuvenating polyamide reverse osmosis membranes by tannic acid treatment. *Separation and Purification Technology***,** v. 100, p. 1-8, 2012.

DALWANI, M.; BENES, N. E.; BARGEMAN, G.; STAMATIALIS, D.; WESSLING, M. Effect of pH on the performance of polyamide/polyacrylonitrile based thin film composite membranes. *Journal of Membrane Science***,** v. 372, n. 1-2, p. 228-238, 2011.

DANG, H. Q.; PRICE, W. E.; NGHIEM, L. D. The effects of feed solution temperature on pore size and trace organic contaminant rejection by the nanofiltration membrane NF270. *Separation and Purification Technology***,** v. 125, p. 43-51, 2014.

DE KLERK, R. J.; JIA, Y.; DAENZER, R.; GOMEZ, M. A.; DEMOPOULOS, G. P. Continuous circuit coprecipitation of arsenic(V) with ferric iron by lime neutralization: Process parameter effects on arsenic removal and precipitate quality. *Hydrometallurgy***,** v. 111-112, p. 65-72, 2012.

DE, S.; BHATTACHARJEE, S.; BHATTACHARYA, P. Development of correlations for mass transfer coefficient in ultrafiltration systems. *Developments in Chemical Engineering and Mineral Processing***,** v. 3, n. 3-4, p. 187-206, 1995.

DEBIK, E.; KAYKIOGLU, G.; COBAN, A.; KOYUNCU, I. Reuse of anaerobically and aerobically pre-treated textile wastewater by UF and NF membranes. *Desalination***,** v. 256, n. 1, p. 174-180, 2010.

DHAR, R.; ZHENG, Y.; RUBENSTONE, J.; VAN GEEN, A. A rapid colorimetric method for measuring arsenic concentrations in groundwater. *Analytica Chimica Acta***,** v. 526, n. 2, p. 203-209, 2004.

DNPM. *Sumário Mineral 2014*. Departamento Nacional de Produção Mineral. 2014

DOWFILMTEC™ a. *Cleaning and Disinfection Procedures for FilmTec™ NF200 and NF270 Elements*. Form n. 609-00388-1006.

DOWFILMTEC™ b. *Product Information: FILMTEC NF90-400 Nanofiltration Element.* Form n. 609-00345-0312.

DOWFILMTEC™, 2012. *ACUMER™ 4300 Polymer Technical Data Sheet.* Form n. 713-00006-0712-EN, 2012.

DRAK, A.; GLUCINA, K.; BUSCH, M.; HASSON, D.; LAÎNE, J.-M.; SEMIAT, R. Laboratory technique for predicting the scaling propensity of RO feed waters. *Desalination***,** v. 132, n. 1, p. 233-242, 2000.

DUBOIS, M.; GILLES, K. A.; HAMILTON, J. K.; REBERS, P.; SMITH, F. Colorimetric method for determination of sugars and related substances. *Analytical chemistry***,** v. 28, n. 3, p. 350-356, 1956.

DYDO, P.; TUREK, M.; CIBA, J.; WANDACHOWICZ, K.; MISZTAL, J. The nucleation kinetic aspects of gypsum nanofiltration membrane scaling. *Desalination***,** v. 164, n. 1, p. 41-52, 2004.

FERNÁNDEZ-TORRES, M.; RANDALL, D.; MELAMU, R.; VON BLOTTNITZ, H. A comparative life cycle assessment of eutectic freeze crystallisation and evaporative crystallisation for the treatment of saline wastewater. *Desalination***,** v. 306, p. 17-23, 2012.

FRANK, M.; WESTERINK, J.; SCHOKKER, A. Recycling of industrial waste water by using a two-step nanofiltration process for the removal of colour. *Desalination,* v. 145, n. 1, p. 69-74, 2002.

FU, F.; WANG, Q. Removal of heavy metal ions from wastewaters: A review. *Journal of Environmental Management,* v. 92, n. 3, p. 407-418, 2011.

FUJIOKA, T.; NGHIEM, L. D.; KHAN, S. J.; MCDONALD, J. A.; POUSSADE, Y.; DREWES, J. E. Effects of feed solution characteristics on the rejection of N-nitrosamines by reverse osmosis membranes. *Journal of Membrane Science,* v. 409, p. 66-74, 2012.

GABELICH, C. J.; RAHARDIANTO, A.; NORTHRUP, C. R.; YUN, T. I.; COHEN, Y. Process evaluation of intermediate chemical demineralization for water recovery enhancement in production-scale brackish water desalting. *Desalination,* v. 272, n. 1, p. 36-45, 2011.

GABELICH, C. J.; WILLIAMS, M. D.; RAHARDIANTO, A.; FRANKLIN, J. C.; COHEN, Y. High-recovery reverse osmosis desalination using intermediate chemical demineralization. *Journal of Membrane Science,* v. 301, n. 1, p. 131-141, 2007.

GAUTAM, A.; MENKHAUS, T. J. Performance evaluation and fouling analysis for reverse osmosis and nanofiltration membranes during processing of lignocellulosic biomass hydrolysate. *Journal of Membrane Science,* v. 451, p. 252-265, 2014.

GERALDES, V. T.; SEMIÃO, V.; DE PINHO, M. N. Flow management in nanofiltration spiral wound modules with ladder-type spacers. *Journal of Membrane Science,* v. 203, n. 1, p. 87-102, 2002.

GETANEH, W.; ALEMAYEHU, T. Metal contamination of the environment by placer and primary gold mining in the Adola region of southern Ethiopia. *Environmental Geology,* v. 50, n. 3, p. 339-352, 2006.

GHAFFOUR, N.; NACEUR, M.; DROUICHE, N.; MAHMOUDI, H. Use of ultrafiltration membranes in the treatment of refinery wastewaters. *Desalination and Water Treatment,* v. 5, n. 1-3, p. 159-166, 2009.

GHERASIM, C.-V.; MIKULÁŠEK, P. Influence of operating variables on the removal of heavy metal ions from aqueous solutions by nanofiltration. *Desalination,* v. 343, p. 67-74, 2014.

GONZÁLEZ, M.; SAUCEDO, I.; NAVARRO, R.; PRÁDANOS, P.; PALACIO, L.; MARTÍNEZ, F.; MARTÍN, A.; HERNÁNDEZ, A. Effect of phosphoric and hydrofluoric acid on the structure and permeation of a nanofiltration membrane. *Journal of Membrane Science,* v. 281, n. 1, p. 177-185, 2006.

GONZÁLEZ, V.; GARCÍA, I.; DEL MORAL, F.; DE HARO, S.; SÁNCHEZ, J.; SIMÓN, M. Spreading of pollutants from alkaline mine drainage. Rodalquilar mining district (SE Spain). *Journal of Environmental Management,* v. 106, p. 69-74, 2012.

GORZALSKI, A. S.; CORONELL, O. Fouling of nanofiltration membranes in full-and bench-scale systems treating groundwater containing silica. *Journal of Membrane Science***,** v. 468, p. 349-359, 2014.

GREENLEE, L. F.; LAWLER, D. F.; FREEMAN, B. D.; MARROT, B.; MOULIN, P. Reverse osmosis desalination: water sources, technology, and today's challenges. *Water Research***,** v. 43, n. 9, p. 2317-2348, 2009.

GREENLEE, L. F.; TESTA, F.; LAWLER, D. F.; FREEMAN, B. D.; MOULIN, P. Effect of antiscalants on precipitation of an RO concentrate: metals precipitated and particle characteristics for several water compositions. *Water Research***,** v. 44, n. 8, p. 2672-2684, 2010.

GWON, E.-M.; YU, M.-J.; OH, H.-K.; YLEE, Y.-H. Fouling characteristics of NF and RO operated for removal of dissolved matter from groundwater. *Water Research***,** v. 37, n. 12, p. 2989-2997, 2003.

HABERT, A. C.; BORGES, C. P.; NOBREGA, R. *Processos de Separação com Membranas*. 1. Rio de Janeiro: e-papers, 2006. 180 p.

HARRIES, R. A field trial of seeded reverse osmosis for the desalination of a scaling-type mine water. *Desalination***,** v. 56, p. 227-236, 1985.

HÄYRYNEN, K.; PONGRÁCZ, E.; VÄISÄNEN, V.; PAP, N.; MÄNTTÄRI, M.; LANGWALDT, J.; KEISKI, R. L. Concentration of ammonium and nitrate from mine water by reverse osmosis and nanofiltration. *Desalination***,** v. 240, n. 1, p. 280-289, 2009.

HEIJMAN, S.; GUO, H.; LI, S.; VAN DIJK, J.; WESSELS, L. Zero liquid discharge: Heading for 99% recovery in nanofiltration and reverse osmosis. *Desalination***,** v. 236, n. 1, p. 357-362, 2009.

HONG, S.; ELIMELECH, M. Chemical and physical aspects of natural organic matter (NOM) fouling of nanofiltration membranes. *Journal of Membrane Science***,** v. 132, n. 2, p. 159-181, 1997.

HOYER, M.; ZABELT, D.; STEUDTNER, R.; BRENDLER, V.; HASENEDER, R.; REPKE, J.-U. Influence of speciation during membrane treatment of uranium contaminated water. *Separation and Purification Technology***,** v. 132, p. 413-421, 2014.

HUANG, Q.; MA, W. A model of estimating scaling potential in reverse osmosis and nanofiltration systems. *Desalination***,** v. 288, p. 40-46, 2012.

HYDRANAUTICS, 2008. *Chemical pretreatment of RO and NF*. Technical Application Bulletin No. 111. DENKO, N. 2008.

JARUSUTTHIRAK, C.; MATTARAJ, S.; JIRARATANANON, R. Influence of inorganic scalants and natural organic matter on nanofiltration membrane fouling. *Journal of Membrane Science***,** v. 287, n. 1, p. 138-145, 2007.

JIA, Y.; DEMOPOULOS, G. P. Coprecipitation of arsenate with iron(III) in aqueous sulfate media: Effect of time, lime as base and co-ions on arsenic retention. *Water Research***,** v. 42, n. 3, p. 661-668, 2008.

JIA, Y.; ZHANG, D.; PAN, R.; XU, L.; DEMOPOULOS, G. P. A novel two-step coprecipitation process using Fe(III) and Al(III) for the removal and immobilization of arsenate from acidic aqueous solution. *Water Research***,** v. 46, n. 2, p. 500-508, 2012.

JUBY, G.; SCHUTTE, C.; VAN LEEUWEN, J. Desalination of calcium sulphate scaling mine water: Design and operation of the SPARRO process. *Water S. A.***,** v. 22, n. 2, p. 161-172, 1996.

KAPPEL, C.; KEMPERMAN, A.; TEMMINK, H.; ZWIJNENBURG, A.; RIJNAARTS, H.; NIJMEIJER, K. Impacts of NF concentrate recirculation on membrane performance in an integrated MBR and NF membrane process for wastewater treatment. *Journal of Membrane Science***,** v. 453, p. 359-368, 2014.

KAYA, Y.; BARLAS, H.; ARAYICI, S. Nanofiltration of Cleaning-in-Place (CIP) wastewater in a detergent plant: Effects of pH, temperature and transmembrane pressure on flux behavior. *Separation and Purification Technology***,** v. 65, n. 2, p. 117-129, 2009.

KAYA, Y.; GÖNDER, Z.; VERGILI, I.; BARLAS, H. The effect of transmembrane pressure and pH on treatment of paper machine process waters by using a two-step nanofiltration process: Flux decline analysis. *Desalination***,** v. 250, n. 1, p. 150-157, 2010.

KOYUNCU, I.; TURAN, M.; TOPACIK, D.; ATES, A. Application of low pressure nanofiltration membranes for the recovery and reuse of dairy industry effluents. *Water science and technology***,** v. 41, n. 1, p. 213-221, 2000.

KRAMER, F. C.; SHANG, R.; HEIJMAN, S. G.; SCHERRENBERG, S. M.; VAN LIER, J. B.; RIETVELD, L. C. Direct water reclamation from sewage using ceramic tight ultra-and nanofiltration. *Separation and Purification Technology***,** v. 147, p. 329-336, 2015.

KRIEG, H.; MODISE, S.; KEIZER, K.; NEOMAGUS, H. Salt rejection in nanofiltration for single and binary salt mixtures in view of sulphate removal. *Desalination***,** v. 171, n. 2, p. 205-215, 2005.

KURT, E.; KOSEOGLU-IMER, D. Y.; DIZGE, N.; CHELLAM, S.; KOYUNCU, I. Pilot-scale evaluation of nanofiltration and reverse osmosis for process reuse of segregated textile dyewash wastewater. *Desalination***,** v. 302, p. 24-32, 2012.

LANGMUIR, D.; MAHONEY, J.; ROWSON, J. Solubility products of amorphous ferric arsenate and crystalline scorodite (FeAsO 4· 2H 2 O) and their application to arsenic behavior in buried mine tailings. *Geochimica et Cosmochimica Acta***,** v. 70, n. 12, p. 2942-2956, 2006.

LANGSCH, J. E.; COSTA, M.; MOORE, L.; MORAIS, P.; BELLEZZA, A.; FALCÃO, S. New Technology for Arsenic Removal from Mining Effluents. *Journal of Materials Research and Technology***,** v. 1, n. 3, p. 178-181, 2012.

LE GOUELLEC, Y. A.; CORNWELL, D.; CHENG, R.; TSENG, T.; VUONG, D.; WATTIER, K.; HARRISON, C.; CHILDRESS, A. *A novel approach to seawater desalination using dual-staged nanofiltration*. Water Environment Research Foundation, 2007. ISBN 1843399709.

LE GOUELLEC, Y. A.; ELIMELECH, M. Calcium sulfate (gypsum) scaling in nanofiltration of agricultural drainage water. *Journal of Membrane Science***,** v. 205, n. 1, p. 279-291, 2002.

LI, K.; WANG, J.; LIU, J.; WEI, Y.; CHEN, M. Advanced treatment of municipal wastewater by nanofiltration: Operational optimization and membrane fouling analysis. *Journal of Environmental Sciences*, 2015.

LIIKANEN, R.; YLI-KUIVILA, J.; TENHUNEN, J.; LAUKKANEN, R. Cost and environmental impact of nanofiltration in treating chemically pre-treated surface water. *Desalination***,** v. 201, n. 1, p. 58-70, 2006.

LIU, M.; LÜ, Z.; CHEN, Z.; YU, S.; GAO, C. Comparison of reverse osmosis and nanofiltration membranes in the treatment of biologically treated textile effluent for water reuse. *Desalination***,** v. 281, p. 372-378, 2011.

LOBO, F. L.; COSTA, M. P.; NOVO, E. M. Time-series analysis of Landsat-MSS/TM/OLI images over Amazonian waters impacted by gold mining activities. *Remote Sensing of Environment***,** v. 157, p. 170-184, 2015.

LUO, J.; WAN, Y. Effects of pH and salt on nanofiltration - a critical review. *Journal of Membrane Science***,** v. 438, p. 18-28, 2013.

LUSILAO-MAKIESE, J.; CUKROWSKA, E.; TESSIER, E.; AMOUROUX, D.; WEIERSBYE, I. The impact of post gold mining on mercury pollution in the West Rand region, Gauteng, South Africa. *Journal of Geochemical Exploration***,** v. 134, p. 111-119, 2013.

LYSTER, E.; KIM, M.-M.; AU, J.; COHEN, Y. A method for evaluating antiscalant retardation of crystal nucleation and growth on RO membranes. *Journal of Membrane Science***,** v. 364, n. 1, p. 122-131, 2010.

MADAENI, S.; KAZEMI, V. Treatment of saturated brine in chlor-alkali process using membranes. *Separation and Purification Technology***,** v. 61, n. 1, p. 68-74, 2008.

MADAENI, S.; MANSOURPANAH, Y. Chemical cleaning of reverse osmosis membranes fouled by whey. *Desalination***,** v. 161, n. 1, p. 13-24, 2004.

MADAENI, S.; SAMIEIRAD, S. Chemical cleaning of reverse osmosis membrane fouled by wastewater. *Desalination***,** v. 257, n. 1, p. 80-86, 2010.

MAGRIOTIS, Z. M.; LEAL, P. V.; DE SALES, P. F.; PAPINI, R. M.; VIANA, P. R.; ARROYO, P. A. A comparative study for the removal of mining wastewater by kaolinite, activated carbon and beta zeolite. *Applied Clay Science***,** v. 91, p. 55-62, 2014.

MARCUCCI, M.; CIABATTI, I.; MATTEUCCI, A.; VERNAGLIONE, G. Membrane technologies applied to textile wastewater treatment. *Annals of the New York Academy of Sciences***,** v. 984, n. 1, p. 53-64, 2003.

MATTARAJ, S.; JARUSUTTHIRAK, C.; CHAROENSUK, C.; JIRARATANANON, R. A combined pore blockage, osmotic pressure, and cake filtration model for crossflow nanofiltration of natural organic matter and inorganic salts. *Desalination***,** v. 274, n. 1-3, p. 182-191, 2011.

MATTARAJ, S.; JARUSUTTHIRAK, C.; JIRARATANANON, R. A combined osmotic pressure and cake filtration model for crossflow nanofiltration of natural organic matter. *Journal of Membrane Science***,** v. 322, n. 2, p. 475-483, 2008.

MCCOOL, B. C.; RAHARDIANTO, A.; FARIA, J. I.; COHEN, Y. Evaluation of chemically-enhanced seeded precipitation of RO concentrate for high recovery desalting of high salinity brackish water. *Desalination***,** v. 317, p. 116-126, 2013.

MCNAUGHT, A. D. *Compendium of chemical terminology*. Blackwell Science Oxford, 1997.

MINNIKANTI, V.; DASGUPTA, S.; DE, S. Prediction of mass transfer coefficient with suction for turbulent flow in cross flow ultrafiltration. *Journal of Membrane Science***,** v. 157, n. 2, p. 227-239, 1999.

MO, Y.; CHEN, J.; XUE, W.; HUANG, X. Chemical cleaning of nanofiltration membrane filtrating the effluent from a membrane bioreactor. *Separation and Purification Technology***,** v. 75, n. 3, p. 407-414, 2010.

MOHAMMAD, A.; TEOW, Y.; ANG, W.; CHUNG, Y.; OATLEY-RADCLIFFE, D.; HILAL, N. Nanofiltration membranes review: Recent advances and future prospects. *Desalination***,** v. 356, p. 226-254, 2015.

MOLDOVAN, B. J.; HENDRY, M. J. Characterizing and quantifying controls on arsenic solubility over a pH range of 1-11 in a uranium mill-scale experiment. *Environmental science & technology***,** v. 39, n. 13, p. 4913-4920, 2005.

MUKHERJEE, R.; MONDAL, M.; SINHA, A.; SARKAR, S.; DE, S. Application of nanofiltration membrane for treatment of chloride rich steel plant effluent. *Journal of Environmental Chemical Engineering***,** v. 4, n. 1, p. 1-9, 2016.

MYAGKAYA, I.; LAZAREVA, E.; GUSTAYTIS, M.; ZHMODIK, S. Gold and silver in a system of sulfide tailings. Part 1: Migration in water flow. *Journal of Geochemical Exploration***,** v. 160, p. 16-30, 2016.

NANDA, D.; TUNG, K.-L.; LI, Y.-L.; LIN, N.-J.; CHUANG, C.-J. Effect of pH on membrane morphology, fouling potential, and filtration performance of nanofiltration membrane for water softening. *Journal of Membrane Science***,** v. 349, n. 1-2, p. 411-420, 2010.

NERY, M. A. C.; SILVA, E. A. *Ouro: Balanço Mineral Brasileiro*. Departamento Nacional de Produção Mineral (DNPM). 2001

NGHIEM, L. D.; HAWKES, S. Effects of membrane fouling on the nanofiltration of pharmaceutically active compounds (PhACs): Mechanisms and role of membrane pore size. *Separation and Purification Technology***,** v. 57, n. 1, p. 176-184, 2007.

NGUYEN, C. M.; BANG, S.; CHO, J.; KIM, K.-W. Performance and mechanism of arsenic removal from water by a nanofiltration membrane. *Desalination***,** v. 245, n. 1, p. 82-94, 2009.

NILSSON, M.; TRÄGÅRDH, G.; ÖSTERGREN, K. The influence of pH, salt and temperature on nanofiltration performance. *Journal of Membrane Science***,** v. 312, n. 1, p. 97-106, 2008.

NING, L.; LIYUAN, Y.; JIRUI, D.; XUGUI, P. Heavy metal pollution in surface water of Linglong gold mining area, China. *Procedia Environmental Sciences***,** v. 10, p. 914-917, 2011.

NISHIMURA, T.; UMETSU, Y. Chemistry on elimination of arsenic, antimony and selenium from aqueous solution with iron(III) species. In: YOUNG, C. A. (Ed.). *Minor Elements*. Littleton: SME, 2000. p.105-112.

OCHANDO-PULIDO, J.; HODAIFA, G.; MARTÍNEZ-FEREZ, A. Permeate recirculation impact on concentration polarization and fouling on RO purification of olive mill wastewater. *Desalination***,** v. 343, p. 169-179, 2014.

OCHANDO-PULIDO, J. M.; FÉREZ, A. M. Impacts of operating conditions on nanofiltration of secondary-treated two-phase olive mill wastewater. *Journal of Environmental Management***,** v. 161, p. 219-227, 2015.

OH, H.-J.; CHOUNG, Y.-K.; LEE, S.; CHOI, J.-S.; HWANG, T.-M.; KIM, J. H. Scale formation in reverse osmosis desalination: model development. *Desalination***,** v. 238, n. 1, p. 333-346, 2009.

ONCEL, M.; MUHCU, A.; DEMIRBAS, E.; KOBYA, M. A comparative study of chemical precipitation and electrocoagulation for treatment of coal acid drainage wastewater. *Journal of Environmental Chemical Engineering***,** v. 1, n. 4, p. 989-995, 2013.

PAGES, N.; YAROSHCHUK, A.; GIBERT, O.; CORTINA, J. L. Rejection of trace ionic solutes in nanofiltration: Influence of aqueous phase composition. *Chemical Engineering Science***,** v. 104, p. 1107-1115, 2013.

PAPASSIOPI, N.; VIRČIKOVÁ, E.; NENOV, V.; KONTOPOULOS, A.; MOLNÁR, L. Removal and fixation of arsenic in the form of ferric arsenates. Three parallel experimental studies. *Hydrometallurgy***,** v. 41, n. 2, p. 243-253, 1996.

PATIL, N. V.; FENG, X.; SEWALT, J. J.; BOOM, R. M.; JANSSEN, A. E. Separation of an inulin mixture using cascaded nanofiltration. *Separation and Purification Technology***,** v. 146, p. 261-267, 2015.

PEETERS, J.; MULDER, M.; STRATHMANN, H. Streaming potential measurements as a characterization method for nanofiltration membranes. *Colloids and Surfaces A: Physicochemical and Engineering Aspects***,** v. 150, n. 1, p. 247-259, 1999.

PÉREZ-GONZÁLEZ, A.; URTIAGA, A.; IBÁÑEZ, R.; ORTIZ, I. State of the art and review on the treatment technologies of water reverse osmosis concentrates. *Water Research***,** v. 46, n. 2, p. 267-283, 2012.

PETRINIC, I.; KORENAK, J.; POVODNIK, D.; HÉLIX-NIELSEN, C. A feasibility study of ultrafiltration/reverse osmosis (UF/RO)-based wastewater treatment and reuse in the metal finishing industry. *Journal of Cleaner Production***,** v. 101, p. 292-300, 2015.

PLOTTU-PECHEUX, A.; HOUSSAIS, B.; DEMOCRATE, C.; GATEL, D.; PARRON, C.; CAVARD, J. Comparison of three antiscalants, as applied to the treatment of water from the River Oise. *Desalination***,** v. 145, n. 1, p. 273-280, 2002.

PORTO, C. G.; PALERMO, N.; PIRES, F. R. M. *Panorama da exploração e produção de ouro no Brasil*. Rio de Janeiro: CETEM, 2002. 1-23 p.

PULLES, W.; JUBY, G.; BUSBY, R. Development of the slurry precipitation and recycle reverse osmosis (SPARRO) technology for desalinating scaling mine waters. *Water science and technology***,** v. 25, n. 10, p. 177-192, 1992.

QI, L.; WANG, X.; XU, Q. Coupling of biological methods with membrane filtration using ozone as pre-treatment for water reuse. *Desalination***,** v. 270, n. 1, p. 264-268, 2011.

QIN, J.-J.; OO, M. H.; WAI, M. N.; WONG, F.-S. Effect of feed pH on an integrated membrane process for the reclamation of a combined rinse water from electroless nickel plating. *Journal of Membrane Science***,** v. 217, n. 1-2, p. 261-268, 2003.

QU, D.; WANG, J.; WANG, L.; HOU, D.; LUAN, Z.; WANG, B. Integration of accelerated precipitation softening with membrane distillation for high-recovery desalination of primary reverse osmosis concentrate. *Separation and Purification Technology***,** v. 67, n. 1, p. 21-25, 2009.

RAHARDIANTO, A.; GAO, J.; GABELICH, C. J.; WILLIAMS, M. D.; COHEN, Y. High recovery membrane desalting of low-salinity brackish water: Integration of accelerated precipitation softening with membrane RO. *Journal of Membrane Science***,** v. 289, n. 1, p. 123-137, 2007.

RAHARDIANTO, A.; MCCOOL, B. C.; COHEN, Y. Reverse osmosis desalting of inland brackish water of high gypsum scaling propensity: kinetics and mitigation of membrane mineral scaling. *Environmental science & technology***,** v. 42, n. 12, p. 4292-4297, 2008.

RAHARDIANTO, A.; MCCOOL, B. C.; COHEN, Y. Accelerated desupersaturation of reverse osmosis concentrate by chemically-enhanced seeded precipitation. *Desalination***,** v. 264, n. 3, p. 256-267, 2010.

RICCI, B. C.; FERREIRA, C. D.; AGUIAR, A. O.; AMARAL, M. C. Integration of nanofiltration and reverse osmosis for metal separation and sulfuric acid recovery from gold mining effluent. *Separation and Purification Technology*, 2015.

RICHARDS, L. A.; VUACHÈRE, M.; SCHÄFER, A. I. Impact of pH on the removal of fluoride, nitrate and boron by nanofiltration/reverse osmosis. *Desalination***,** v. 261, n. 3, p. 331-337, 2010.

RICHMOND, W. R.; LOAN, M.; MORTON, J.; PARKINSON, G. M. Arsenic removal from aqueous solution via ferrihydrite crystallization control. *Environmental science & technology***,** v. 38, n. 8, p. 2368-2372, 2004.

RIERA, F. A.; SUÁREZ, A.; MURO, C. Nanofiltration of UHT flash cooler condensates from a dairy factory: Characterisation and water reuse potential. *Desalination***,** v. 309, p. 52-63, 2013.

RIETMAN, B. *Cleaning spiral wound membrane modules with a two phase solution*. 2013. 85 p. Thesis (Master of Science in Civil Engineering) - Department of Water Management, Delft University of Technology, Delft, 2013.

ROY, Y.; SHARQAWY, M. H.; LIENHARD, J. H. Modeling of flat-sheet and spiral-wound nanofiltration configurations and its application in seawater nanofiltration. *Journal of Membrane Science***,** v. 493, p. 360-372, 2015.

SALGADO, C. M.; PALACIO, L.; PRÁDANOS, P.; HERNÁNDEZ, A.; GONZÁLEZ-HUERTA, C.; PÉREZ-MAGARIÑO, S. Comparative study of red grape must nanofiltration: Laboratory and pilot plant scales. *Food and Bioproducts Processing***,** v. 94, p. 610-620, 2015.

SÁNCHEZ-ANDREA, I.; SANZ, J. L.; BIJMANS, M. F.; STAMS, A. J. Sulfate reduction at low pH to remediate acid mine drainage. *Journal of Hazardous Materials***,** v. 269, p. 98-109, 2014.

SAWYER, C. N.; MCCARTY, P. L.; PARKIN, G. F. *Chemistry for environmental engineering and science*. New York: McGraw-Hill, 2003.

SCHAEP, J.; VAN DER BRUGGEN, B.; VANDECASTEELE, C.; WILMS, D. Influence of ion size and charge in nanofiltration. *Separation and Purification Technology***,** v. 14, n. 1, p. 155-162, 1998.

SCHÄFER, A. I.; FANE, A. G.; WAITE, T. D. *Nanofiltration: principles and applications.* Elsevier, 2005. ISBN 1856174050.

SEMIÃO, A. J.; SCHÄFER, A. I. Estrogenic micropollutant adsorption dynamics onto nanofiltration membranes. *Journal of Membrane Science***,** v. 381, n. 1, p. 132-141, 2011.

SETHI, S.; WIESNER, M. R. Cost modeling and estimation of crossflow membrane filtration processes. *Environmental engineering science***,** v. 17, n. 2, p. 61-79, 2000.

SHETTY, G. R.; CHELLAM, S. Predicting membrane fouling during municipal drinking water nanofiltration using artificial neural networks. *Journal of Membrane Science***,** v. 217, n. 1, p. 69-86, 2003.

SHU, L.; WAITE, T.; BLISS, P.; FANE, A.; JEGATHEESAN, V. Nanofiltration for the possible reuse of water and recovery of sodium chloride salt from textile effluent. *Desalination***,** v. 172, n. 3, p. 235-243, 2005.

SIERRA, C.; SAIZ, J. R. Á.; GALLEGO, J. L. R. Nanofiltration of Acid Mine Drainage in an Abandoned Mercury Mining Area. *Water, Air, & Soil Pollution***,** v. 224, n. 10, p. 1-12, 2013.

SIMATE, G. S.; NDLOVU, S. Acid mine drainage: Challenges and opportunities. *Journal of Environmental Chemical Engineering***,** v. 2, n. 3, p. 1785-1803, 2014.

SIMON, A.; MCDONALD, J. A.; KHAN, S. J.; PRICE, W. E.; NGHIEM, L. D. Effects of caustic cleaning on pore size of nanofiltration membranes and their rejection of trace organic chemicals. *Journal of Membrane Science***,** v. 447, p. 153-162, 2013.

SOHRABI, M.; MADAENI, S.; KHOSRAVI, M.; GHAEDI, A. Chemical cleaning of reverse osmosis and nanofiltration membranes fouled by licorice aqueous solutions. *Desalination***,** v. 267, n. 1, p. 93-100, 2011.

SONG, Y.; GAO, X.; GAO, C. Evaluation of scaling potential in a pilot-scale NF–SWRO integrated seawater desalination system. *Journal of Membrane Science***,** v. 443, p. 201-209, 2013.

SUBRAMANI, A.; CRYER, E.; LIU, L.; LEHMAN, S.; NING, R. Y.; JACANGELO, J. G. Impact of intermediate concentrate softening on feed water recovery of reverse osmosis process during treatment of mining contaminated groundwater. *Separation and Purification Technology***,** v. 88, p. 138-145, 2012.

TANG, C. Y.; KWON, Y.-N.; LECKIE, J. O. Effect of membrane chemistry and coating layer on physiochemical properties of thin film composite polyamide RO and NF membranes: II. Membrane physiochemical properties and their dependence on polyamide and coating layers. *Desalination***,** v. 242, n. 1, p. 168-182, 2009.

TANHAEI, B.; CHENAR, M. P.; SAGHATOLESLAMI, N.; HESAMPOUR, M.; KALLIOINEN, M.; SILLANPÄÄ, M.; MÄNTTÄRI, M. Removal of nickel ions from aqueous solution by micellar-enhanced ultrafiltration, using mixed anionic–non-ionic surfactants. *Separation and Purification Technology***,** v. 138, p. 169-176, 2014.

TEIXEIRA, M.; ROSA, M.; NYSTROM, M. The role of membrane charge on nanofiltration performance. *Journal of Membrane Science***,** v. 265, n. 1-2, p. 160-166, 2005.

TRISZCZ, J. M.; PORTA, A.; EINSCHLAG, F. S. G. Effect of operating conditions on iron corrosion rates in zero-valent iron systems for arsenic removal. *Chemical Engineering Journal***,** v. 150, n. 2, p. 431-439, 2009.

TU, K. L.; NGHIEM, L. D.; CHIVAS, A. R. Coupling effects of feed solution pH and ionic strength on the rejection of boron by NF/RO membranes. *Chemical Engineering Journal***,** v. 168, n. 2, p. 700-706, 2011.

TWIDWELL, L.; MCCLOSKEY, J. Removing arsenic from aqueous solution and long-term product storage. *JOM***,** v. 63, n. 8, p. 94-100, 2011.

USA. *Toxicological profile for arsenic.* U.S. Department of Health and Human Services. Atlanta. 2007.

VACLAV, P.; EVA, G. Desalting of Acid Mine Drainage by Reverse Osmosis Method – Field Tests 9th International Mine Water Congress, 2005. Oviedo, Spain.

VAN GAUWBERGEN, D.; BAEYENS, J. Macroscopic fluid flow conditions in spiral-wound membrane elements. *Desalination***,** v. 110, n. 3, p. 287-299, 1997.

VAN GESTEL, T.; VANDECASTEELE, C.; BUEKENHOUDT, A.; DOTREMONT, C.; LUYTEN, J.; LEYSEN, R.; VAN DER BRUGGEN, B.; MAES, G. Salt retention in nanofiltration with multilayer ceramic TiO 2 membranes. *Journal of Membrane Science***,** v. 209, n. 2, p. 379-389, 2002.

VAN PAASSEN, J. A.; KRUITHOF, J. C.; BAKKER, S. M.; KEGEL, F. S. Integrated multi-objective membrane systems for surface water treatment: pre-treatment of nanofiltration by riverbank filtration and conventional ground water treatment. *Desalination***,** v. 118, n. 1, p. 239-248, 1998.

VEDAVYASAN, C. Combating water shortages with innovative uses of membranes. *Desalination***,** v. 132, n. 1, p. 345-347, 2000.

VISSER, T.; MODISE, S.; KRIEG, H.; KEIZER, K. The removal of acid sulphate pollution by nanofiltration. *Desalination***,** v. 140, n. 1, p. 79-86, 2001.

VOGEL, D.; SIMON, A.; ALTURKI, A. A.; BILITEWSKI, B.; PRICE, W. E.; NGHIEM, L. D. Effects of fouling and scaling on the retention of trace organic contaminants by a nanofiltration membrane: the role of cake-enhanced concentration polarisation. *Separation and Purification Technology***,** v. 73, n. 2, p. 256-263, 2010.

WANG, D.-X.; SU, M.; YU, Z.-Y.; WANG, X.-L.; ANDO, M.; SHINTANI, T. Separation performance of a nanofiltration membrane influenced by species and concentration of ions. *Desalination***,** v. 175, n. 2, p. 219-225, 2005.

WANG, X.-L.; TSURU, T.; TOGOH, M.; NAKAO, S.-I.; KIMURA, S. Evaluation of pore structure and electrical properties of nanofiltration membranes. *Journal of chemical engineering of Japan***,** v. 28, n. 2, p. 186-192, 1995.

WANG, X.; LIU, W.; LI, D.; MA, W. Arsenic (V) removal from groundwater by GE-HL nanofiltration membrane: effects of arsenic concentration, pH, and co-existing ions. *Frontiers of Environmental Science & Engineering in China***,** v. 3, n. 4, p. 428-433, 2009.

WANG, Y.-N.; TANG, C. Y. Protein fouling of nanofiltration, reverse osmosis, and ultrafiltration membranes—the role of hydrodynamic conditions, solution chemistry, and membrane properties. *Journal of Membrane Science***,** v. 376, n. 1, p. 275-282, 2011.

WANG, Z.; LIU, G.; FAN, Z.; YANG, X.; WANG, J.; WANG, S. Experimental study on treatment of electroplating wastewater by nanofiltration. *Journal of Membrane Science***,** v. 305, n. 1-2, p. 185-195, 2007.

WEI, X.; WANG, Z.; FAN, F.; WANG, J.; WANG, S. Advanced treatment of a complex pharmaceutical wastewater by nanofiltration: Membrane foulant identification and cleaning. *Desalination***,** v. 251, n. 1, p. 167-175, 2010.

WILDEMAN, T.; PINTO, A.; TONDO, L.; ALVES, L. Passive treatment of a cyanide and arsenic laden process water at the RPM Gold Mine, Minas Gerais, Brazil. Proceedings, 7th International Conference on Acid Rock Drainage, 26Á30 March, 2006. p.2377Á2384.

WILF, M. *The Guidebook to Membrane Technology for Wastewater Reclamation*. Hopkinton: Balaban Desalinations Publications, 2010. ISBN ISBN 0-86689-067-x.

XIA, S.; DONG, B.; ZHANG, Q.; XU, B.; GAO, N.; CAUSSERANDA, C. Study of arsenic removal by nanofiltration and its application in China. *Desalination***,** v. 204, n. 1, p. 374-379, 2007.

XU, P.; CAPITO, M.; CATH, T. Y. Selective removal of arsenic and monovalent ions from brackish water reverse osmosis concentrate. *Journal of Hazardous Materials***,** v. 260, p. 885-891, 2013.

XU, P.; DREWES, J. E.; BELLONA, C.; AMY, G.; KIM, T.-U.; ADAM, M.; HEBERER, T. Rejection of emerging organic micropollutants in nanofiltration-reverse osmosis membrane applications. *Water Environment Research*, p. 40-48, 2005.

YAN, L.; WANG, Y.; MA, H.; HAN, Z.; ZHANG, Q.; CHEN, Y. Feasibility of fly ash-based composite coagulant for coal washing wastewater treatment. *Journal of Hazardous Materials***,** v. 203, p. 221-228, 2012.

YU, S.; LIU, M.; MA, M.; QI, M.; LÜ, Z.; GAO, C. Impacts of membrane properties on reactive dye removal from dye/salt mixtures by asymmetric cellulose acetate and composite polyamide nanofiltration membranes. *Journal of Membrane Science***,** v. 350, n. 1-2, p. 83-91, 2010.

YUAN, P.-Q.; KONG, N.; CHENG, Z.-M.; SEMIAT, R. Electrostatic potential on anti-scalants modified CaCO 3 (104) surface: A molecular simulation study. *Desalination***,** v. 238, n. 1, p. 246-256, 2009.

ZARGA, Y.; BOUBAKER, H. B.; GHAFFOUR, N.; ELFIL, H. Study of calcium carbonate and sulfate co-precipitation. *Chemical Engineering Science***,** v. 96, p. 33-41, 2013.

ZULAIKHA, S.; LAU, W.; ISMAIL, A.; JAAFAR, J. Treatment of restaurant wastewater using ultrafiltration and nanofiltration membranes. *Journal of Water Process Engineering*, 2014.